DEVELOPMENT AND UNCERTAINTY QUANTIFICATION OF HURRICANE SURGE RESPONSE FUNCTIONS AND SEA-LEVEL RISE ADJUSTMENTS FOR COASTAL BAYS

Nicholas Ramsey Taylor

Thesis submitted to the faculty of the Virginia Polytechnic Institute and State University in partial fulfillment of the requirements for the degree of

Master of Science
In
Civil Engineering

Jennifer L. Irish, Committee Chair
Nina Stark
Robert Weiss

April 28, 2014
Blacksburg, VA

Keywords: Storm Surge, Hazard Assessment, Coastal Flooding, Hurricane, Sea-Level Rise

Development and Uncertainty Quantification of Hurricane Surge Response Functions and Sea-Level Rise Adjustments for Coastal Bays

Nick R. Taylor

ABSTRACT

Reliable and robust methods of extreme value based hurricane surge prediction, such as the Joint Probability Method (JPM), are critical in the coastal engineering profession. The JPM has become the preferred surge hazard assessment method in the United States; however, it has a high computational cost: one location can require hundreds of simulated storms, and more than ten thousand computational hours to complete. Optimal sampling methods that use physics based surge response functions (SRFs), can reduce the required number of simulations. This study extends the development of SRFs to bay interior locations at Panama City, Florida. Mean SRF root-mean-square (RMS) errors for open coast and bay interior locations were 0.34 m and 0.37 m, respectively; comparable to expected ADCIRC model errors (~0.3 m—0.5 m). Average uncertainty increases from open coast and bay SRFs were 10% and 12%, respectively.

Long-term climate trends, such as rising sea levels, introduce nonstationarity into the simulated and historical surge datasets. A common approach to estimating total flood elevations is to take the sum of projected sea-level rise (SLR) and present day surge (static approach); however, this does not account for dynamic SLR effects on surge generation. This study demonstrates that SLR has a significant dynamic effect on surge in the Panama City area, and that total flood elevations, with respect to changes in SLR, are poorly characterized as static increases. A simple adjustment relating total flood elevation to present day conditions is proposed. Uncertainty contributions from these SLR adjustments are shown to be reasonable for surge hazard assessments.

ACKNOWLEDGEMENTS

First, I would like to express my sincerest thanks to my advisor, Dr. Jennifer L. Irish, for her continual support, guidance, and patience, throughout my graduate studies. It was her support that brought me to Virginia Tech, her guidance that fostered my own skills and enthusiasm for this field of study, and her patience that made graduation possible. I couldn't have asked for a better mentor.

I would also like to thank my committee members, Dr. Nina Stark and Dr. Robert Weiss, for their encouragement and insightful comments throughout this work.

I gratefully acknowledge Dr. Scott C. Hagen, Dr. James M. Kaihatu, Matthew V. Bilskie, and Patrick W. McLaughlin, for their many contributions to this work.

This material is based on the work supported by the National Sea Grant College Program of the U.S. Department of Commerce's National Oceanic and Atmospheric Administration (Grant No. NA10OAR4170099. The views expressed here do not necessarily reflect the views of this organization.

TABLE OF CONTENTS

LIST OF TABLES

LIST OF FIGURES

NOMENCLATURE

RMW	Radius of maximum winds
JPM	Joint Probability Method
OS	Optimal sampling
JPM-OS	Joint Probability Method with optimal sampling
EST	Empirical Simulation Technique
EVA	Extreme value analysis
PDF	Probability density function
PBL	Planetary boundary layer
JPM-OS-Q	Quadrature based optimal sampling
JPM-OS-SG	Sparse grid optimal sampling
JPM-OS-RS	Response surface optimal sampling
SRF	Surge response function
RMS	Root mean square
MSL	Mean sea level
SST	Sea surface temperature
ENSO	El Niño-Southern Oscillation
SLR	Sea-level rise
IPCC	Intergovernmental Panel on Climate Change
GMST	Global mean surface temperature
NOAA	National Oceanic and Atmospheric Administration
FEMA	Federal Emergency Management Agency
AFB	Air force base
WRF	Wave response function

$\vec{\mathbf{V}}$	Hurricane wind field velocity
R	Radius of curvature
ρ_a	Density of air
p	Hurricane pressure field
f	Coriolis parameter
ζ	Surge relative to still water level
$\vec{\boldsymbol{U}}$	Depth averaged horizontal water velocity vector
$\boldsymbol{U}_x$	x-component of depth averaged horizontal water velocity
$\boldsymbol{U}_y$	y-component of depth averaged horizontal water velocity
h_b	Average still water depth
τ_{bf}	Bottom stress term
g	Gravitational acceleration constant
α	Effective earth elasticity factor
η	Newtonian equilibrium tide potential
ρ_0	Reference density of water
τ_s	Surface wind stress term
ζ_w	Wind driven surge
L	Cross shore shallow water continental shelf width
C_d	Drag coefficient

$T(\zeta)$	Return period
λ_T	Hurricane landfall occurrence rate
$F(\zeta)$	Cumulative surge distribution function
R_p	Hurricane pressure radius
c_p	Hurricane central pressure
v_f	Hurricane forward velocity
θ	Hurricane track angle
x_0	Hurricane landfall position
Φ	Surge model term
ε_z	Model uncertainty
$\vec{\boldsymbol{G}}_{\boldsymbol{V}}$	Geostrophic wind field
$\vec{\boldsymbol{C}}_{\boldsymbol{V}}$	Hurricane forward velocity (vector)
h	Atmospheric boundary layer height
Δp	Difference between ambient and hurricane central pressure
A, B	Scaling parameters (Holland 1980)
x_p	Hurricane peak surge position
λ	Nondimensional coefficient
x'	Dimensionless alongshore parameter
x	Location of interest
R_{thres}	Threshold R_p value
a_1, a_2, b_1, b_2	Location dependent, dimensionless scaling coefficients
K	Dimensionless constant
γ_0	Reference specific weight of water
ζ'	Dimensionless surge parameter
m_x	Location dependent scaling coefficient
$\lambda(x_0)$	Ratio between relative maximum peak surge location and R_p
c	Dimensionless constant
$L_{30}(x_0)$	Cross shore distance from shoreline to 30 m depth contour, at x_0
L_{30-ref}	Reference value of L_{30}
m_2, α, β	Location dependent scaling coefficients
Δp_{max}	Maximum theoretical hurricane intensity (Tonkin *et al.* 2000)
$\left[R_p/L_{30}\right]_{ref}$	Maximum R_p/L_{30} value
a, b, c	Regression coefficients
$p_{\Delta SST}$	Future predicted hurricane central pressure
ΔSST	Increase in sea surface temperature
ε_p	Uncertainty in ΔSST dependent central pressure increases
$\varepsilon_{\Delta SST}$	Uncertainty in ΔSST predictions
$\lambda_{\Delta SST}$	Future predicted hurricane annual landfall occurrence rate
λ_T	Hurricane annual landfall occurrence rate
ε_λ	Uncertainty in ΔSST dependent occurrence rate changes
ε_{tide}	Tide model uncertainty
ε_{model}	Hydrodynamic and wind model uncertainty
ε_B	Uncertainty in Holland (1980) B scaling parameter

ε_{waves}	Wave model uncertainty
ε_{wind}	Wind model uncertainty
$\varepsilon_{residual}$	Residual uncertainties
ε_{a}	Aleatory uncertainty
ε_{0}	Present day aleatory uncertainty
ε_{SLR}	SLR uncertainty
Z	Total maximum flood elevation
T_{Z}	Total maximum flood elevation return period
ϕ	SRF model term
ε_{SRF}	SRF uncertainty
ε_{SLR}	SLR uncertainty
Z_{SLR}	Total flood elevation at projected SLR, relative to present day MSL
Z_{0}	Present day total flood elevation
k, l	Location-dependent fit coefficients

CHAPTER 1

INTRODUCTION

Hurricanes continue to pose one of the most substantial risks to coastal communities. Damages inflicted from heavy wind, rain, and inland flooding can be considerable; without adequate preparations, these storms will continue to cause catastrophic damages and losses of life. To safeguard coastal communities against hurricane surge, extreme value analysis (EVA) methods are used to predict the likelihood of hurricane surge events. The estimated surge probabilities provided by these EVA methods, referred to as hazard assessments, are used by coastal engineers, planners, and developers to create surge barriers, evacuation plans, early warning systems, and other protective measures. Therefore, reliable and robust methods of hurricane surge estimation, such as the Joint Probability Method (JPM), play a critical role in reducing the damage these storms inflict on lives and property.

One of the most damaging aspects of hurricanes is the sudden and sustained increase in water levels, known as surge. As a hurricane approaches land, shoreline water levels slowly begin to rise, reaching peak heights at some point along the storm's path. These heights can be quite large; in 2008, Hurricane Katrina caused peak surges in excess of 6.0 m along the coasts of Louisiana and Mississippi (*e.g.,* Smith *et al.* 2010, Irish *et al.* 2013). Peak surge levels are directly correlated with the maximum overland flooding extent that a hurricane can potentially cause. Therefore, hurricane hazard assessments often focus on peak surge heights when referring to surge "levels."

Peak surge heights, or surge levels, are affected by several hurricane characteristics. Higher surges are caused by both stronger storms (as defined by central pressure), and larger storms. Surge levels also tend to be higher at points along a coastline where storms make landfall. Forward velocity and track angle also influence surge levels; typically, higher surges are caused by slower moving storms, and by storms striking coasts at perpendicular angles. Storm hazard assessments such as the JPM can predict surge occurrence rates by relating these hurricane characteristics, or "parameters," to surge levels.

Traditional extreme value analysis (EVA) methods apply probability distributions to available historical data; in essence, the return periods obtained from these analyses are the interpolated results of a regression analysis. The accuracy of return period estimates obtained from historical surge records alone is dependent on both the length of the record, and the number of events in the record data. Estimates of probable surge magnitudes are frequently sought at 50, 100, or 500 year return periods; any of these which exceed the historical record length are, by definition, extrapolated values (Klemes 1986). Hurricanes are relatively rare events, and hurricane surge displays considerable dependence on landfall location and size, as well as intensity. Because these storms are so rare, historical surge records do not provide enough data to sufficiently cover the range of meteorological parameters. As a result, historical surge records alone lack the statistical variability required for robust EVA applications.

The JPM, introduced by Ho and Meyers (1975), circumvents the shortcomings associated with other EVA techniques by allowing all possible statistical events to be considered in the analysis. As opposed to directly applying a frequency distribution to hurricane surge, the JPM uses statistical distributions of each hurricane meteorological parameter. By applying a surge value to each combination of hurricane parameters, a population of surge values can be generated with sufficient variability to produce robust results. Additionally, removing the dependence on historical surge data mitigates the inaccuracies resulting from extrapolated values.

To obtain surge estimates that correspond to the hurricane parameter combinations used in the JPM, hydrodynamic simulations are used to supplement historical records; however, these simulations are often significant sources of epistemic error (*e.g.,* Resio *et al.* 2009, Irish and Resio 2013, Resio *et al.* 2013). Models that provide accurate surge estimates use advanced numerical methods, highly resolved spatial domains, and require access to advanced computational resources of limited availability. Optimal sampling (OS) techniques are employed to reduce the number of required hydrodynamic simulations; continual efforts are made to improve upon existing OS techniques, or to develop new ones.

Traditional EVA is based on a stationary assumption; population datasets require an absence of long term trends. This assumption is invalidated by climate driven changes in sea surface temperature (SST) and sea-level rise (SLR) conditions, and must be considered in hurricane hazard assessments. Several studies have shown a relationship between increasing SST and hurricane central pressures (*e.g.,* Knutson and Tuleya 2004, 2008, Knutson *et al.* 2010); by affecting changes to the pressure probability distribution, return period adjustments can be made from a statistical aspect, with little or no additional hydrodynamic simulations required (*e.g.,* Irish and Resio 2013). Increases in SLR, in contrast, alter surge levels; the significance of this effect varies by location. Open coast areas often experience negligible effects, while the effects at bay interior locations may be more substantial, depending on bathymetric and geographic features (*e.g.,* Mousavi *et al.* 2011). Therefore, return period adjustments for SLR trends must be incorporated through additional hydrodynamic simulations, to inform surge response function (SRF) and SLR development.

This study will focus on the SRF method of optimal sampling, a method which uses physical scaling laws to develop continuous expressions relating surge to hurricane meteorological parameters. JPM based hazard assessments coupled with SRFs (*e.g.,* Irish *et al.* 2009, Song *et al.* 2012) have shown high levels of accuracy at open coast regions of the northern Gulf of Mexico coastline. Applications have been limited to four locations, spaced over alongshore distances of 90 km (Irish *et al.* 2009) or 560 km (Song *et al.* 2012). It will be demonstrated that SRFs are effective when simulated surge data availability is limited to a 90 km alongshore extent. Furthermore, SRF development will be extended to bay interior locations. Finally, a linear model relating SLR to total flood elevations will be proposed. The results of this model will be used to gain physical insight into the implications of SLR on flooding hazards at open coast, and bay interior, locations.

CHAPTER 2

LITERATURE REVIEW

2.1 Hurricane Parameters

Extreme value based methods of hurricane hazard assessment that are both accurate and robust consider all meteorological characteristics that affect surge magnitudes. Modern assessment techniques use separate distributions of each storm parameter in order reduce sampling variability. Additionally, these parameters are the basis for the response function model, introduced in later sections, which is used to estimate corresponding surge values. The following section provides an overview of the physical mechanisms that relate storm surge generation to its primary statistical parameters—central pressure, pressure radius, and landfall position—as well as, to a lesser extent, forward velocity and track angle. Emphasis is placed on defining the physical relationships that govern the intensity and pressure radius parameters, introducing the hydrodynamic equation regarding the transfer of momentum between hurricane wind fields and a water column, and illustrating the relationship between surge height and continental shelf width.

2.1.1 Central Pressure and Radius of Maximum Winds

A hurricane's high-intensity wind field is sustained by the balance of pressure, centripetal, and Coriolis forces at the radius of maximum winds (RMW). In regions of the wind field that lie outside of the RMW, the Coriolis force acts in a direction normal to wind velocity, and a circular pattern begins to develop. A steady-state force balance, with the underlying assumption of slow wind field evolution over time, is expressed by the gradient wind equation (Rossby 1940, Smith 1968) as:

$$\frac{|\vec{\mathbf{V}}|^2}{R} + \frac{1}{\rho_a}\frac{dp}{d\hat{n}} + f|\vec{\mathbf{V}}| = 0 \tag{1}$$

$\vec{\mathbf{V}}$	=	Hurricane wind field velocity
R	=	Radius of curvature
ρ_a	=	Density of air
p	=	Hurricane pressure field
f	=	Coriolis parameter

Equation 1 is defined in terms of normal and tangential components. Pressure force is directed along the normal axis towards the storm center, while Coriolis and centripetal forces are directed along the normal axis away from the storm center.

Hurricane pressure fields are generally categorized by their central pressures, while storm size can be defined by its value corresponding to maximum wind velocity. As hurricane pressure field gradients increase, the Coriolis force magnitude becomes negligible, and wind velocity can be approximated as a balance between pressure and centripetal forces:

$$\frac{|\vec{\mathbf{V}}|^2}{\mathrm{R}} = -\frac{1}{\rho_a}\frac{dp}{d\hat{n}} \tag{2}$$

The pressure gradient force in Equation 2 is dependent on both hurricane size and intensity. As a result, a separation between the RMW and the maximum pressure gradient location exists; the ratio between hurricane pressure radius (R_p) and RMW can range from 0.5 to 0.9 for Holland B parameter values between 1 and 2.5, respectively (Holland 1980). Many Joint Probability Method (JPM) studies, therefore, classify storm size in terms of R_p (*e.g.,* Resio *et al.* 2009, Toro *et al.* 2010a, Irish and Resio 2013).

2.1.2 Landfall Position

Hurricane surge at nearshore locations is generated primarily by hurricane wind and, to a lesser extent, pressure fields. Surge can be modeled using the depth-integrated, shallow water representation of the mass and momentum conservation equations (*e.g.,* Westerink *et al.* 1992, Blain *et al.* 1998, Dawson and Profit 2004):

$$\frac{\partial \zeta}{\partial t} + \nabla \cdot \left[\vec{\boldsymbol{U}}(\zeta + h_b)\right] = 0 \tag{3}$$

$$\frac{D\boldsymbol{U}_x}{Dt} + \frac{D\boldsymbol{U}_y}{Dt} + \tau_{bf}\vec{\boldsymbol{U}} + f\hat{k} \times \vec{\boldsymbol{U}} + g\nabla(\zeta - \alpha\eta) = -\frac{1}{\rho_0}\nabla p + \frac{\tau_s}{\rho_0(\zeta + h_b)} \tag{4}$$

ζ = Surge relative to still water level
$\vec{\boldsymbol{U}}$ = Depth averaged horizontal water velocity vector
$\boldsymbol{U}_x$ = x-component of depth averaged horizontal water velocity
$\boldsymbol{U}_y$ = y-component of depth averaged horizontal water velocity
h_b = Average still water depth
τ_{bf} = Bottom stress term
g = Gravitational acceleration constant
α = Effective earth elasticity factor
η = Newtonian equilibrium tide potential
ρ_0 = Reference density of water
τ_s = Surface wind stress term

The left-side terms in the momentum equation (Equation 4) include bottom friction, Coriolis, and tidal forces. Hurricane effects are incorporated as pressure and wind forces on the right side of Equation 4, with the transfer of momentum from the wind field to the water column included as a surface stress term.

As a hurricane approaches landfall, the wind force typically predominates storm surge generation, as its magnitude increases with decreasing bathymetric depth. Resio and Westerink (2008) define wind driven surge at nearshore locations as proportional to surface stress and cross-shore geometry, based on a steady state solution to the linear, depth integrated, one dimensional form of Equation 4:

$$\zeta_w \propto \frac{\rho_a C_d |\vec{\mathbf{V}}|^2}{g h_b} L \tag{5}$$

ζ_w = Wind driven surge
L = Cross shore shallow water continental shelf width
C_d = Drag coefficient

The inclusion of the continental shelf width term in Equation 5 provides physical evidence that storm surge generation varies according to coastal features. Consequently, landfall position, and its relation to corresponding *L* values, is introduced as a significant parameter influencing surge generation. Other physical implications must also be considered during surge response function development; these will be addressed in later sections.

2.1.3 Forward Velocity and Track Angle

In addition to the three significant hurricane parameters identified thus far, a study by Irish *et al.* (2008) demonstrates that surge can also be influenced by forward velocity and track angle, although to a lesser extent than pressure, size, or landfall position. A 20% variation in peak surge values is reported for forward speed differences of 50%, at locations along the Gulf of Mexico coastline. Additionally, a 10% peak surge variation was observed for track angles ranging between -50^{o} and +30^{o} (Irish *et al.* 2008). These findings provide evidence that both forward velocity and track angle are additional parameters to be considered in surge analysis. However, many studies conducting this type of analysis (*e.g.*, Irish *et al.* 2009, Irish *et al.* 2011, Song *et al.* 2012) do not consider these parameters to be significant, due to their relatively low influence on peak surge values.

2.1.4 Section Summary

This section has identified the five parameters responsible for most of the variability in hurricane surge. The force balance between pressure forces and centripetal forces near the RMW establishes hurricane central pressure, and pressure radius, as important parameters influencing hurricane surge. Additionally, integration of the shallow water momentum equations in the alongshore direction defines the relationship between wind driven surge and continental shelf width, and establishes landfall position as a third influential parameter. Hurricane track angle and forward velocity have also been shown to influence surge generation, although their effects are less significant.

2.2 Extreme Value Analysis and Optimal Sampling Methods

Extreme value based hurricane hazard assessments that consider statistical possibilities beyond the recorded data must supplement historical surge records with artificial data. This supplementary data is developed using hydrodynamic hurricane surge models; selecting which model setup to use involves compromises between accuracy and computational resources. Techniques that reduce the number of additional storms required are used in conjunction with surge frequency analysis methods, in order to make use of high resolution hydrodynamic models more feasible. This section provides an overview of surge frequency analysis and the JPM; an introduction to ADCIRC, a frequently used hurricane surge model; and a review of optimal sampling (OS) techniques for coupled JPM application (JPM-OS).

2.2.1 Overview

In the 1960's, coastal planners became aware of the influence that local coastline features have on storm surge generation, and began to apply extreme value statistics to surge frequency analysis. These methods apply extreme value distributions to measured surge data, and express annual exceedance probabilities as return periods (*e.g.*, Yang *et al.* 1970, Scheffner *et al.* 1996, Resio *et al.* 2009):

$$T(\zeta) = \frac{1}{\lambda_T[1-F(\zeta)]} \tag{6}$$

$T(\zeta)$ = Return period
λ_T = Hurricane landfall occurrence rate
$F(\zeta)$ = Cumulative surge distribution function

Statistical methods such as the Empirical Simulation Technique (EST) use bootstrapping methods to estimate return periods using only recorded hurricane surge data (*e.g.*, Divoky and Resio 2007). However, historical surge records do not contain enough data to cover the range of hurricane parameters. These records constitute a small percentage of a full statistical sample, and any return period estimates derived from their use will contain large amounts of statistical uncertainty. As a result, substantial differences in return period values will occur for estimates at the same location, using different historical surge records.

A study by Divoky and Resio (2007) estimated 50, 100, and 500 year return periods along an idealized coastline 1000 miles in length, using EST techniques. Ten separate 65-year historical surge records were created for this hypothetical coastline. Each historical record consisted of a random sample of hurricanes taken from a large pool of simulated hurricanes, with an occurrence rate of 5E-4 km/yr. Theoretical values were estimated using a JPM analysis of the entire synthetic hurricane set. Divoky and Resio (2007) reported the standard deviations of 50, 100, and 500-year return period estimates among the 10 historical surge records as 1.66 m, 2.44 m, and 5.52 m, respectively. This degree of variability demonstrates the unreliability of extreme value analysis (EVA) methods based solely on historical records.

2.2.2 Joint Probability Method

The JPM was first applied to hurricane surge by Ho and Meyers (1975), and has been shown to provide more reliable estimates than the EST method (*e.g.,* Divoky and Resio 2007, Resio *et al.* 2009). Unlike methods that use only historical surge data, the JPM considers all possible parameter sets in the analysis (Divoky and Resio 2007). A probability density function (PDF) is assigned to each storm parameter (*e.g.*, Resio *et al.* 2009, Irish *et al.* 2009, Irish and Resio 2013):

$$p\left(c_p, R_p, v_f, \theta, x_0\right) = p(c_p|x_0) \cdot p(R_p|c_p) \cdot p(v_f|\theta) \cdot p(\theta|x_0) \cdot p(\lambda_T, x_0) \tag{7}$$

c_p = Hurricane central pressure
R_p = Hurricane pressure radius
v_f = Hurricane forward velocity
θ = Hurricane track angle, relative to shore normal direction
x_0 = Hurricane landfall position

Return periods are found by integrating Equation 7, often by numerical means:

$$F(\zeta) = \int_{c_p} \int_{R_p} \int_{v_f} \int_{\theta} \int_{x_0} p(c_p, R_p, v_f, \theta, x_0)\, H[\zeta - \Phi(c_p, R_p, v_f, \theta, x_0) + \varepsilon_z]$$

$$x_0 d\theta dv_f dR_p dc_p \tag{8}$$

Φ = Surge model term
ε_z = Model uncertainty

In comparison to the EST, return period estimates obtained using the JPM have substantially less variability. Divoky and Resio (2007) compared the variability in the JPM to that of the EST by evaluating the standard deviation of the 50, 100, and 500-year return period estimates, among 10 different sets of simulated hurricanes. The meteorological data used to construct hurricane parameter PDFs spanned a 65-year period. Standard deviations of the 50, 100, and 500-year return period estimates were 0.27 m, 0.31 m, and 0.47 m, respectively. These deviations, which are considerably lower than those from the EST, demonstrate that the JPM is a reliable statistical method for coastal surge hazard assessment.

2.2.3 Numerical Models

The JPM reduces variability in return period estimates by evaluating the PDFs of hurricane meteorological parameters; however, most storm parameter combinations do not have readily available surge estimates. Numerical models capable of simulating hypothetical storm events to a high degree of accuracy must be used to provide surge estimates for JPM inputs. Several studies that have accurately modeled hurricane surge (*e.g.*, Binder *et al.* 2009, Bacopoulos *et al.* 2012) have used the Planetary Boundary Layer (PBL) wind field model described by Thompson and Cardone (1996). The PBL model simulates a hurricane wind field by finding a numerical solution for the balance of forces described by Equation 1, vertically averaged over the atmospheric boundary layer:

$$f\hat{k} \times \left(\vec{\boldsymbol{V}} - \vec{\boldsymbol{G}}_{\boldsymbol{V}}\right) + \frac{1}{\rho_a}\nabla p + \frac{C_d}{h}\left|\vec{\boldsymbol{V}} + \vec{\boldsymbol{C}}_{\boldsymbol{V}}\right|\left(\vec{\boldsymbol{V}} + \vec{\boldsymbol{C}}_{\boldsymbol{V}}\right) = 0 \qquad (9)$$

$$p = c_p + \Delta p e^{-A/r^B} \qquad (10)$$

$\vec{\boldsymbol{G}}_{\boldsymbol{V}}$	=	Geostrophic wind field
$\vec{\boldsymbol{C}}_{\boldsymbol{V}}$	=	Hurricane forward velocity (vector)
h	=	Atmospheric boundary layer height
Δp	=	Difference between ambient and hurricane central pressure
A, B	=	Scaling parameters (Holland 1980)

The Holland model (1980), with specified inputs for intensity and RMW, is used as the pressure field model. Steady state solutions to Equations 9 and 10 are determined for specified time intervals; this allows control over landfall position, track angle, and forward velocity in all simulations. The pressure and wind field created by the hurricane atmospheric model is used by hydrodynamic model to calculate surface wind stresses.

ADCIRC is a finite element based hydrodynamic model that has been used to accurately estimate hurricane surge for both hypothetical storm scenarios and historical hurricanes (*e.g.*, Bacopoulos *et al.* 2012, Dietrich *et al.* 2013, Ferreira *et al.* 2013). A study by Westerink *et al.* (2008) estimated ADCIRC model uncertainty using simulations of Hurricanes Betsy (1965) and Andrew (1992). A total of 67 recorded peak surge measurements were compared to the simulated results; mean absolute error and standard deviations of 0.30 m and 0.37 m, respectively, were reported.

2.2.4 Optimal Sampling

Although hydrodynamic models are accurate enough to fully supplement historical data records in extreme value surge analysis, the computational requirements of these models can be prohibitive. A single ADCIRC simulation can require on the order of 10,000 computational hours to complete (Irish *et al.* 2009), and adequate coverage of all storm parameter combinations in a 5-dimensional scheme can require thousands of simulations. It is therefore necessary to incorporate optimization techniques that reduce the number of required simulations. Optimal sampling is based on one of two types of methods; quadrature, and interpolation based schemes (*e.g.,* Toro *et al.* 2010, Niedoroda *et al.* 2010, Condon and Sheng 2012).

Quadrature based optimal sampling (JPM-OS-Q) uses Bayesian quadrature to select storm parameter combinations. Integration of the JPM parameter space is accomplished by numerical means; an importance factor is assigned to each parameter combination prior to integration (*e.g.,* Toro *et al.* 2010). This factor is based on the relative importance of the storm scenario, and its value is determined during the sampling process. A drawback to this method is the exponential relationship between the number of parameters included in an analysis, and the number of optimal samples required for scheme stability (Toro *et al.* 2010). Use of the JPM-OS-Q method is currently limited to five dimensions, and precludes incorporating additional parameters, such as the Holland B parameter, into the JPM.

Interpolation based optimal sampling methods use different means of interpolating the surge response for all possible parameter combinations from a small subset of storms. The sparse grid (JPM-OS-SG) scheme, introduced by Condon and Sheng (2012), uses multi-adaptive regression splines for surge response interpolation. Population and numerical integration of the JPM parameter space is accomplished through the use of an anisotropic sparse grid that creates added resolution for more influential storm parameters. The response surface (JPM-OS-RS) scheme (*e.g.,* Resio *et al.* 2007, Toro *et al.* 2010, Condon and Sheng 2012), in contrast, is based on more conventional methods. Optimal sampling is achieved by introducing greater variability into the central pressure and storm radius parameters. Initial surge response surfaces, with respect to central pressure and storm radius, are created at fixed values of landfall position, forward velocity, and track angle. The method is extended into higher dimensions by interpolating between response surfaces for the remaining (less influential) parameters, at different fixed values.

An alternative means of optimal sampling, introduced by Irish *et al.* (2009), involves optimal sampling using surge response functions. In contrast to quadrature and response surface schemes, surge response function (SRF) methods use physics based arguments to create continuous functions of surge, with hurricane meteorological parameters as the independent variables. This allows continuous, rather than discrete, surge PDFs to be developed (Irish *et al.* 2009). Furthermore, the algebraic form of SRFs (*e.g.,* Irish *et al.* 2009, Song *et al.* 2012) allows for rapid calculation of surge values; this reduces the computational burden associated with traditional JPM applications.

2.2.5 Section Summary

This section has introduced the main concepts, as well as the rationale, behind surge hazard assessments using JPM-OS techniques. The JPM captures the variability in surge data by considering, to a practical limit, all possible hurricane combinations. Hydrodynamically simulated surge data supplements historical surge records in order to create a complete dataset for analysis. Because accurate hydrodynamic simulations involve high computational demands, the JPM is coupled with OS techniques to reduce the number of required hydrodynamic simulations.

2.3 Surge Response Functions

SRFs estimate hurricane surge values using the governing hydrodynamic relationships, discussed previously. The resulting equations constitute a statistical surge model capable of creating a synthetic surge population. This method is considered an optimal sampling technique because it uses a regression function, fitted to a small subset of hydrodynamically simulated storms, to estimate hypothetical surge values. Surge populations created using SRFs are, therefore, derived from available historical and hydrodynamically simulated data.

This section gives an overview of the SRF development process. Emphasis is placed on the physical justifications for each SRF model component, and the inclusion of continental shelf width as a scaling term.

2.3.1 Dimensionless Alongshore Parameter

Because surge varies due to storm and coastline characteristics, SRFs must account for both sources of variability. Application of SRFs to the Texas coastline establish the physical scaling laws for bathymetric effects by analyzing the alongshore surge distribution due to storms with varying hurricane meteorological parameters. Irish *et al.* (2009) defines a first order linear relationship between storm landfall position and storm radius as:

$$x_p - x_0 = \lambda R_p \tag{11}$$

x_p = Hurricane peak surge position
λ = Nondimensional coefficient

Physically, λ represents the ratio of the offset distance between landfall position and peak surge position, to storm size. This relationship is used to define a dimensionless alongshore response function for any location of interest relative to the peak surge position:

$$x' = \frac{x - x_0}{R_p} - \lambda \tag{12}$$

x'	=	Dimensionless alongshore parameter
x	=	Location of interest

Irish *et al.* (2009) estimates λ as a location dependent constant (Figure 2-1); average percent errors for numerically simulated values of $x_p - x_0$, and values predicted using Equation 11, were approximately 17%.

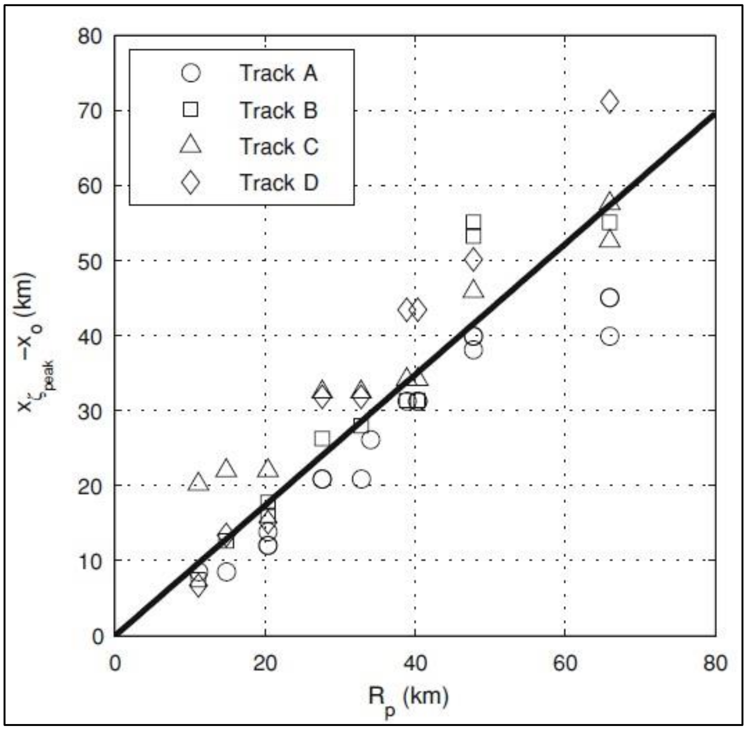

Figure 2-1 Simulated alongshore location of peak surge versus storm size for all simulated storms. The R^2 value was determined to be 0.85 for all storms (from Irish *et al.* 2009)

Storm surge tends to vary smoothly for changes in both size and intensity; however, Equation 12 does not account for some of the complexities in pressure-radius response surfaces caused by certain types of storms. Irish *et al.* (2009) developed surge response surfaces, with respect to central pressure and storm radius, for the Rockport, TX coastline; these effects appear as "ridges" in the response surfaces, and are restricted to a class of storms with relatively small radii that make landfall near locations of interest. The response surfaces for locations close to, and east of, hurricane landfall positions display significant ridges. Locations close to, and west of, landfall position show less pronounced ridges in their response surfaces. These ridges have the greatest impact on storms with radii less than, or equal to, 25 km.

To incorporate hurricanes with relatively small storm radii, landfall positions close to locations of interest, Irish *et al.* (2009) introduces the following revision to the x' parameter:

$$x' = \frac{x-x_0}{R_p} - \lambda - F\left(1 - \frac{R_p}{R_{thres}}\right) H\left(1 - \frac{R_p}{R_{thres}}\right)$$

$$F\left(1 - \frac{R_p}{R_{thres}}\right) = \begin{cases} a_1\left(1 - \frac{R_p}{R_{thres}}\right) + b_1 & for \quad -\lambda \le x' \le 0 \\ a_2\left(1 - \frac{R_p}{R_{thres}}\right) + b_2 & for \quad 0 < x' \le \lambda \\ 0 & for \quad \lambda < |x'| \end{cases} \tag{13}$$

R_{thres} = Threshold R_p value
a_1, a_2, b_1, b_2 = Location dependent, dimensionless scaling coefficients

Equation 13 adjusts the relatively small storms using a first order regression of their dimensionless alongshore deviation. The threshold parameter (R_{thres}) varies by region, but is assumed constant for all locations within a study area.

2.3.2 Dimensionless Surge Parameter

Hydrodynamic scaling laws for surge magnitudes are based on the one dimensional shallow water momentum equations. A first order solution, with constant values for continental shelf width and depth, demonstrates that surge scales linearly with hurricane intensity (Irish and Resio 2010):

$$\zeta = \frac{C_d K L}{h_b} \frac{\Delta p}{\gamma_0} \tag{14}$$

K = Dimensionless constant
γ_0 = Reference specific weight of water

The constant K depends on the pressure distribution model characteristics. Irish *et al.* (2009) defines the dimensionless surge parameter as a function of storm intensity using this first order approximation for surge (Equation 14):

$$\zeta' = \frac{\gamma_0 \zeta}{\Delta p} + m_x \Delta p \qquad (15)$$

ζ' = Dimensionless surge parameter
m_x = Location dependent scaling coefficient

The second term in Equation 15 accounts for additional wind generated drag effects. Equations 13 and 15 describe the dimensionless alongshore and surge response functions; Irish *et al.* (2009) describes the process that uses these equations to develop algebraic SRF models along a portion of the Texas coastline, with a maximum root mean square (RMS) error of 0.43 meters.

2.3.3 Incorporation of Continental Shelf Width into Dimensionless Alongshore Distance

To investigate the effect of variable bathymetry, Song *et al.* (2012) incorporates continental shelf width scaling into Equations 13 and 15, where continental shelf width is defined as the cross-shore distance to the 30 m depth contour (L_{30}). Figure 2-2 shows the alongshore surge distributions of four storms of fixed intensity along tracks that make landfall near four locations along the Texas open coast. It is demonstrated that surge generation is relatively insensitive to changes in storm size for locations along the lower Texas coast, where L_{30} values are low (Song *et al.* 2012). Alongshore surge distributions in areas featuring larger L_{30} values, in contrast, show higher sensitivity.

One consequence of greater bathymetric variation demonstrated in this study is the introduction of variability into λ. Song *et al.* (2012) hypothesized that the relationship between continental shelf width and λ, for areas with significant bathymetric variability, is linear, until an

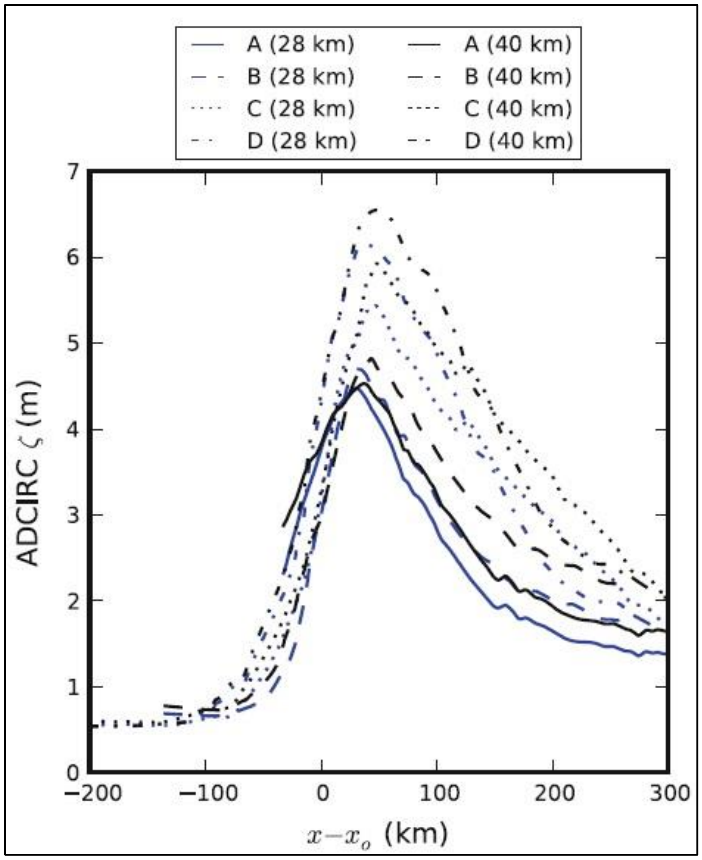

Figure 2-2 Maximum ADCIRC simulated surge values versus alongshore distance for selected tracks when $p_c = 900$ mb and $R_p = 28$ km (blue) and 40 km (black). Surge profile origins for alongshore distance correspond to storm landfall position (from Song *et al.* 2012).

asymptotic value of approximately 1.0 is reached. Figure 2-3 shows the relationship presented by Song *et al.* (2012) between continental shelf widths and λ, for the upper and lower Texas coast. Because continental shelf width increases monotonically along the coast of Texas, higher values along the horizontal axis in Figure 2-3 correspond to locations on the upper Texas coast; lower values on the horizontal axis correspond to locations along the lower Texas coast. Variations in λ follow expected trends along most of the Texas coastline; the asymptotic value for regions along the upper Texas coast, where L_{30} values exceed most storm radii, is 0.88 (Song *et al.* 2012). However, λ reaches a peak value of 1.15 where the shelf width is 40 km, halfway between Matagorda and Galveston; Song *et al.* (2012) reasons that this large λ value arises from the sudden increase in width and change in orientation of the continental shelf at this location.

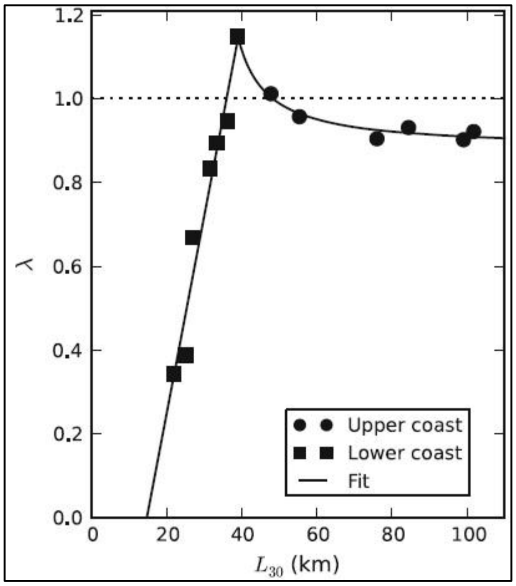

Figure 2-3 Relationship between lambda values and 30-m depth contour (from Song *et al.* 2012).

Based on the relationship between λ and continental shelf width, Song *et al.* (2012) redefines λ as a variable, dependent on L_{30} values at storm landfall position. Furthermore, the alongshore surge distributions in Figure 2-2 show increasing asymmetry at locations with wider continental shelves (Song *et al.* 2012). To account for this, x' is scaled by the ratio of storm size to shelf width:

$$x' = \frac{x-x_0}{R_p} - \lambda(x_0) + cH\left(\frac{L_{30}(x_0)}{L_{30-ref}} - 1\right) H\left(\frac{x-x_0}{R_p} - \lambda(x_0) - 1\right)\left(\frac{R_p}{L_{30}(x_0)}\right) -$$

$$F\left(1 - \frac{R_p}{R_{thres}}\right) H\left(1 - \frac{R_p}{R_{thres}}\right) \qquad (16)$$

$\lambda(x_0)$	=	Ratio between relative maximum peak surge location and R_p
c	=	Dimensionless constant
$L_{30}(x_0)$	=	Cross shore distance from shoreline to 30 m depth contour, at x_0
L_{30-ref}	=	Reference value of L_{30}

The parameters c and L_{30-ref} in Equation 16 are regional constants.

2.3.4 Incorporation of Continental Shelf Width into Dimensionless Surge

Continental shelf width is also shown to limit alongshore surge magnitudes. Equation 14, which gives a 1-dimensional solution to the shallow water momentum equation, assumes that the full distance of the cross shore shelf width is available for surge generation (Irish and Resio 2010). For regions with low L_{30} values, this will often be the case. However, Song *et al.* (2012) shows that this assumption is not always valid for areas with larger L_{30} values. Along the north Texas coast; where L_{30} often exceeds storm size, cross shore distance available for alongshore surge generation is limited by storm size. Song *et al.* (2012) incorporates the relative influence of shelf width and hurricane radius on alongshore surge generation, as R_p/L_{30}. Figure 2-4, from Song *et al.* (2012) shows the relationship between R_p/L_{30} and ADCIRC simulated peak surge magnitudes (ζ_p) for storms of fixed intensity and varying size. For fixed radii, peak surge follows a monotonic, nearly linear relationship with increasing R_p/L_{30}.

Song *et al.* (2012) incorporates R_p/L_{30} into the dimensionless surge parameter (Equation 15) as follows:

$$\zeta' = \frac{\gamma_0 \zeta}{\Delta p} + m_2(x,x')\left(\frac{\Delta p}{\Delta p_{max}}\right)^{\alpha(x,x')}\left(\frac{R_p/L_{30}(x_0)}{\left[R_p/L_{30}\right]_{ref}}\right)^{\beta(x,x')}$$

$$[m_2(x,x'),\alpha(x,x'),\beta(x,x')] = \begin{cases}[m_{2L}(x),\alpha_L(x),\beta_L(x)] & for\ x' < 0 \\ [m_{2R}(x),\alpha_R(x),\beta_R(x)] & for\ x' \geq 0\end{cases} \tag{17}$$

m_2, α, β	=	Location dependent scaling coefficients
Δp_{max}	=	Maximum theoretical hurricane intensity (Tonkin *et al.* 2000)
$\left[R_p/L_{30}\right]_{ref}$	=	Maximum R_p/L_{30} value

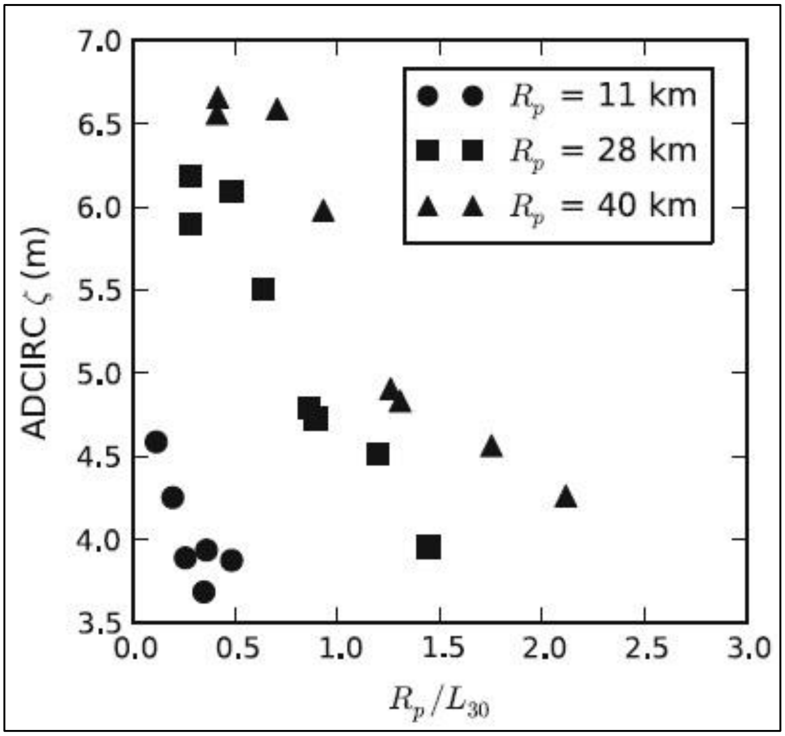

Figure 2-4 Ratio between storm size and cross-shore distance between shoreline and 30-m depth contour versus highest alongshore maximum ADCIRC simulated surge for 900 mb intensity storms (from Song *et al.* 2012).

To express the influence of shelf width on surge magnitude as a dimensionless quantity, R_p/L_{30} is incorporated into the wind generated drag effects term of Equation 15. The regression coefficients $\alpha(x,x')$ and $\beta(x,x')$ are weighting parameters, and determine the relative influence of storm intensity and R_p/L_{30} on surge generation.

2.3.5 SRF Regression Model

Equations 16 and 17 define the x' and ζ' formulations suited for SRF model development in regions with high bathymetric variability. Irish *et al.* (2009) and Song *et al.* (2012) predict the surge value for any hypothetical storm as a function of its parameters by fitting a multi-term exponential distribution to selected ADCIRC surge data in the dimensionless $x'-\zeta'$ plane:

$$\zeta'(x') = a_1 e^{-\left(\frac{x'-b_1}{c_1}\right)} + a_2 e^{-\left(\frac{x'-b_2}{c_2}\right)} + \cdots + a_n e^{-\left(\frac{x'-b_n}{c_n}\right)} \quad (18)$$

a, b, c = Regression coefficients

In the absence of ADCIRC simulated surge values, Equation 18 can be used to estimate the value of ζ' as a function of x' for any given set of surge parameters $[\Delta p, R_p, x_0, L_{30}(x_0)]$. Equations 16 and 17, due to their positive—negative dependence, are expressed as piecewise functions (Figure 2-5).

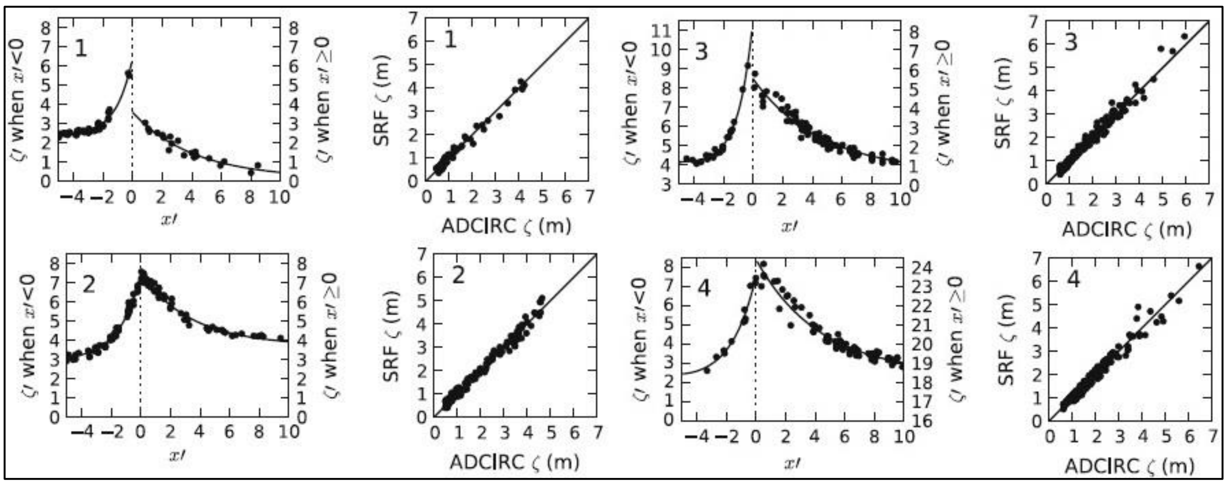

Figure 2-5 Surge response functions developed for the entire Texas open coast using Equations 16, 17, and 18 (left) and SRF-predicted versus ADCIRC-simulated peak surge (right) for selected locations (from Song *et al.* 2012).

2.3.6 Section Summary

This section has introduced the development processes of x' and ζ' in the dimensionless SRF model. Considerations in the x' dimension include the nondimensional distance between hurricane peak surge and landfall position, as well as the effects of small storms with landfall locations near SRF points, and L_{30} asymmetry effects. Development of the ζ' term is based on a first order approximation with respect to hurricane central pressure. Further adjustments, based on central pressure and L_{30}, are also incorporated into the ζ' term. Hurricane hazard assessments that use JPM-OS coupled with SRFs (*e.g.*, Irish *et al.* 2009, Song *et al.* 2012) have succeeded in reducing the number of required hydrodynamic simulations by 75%.

2.4 Long Term Climate Trends

Long-term climate trends, such as increases in sea surface temperature (SST) or mean sea level (MSL) introduce nonstationarity into statistical populations. Long-term climate based trends are present in both the hurricane central pressure PDF, and the global eustatic MSL; these trends are result of global mean increases and decreases in SST. Therefore, JPM based hazard assessments must incorporate these trends into the PDFs, as well as the hydrodynamic model and SRFs, in order to avoid error accumulation. Short term trends, such as the El Niño-Southern Oscillation (ENSO) effect, do not cause changes in baseline probability distributions (Irish *et al.* 2011).

This section introduces the relationship between rising SST and hurricane meteorological parameters, as well as the trend between sea level rise (SLR) and surge generation, as they pertain to the JPM. Emphasis is placed on establishing continuous relationships between climate conditions, hurricane parameters, and surge.

2.4.1 Effects of Sea Surface Temperature on Hurricane Meteorological Parameters

The Intergovernmental Panel on Climate Change (IPCC) projects global mean surface temperatures (GMST) by the 2100s to rise between 1.1 and 6.4^{o}C, relative to GMST levels in the year 2000 (IPCC 2007). These elevated GMST, and corresponding SST values, can cause changes in average hurricane intensity (Knutson and Tuleya 2004, 2008), as well as landfall occurrence rates (*e.g.*, Holland and Webster 2007, Bender *et al.* 2010, Knutson *et al.* 2010). By comparing simulated hurricane intensification across four convective parameterization schemes, and two climate models, Knutson and Tuleya (2004, 2008) projected an average 14% intensification for SST increases between 0.8^{o}C and 2.4^{o}C. Knutson *et al.* (2010) also reports a rising trend in hurricane intensity, and predicts central pressure increases of 2% to 11% by the 2100s. Hazard assessments that consider time dependent trends in hurricane intensity (*e.g.*, Mousavi *et al.* 2011, Irish and Resio 2013) adjust central pressure distributions as a simplified function of increased SST:

$$p_{\Delta SST} = c_p - \left[\left(0.08 + \varepsilon_p\right)\left(\Delta SST + \varepsilon_{\Delta SST}\right)\right]\Delta p \tag{19}$$

$p_{\Delta SST}$ = Future predicted hurricane central pressure
ΔSST = Increase in sea surface temperature
ε_p = Uncertainty in ΔSST dependent central pressure increases
$\varepsilon_{\Delta SST}$ = Uncertainty in ΔSST predictions

An 8% mean increase in hurricane central pressure is assumed for every +1^{o}C ΔSST.

There is less certainty, and conflicting evidence, concerning the relationship between hurricane frequencies and ΔSST levels. Holland and Webster (2007) examined historical records of tropical cyclones in the north Atlantic; the number of cyclones between 1995 and 2005 is shown to have increased by 50% compared to the number of occurrences between 1931 and 1994. The proportion of tropical cyclones that evolve into hurricanes is shown to remain constant between these two time periods, and likely mirrors the tropical cyclone frequency trend (Holland and Webster 2007). In contrast to these findings, Bender *et al.* (2010) predicts that ΔSST dependent tropical cyclone occurrences over an 80 year period will decrease between 4% and 49%; the projected hurricane occurrences approximate these values. However, the occurrences for hurricanes of Category 3 or higher ranged between decreases of 60% and increases of 40%. A 19% mean decrease in hurricane occurrence rates is predicted for every +1^{o}C ΔSST (Bender *et al.* 2010):

$$\lambda_{\Delta SST} = \lambda_T[1 - (0.19 + \varepsilon_\lambda)(\Delta SST + \varepsilon_{\Delta SST})] \tag{20}$$

$\lambda_{\Delta SST}$ = Future predicted hurricane annual landfall occurrence rate
λ_T = Hurricane annual landfall occurrence rate
ε_λ = Uncertainty in ΔSST dependent occurrence rate changes

2.4.2 Effects of Sea Level Rise on Hurricane Surge

Because hurricane hazard assessments must incorporate SLR projections into the total flood hazard, it is necessary to provide formal definitions for the terms "surge," "SLR," and "total flood elevation." SLR refers to the increase in eustatic MSL before hurricane effects are considered. SLR levels of zero indicate "present day" conditions. Surge is used to measure the water elevation increase due to hurricane effects alone, and is measured relative to MSL. Total flood elevation includes both surge and SLR. A definition sketch of these terms is provided in Figure 2-6.

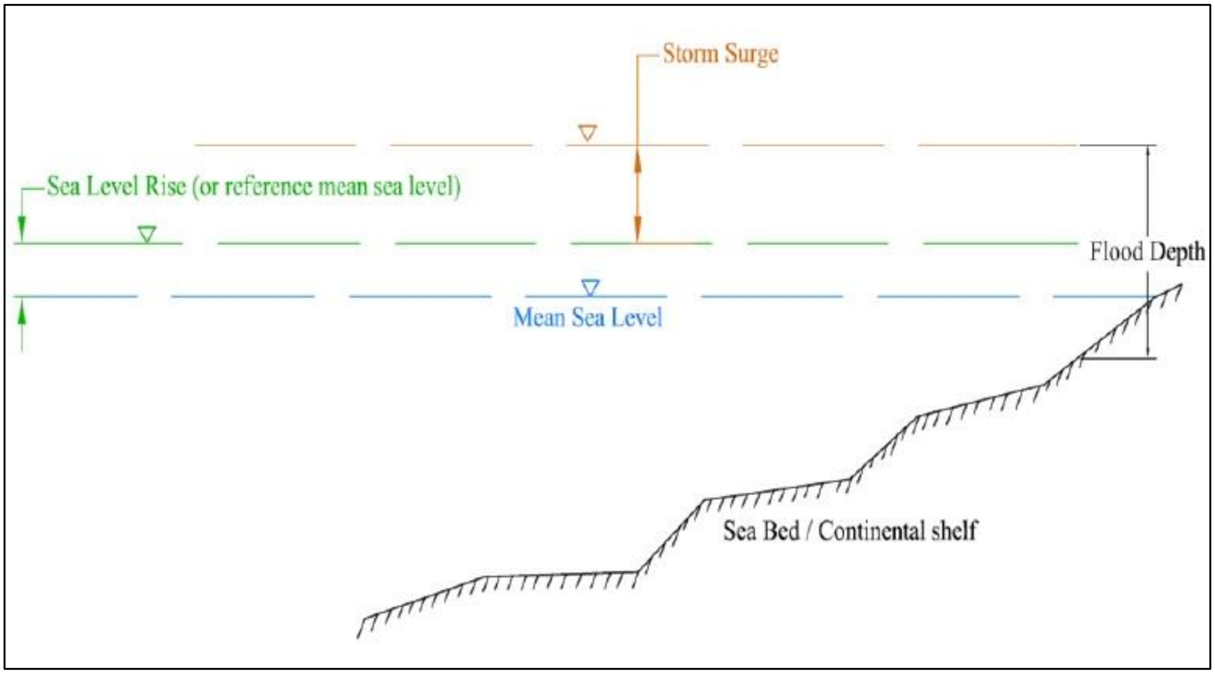

Figure 2-6 Definition sketch of surge, SLR, and total flood elevation (from Udoh 2012).

Rising sea levels alter the shallow water depth and distance, which may increase the likelihood of future flooding, thereby affecting surge generation (*e.g.*, Smith *et al.* 2010, Irish *et al.* 2013). The magnitudes of these SLR induced effects vary substantially for different coastal regions. Generally, SLR effects on hurricane surge are negligible at open coast locations, in areas where SLR does not cause significant changes in coastal topography; supporting evidence of this is provided by Mousavi *et al.* (2011) for Corpus Christi, TX, and Lin *et al.* (2012) for New York City, NY. Other coastal regions, such as open coast locations near New Orleans, experience topographical changes, and considerable surge generation effects, with corresponding SLR increases (*e.g.,* Smith *et al.* 2010). The increases in peak surge generation were hypothesized to be caused by the flooded marshlands becoming a large, shallow extension of the Gulf of Mexico (Smith *et al.* 2010); effectively increasing the shallow water distance available for surge generation.

Significant changes in SLR induced surge response can also be expected within coastal bay interiors. Mousavi *et al.* (2011) investigated the surge response characteristics of Corpus Christi Bay, a shallow bay enclosed by low-elevation barrier islands. Locations inside Corpus Christi Bay, sufficiently spaced from the barrier islands, showed significant reductions in surge generation with respect to SLR increases. It is likely that the bathymetric and geographic features of coastal bays, including inlet geometry and the characteristics of any existing barrier islands, will impact SLR based surge response.

2.*4.3 Section Summary*

This section has introduced the effects of long term, climate driven trends on hurricane surge generation. The relationship between SST increases and average hurricane intensification, quantified in Equation 24, may be used to enact adjustments to regional PDFs for central pressure, for any desired SST projection. Changes in SLR, however, cannot be accounted for through adjustments to hurricane probability distributions; these effects must be quantified in the hydrodynamic and SRF surge models.

2.5. Sources and Quantities of Uncertainty

Assumptions and simplifications in the PDFs that describe hurricane parameters, as well as the hydrodynamic and SRF models that estimate surge, cause uncertainty in return period estimates. The magnitude of these uncertainties can be considerable; confidence bars for return periods in the 50 to 500-year range near New Orleans, LA, show uncertainty contributions on the order of 0.5 m to 1.0 m (Resio *et al.* 2013). It is therefore critical to account for the uncertainty in deterministic return period estimates, in order to avoid under-predicting surge design values.

This section outlines the procedures for quantifying the two separate types of uncertainty, epistemic and aleatory uncertainty, that contribute to the total uncertainty in JPM-OS return period estimates. Emphasis is placed on identifying the type of uncertainty associated with hydrodynamic, SRF, and PDF models, and defining independent sources of uncertainty.

2.5.1 Epistemic Uncertainty

Quantifying uncertainty in hydrodynamic surge and SRF models is based on evaluating the total epistemic uncertainty. This can be estimated as the summation of all independent uncertainty terms, expressed by their variance (*e.g.,* Resio *et al.* 2009):

$$\varepsilon_z^2 = \varepsilon_{tide}^2 + \varepsilon_{model}^2 + \varepsilon_B^2 + \varepsilon_{waves}^2 + \varepsilon_{wind}^2 + \varepsilon_{residual}^2 \tag{21}$$

ε_{tide}	=	Tide model uncertainty
ε_{model}	=	Hydrodynamic and wind model uncertainty
ε_B	=	Uncertainty in Holland (1980) B scaling parameter
ε_{waves}	=	Wave model uncertainty
ε_{wind}	=	Wind model uncertainty
$\varepsilon_{residual}$	=	Residual uncertainties

Epistemic uncertainty can be considerable; the computational models contribute the most to the total uncertainty, especially when PBL generated wind fields are used (Resio *et al.* 2009). Estimates of ε_z for the northern Gulf of Mexico coastline range between 0.70 m (Resio *et al.*

2013) to 1.0 m (Irish and Resio 2013). Contributions to model uncertainty from the additional use of SRFs can be quantified using the RMS error as an estimator.

2.5.2 Aleatory Uncertainty

Hurricane hazard assessments compensate for long term climate trends through statistical, rather than physical, models. To quantify the uncertainty in surge forecasts that incorporate future SST and SLR projections, aleatory uncertainty must also be considered. Irish and Resio (2013) define the aleatory uncertainty in the JPM model as:

$$\varepsilon_a^2 = \varepsilon_0^2 + [\varepsilon_{\Delta SST}^2 + \varepsilon_p^2 + \varepsilon_\lambda^2 + \varepsilon_{SLR}^2] \quad (22)$$

ε_a = Aleatory uncertainty
ε_0 = Present day aleatory uncertainty
ε_{SLR} = SLR uncertainty

Present day aleatory uncertainty results mainly from limited storm sample sizes; this can be estimated by fitting a Gumbel distribution to present day surge values at any location, and estimating the variance as a function of the return period (Gringorten 1963). The additional sources of aleatory error in Equation 22 originate from the statistical relationships between SST, and corresponding changes in central pressure and hurricane landfall occurrence rates.

With the exception of hurricane rates of occurrence, climate contributions to aleatory uncertainty are low. Irish and Resio (2013) compare the sensitivity of estimated surge return periods at 50, 100, and 500 years, to the uncertainty contributions in projected mean SST and SLR conditions. Aleatory uncertainties from mean SST projections contributed no more than 0.02 m to the 50, 100, and 500-year return period estimates, while uncertainties from mean SLR projections contributed less than 0.01 m. Furthermore, uncertainty contributions to surge return period estimates from mean SLR projections will remain low, no more than 0.03 m over the next century, in regions where surge magnitudes scale linearly with SLR (Irish and Resio 2013). It should be noted that these estimates do not consider uncertainty contributions from the mean SST or SLR projections themselves, which can be considerable (Irish and Resio 2013).

2.5.3 Section Summary

This section has defined uncertainty quantification in hurricane hazard assessments, in terms of total standard deviation. Aleatory uncertainty contributions are errors included in the statistical distributions; contributions from climate bases sources are shown to be on the order of 3 cm or lower, in most cases. Contributions to the epistemic uncertainty component include error sources in the surge modeling, such as tides, wind, waves, or aspects of the numerical models themselves. In the Gulf Coast region, epistemic uncertainties range between 0.70 m and 1.0 m; although this remains the largest contributor to net uncertainty, improved numerical surge models are continually being sought to reduce epistemic error magnitudes.

2.6 Research Goals

Surge hazard assessments using JPM-OS coupled with SRFs (*e.g.*, Irish *et al.* 2009, Song *et al.* 2012) have shown high levels of accuracy at open coast regions of the northern Gulf of Mexico coastline. However, SRF development has been restricted to a small number of locations along the open coast of Texas. It will be demonstrated that SRFs are effective when simulated surge data availability is limited to a 90 km alongshore extent. Furthermore, SRF development will be extended to bay interior locations. Finally, a linear model relating SLR to total flood elevations will be proposed. The results of this model will be used to gain physical insight into the implications of SLR on flooding hazards at open coast, and bay interior, locations. Finally, the epistemic uncertainty contributions for these SRF and SLR models will be evaluated, based on the uncertainty estimates provided in Resio *et al.* 2013. By developing SRFs at 1000 m intervals alongshore intervals, a clear idea of the expected accuracy in SRF-based surge predictions can be obtained. Furthermore, large-scale SRF applications, such as the creation of return period based flood inundation maps, will become feasible.

CHAPTER 3

DEVELOPMENT AND UNCERTAINTY QUANTIFICATION OF HURRICANE SURGE RESPONSE FUNCTIONS FOR HAZARD ASSESSMENT IN COASTAL BAYS

Nick R. Taylor, Jennifer L. Irish, Ikpoto E. Udoh, Matthew V. Bilskie, Scott C. Hagen

3.1 Introduction and Background

Hurricanes continue to pose one of the most substantial risks to coastal communities, and the surges caused by these intense storms are a primary source of catastrophic damage. Reliable and robust methods of hurricane surge estimation are critical in reducing the damage that these storms inflict on lives and property. To obtain accurate and robust surge hazard assessments, it is essential that the full range of meteorological hurricane possibilities be considered. In the past, extreme value analysis (EVA) methods applied single distributions to recorded historical surge data (*e.g.,* Yang *et al.* 1970, Fallah *et al.* 1976). After Hurricane Katrina, attempts to improve the accuracy of return period based estimates led to the prevalent use of the Joint Probability Method (JPM) in the United States (*e.g.,* Liu *et al.* 2006, Niedoroda *et al.* 2010). The JPM, which reduces statistical uncertainty in surge data by supplementing historical storms with simulated synthetic storms, is computationally demanding; optimal sampling (OS) techniques are used in conjunction with the JPM to reduce the number of required simulations (JPM-OS). Currently, OS techniques can be categorized into three primary groups; interpolation schemes (Resio *et al.* 2007, Condon and Sheng 2012), quadrature schemes (Toro *et al.* 2010), and surge response function (SRF) schemes (*e.g.,* Resio *et al.* 2009, Irish *et al.* 2009).

Throughout this study, the terms “surge,” “sea-level rise,” and “total flood elevation” will be referred to. Sea-level rise (hereafter SLR) refers to the increase in eustatic mean water elevation (mean sea level, hereafter MSL), before hurricane effects are considered. SLR levels of zero indicate "present day" conditions. Surge is used to measure the water elevation increase due to hurricane effects alone, and is measured relative to MSL. Total flood elevation includes both surge and SLR.

SLR influences on total flood elevation, as well as surge generation, will be classified as either "static" or "dynamic." Static changes in the total flood elevation refer to circumstances where the total flood elevation is well characterized by the summation of SLR and present day surge. In this context, "static" implies that the difference in relative surge levels is zero. Dynamic changes in the total flood elevation refer to circumstances where the total flood elevation is not well characterized by the summation of SLR and present day surge, and the relative difference in surge levels deviates significantly from zero. Because the static situation causes the difference in relative surge levels to be zero, further discussion regarding SLR effects on surge generation refer to dynamic effects, unless explicitly stated otherwise.

This study seeks to incorporate the effects of SLR into the SRF approach, while making the most efficient use of the information from the hydrodynamic surge models. The SRFs, developed initially for open coast locations, will be applied to alongshore bay locations. An approach for integrating SLR into the SRFs will also be introduced, in order to improve the accuracy of total flood elevation predictions at future projected SLR conditions. It will be shown that the dynamic SLR contributions to total flood elevations can be characterized by a simple adjustment model, at locations along the open coast and bay interior. Finally, epistemic uncertainty contributions from the SRF model, and the SLR adjustment, will be presented to demonstrate that these error contributions are small.

3.1.1 Site Description

This study focuses on an 89 kilometer span of coastline in Panama City, FL (Bay County, Figure 3-1). The region has a permanent population of approximately 160,000, as well as a substantial annual tourist population. Most of the region's bathymetry features a continental shelf with gradual alongshore variation; to the west, shore normal distances between the coastline and the 30 m bathymetric contour (L_{30}) range between 14 and 40 km. The rate of continental shelf expansion increases west of Panama City, with L_{30} values increasing from 21 to 66 km.

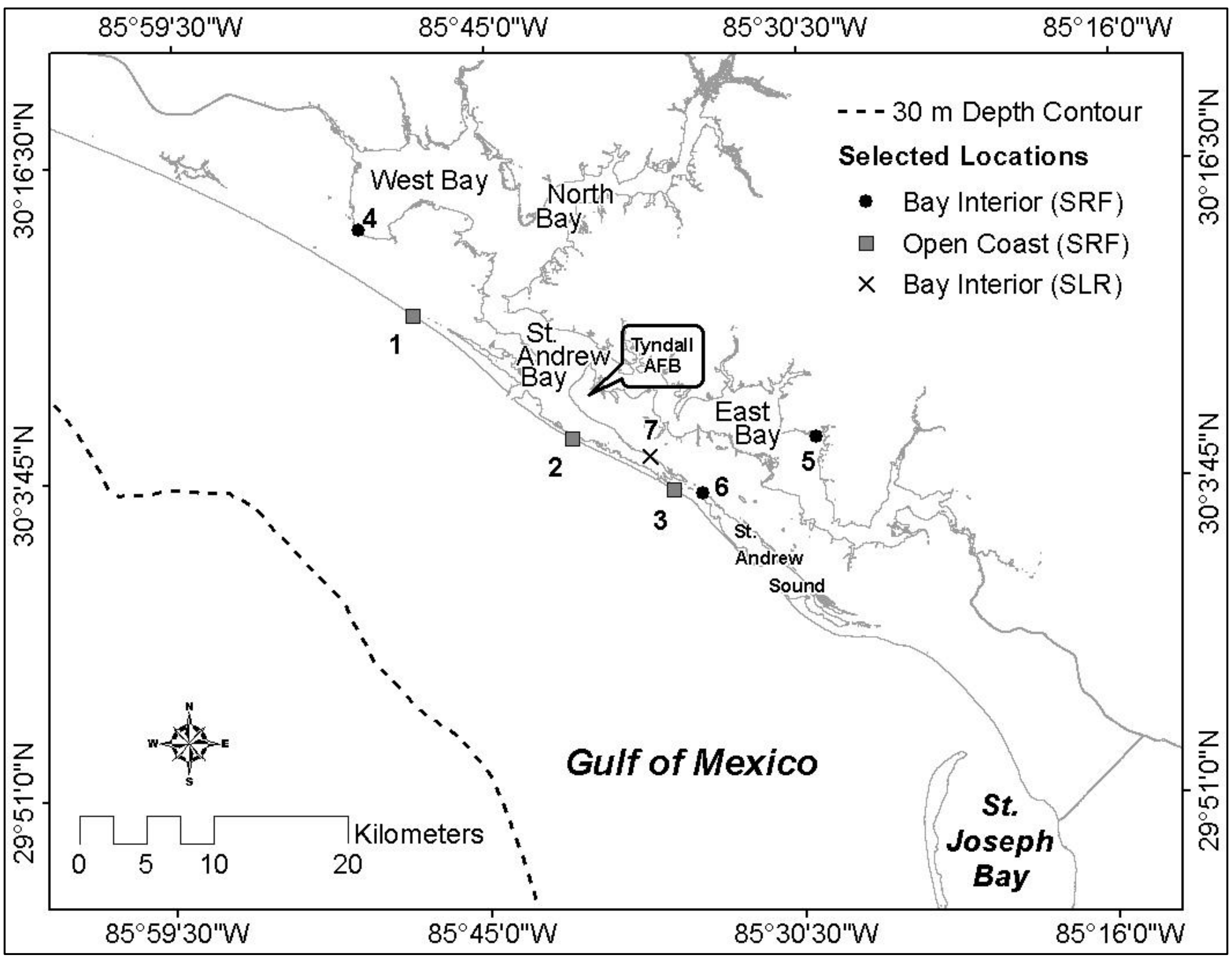

Figure 3-1 Panama City, FL location map.

Panama City's bay is subdivided into four conjoined bodies; West Bay, North Bay, East Bay, and St. Andrew Bay. A chain of barrier islands forms the St. Andrew Sound, an enclosed body of water with a single inlet, as well as the eastern section of St. Andrew Bay. West Bay, North Bay, East Bay, and St. Andrew Sound are shallow bays, with mean depths of 2.55 m, 3.58 m, 3.19 m, and 1.73 m, respectively. The mean depth of St. Andrew Bay is 6.15 m.

3.1.2 Sea Level Rise Trends

Long term climate trends, such as increases in sea surface temperatures (SST) or MSL, introduce nonstationarity into statistical populations. Because surge frequency analyses often focus on return periods in the 50 to 500 year range, accuracy can be significantly improved by accounting for these trends. Long-term SLR is mainly driven by thermal expansion and ice sheet losses, primarily from Greenland and Antarctica (*e.g.*, Rahmstorf 2007, IPCC 2007, Pfeffer *et al.* 2008, Yin *et al.* 2011). Future SLR projections, based on six global emission scenarios, are provided by the Intergovernmental Panel on Climate Change (IPCC 2007). These projected increases, which range from 0.18 m to 0.59 m by the year 2100 for the lowest (B1) and highest (A1FI) respective scenarios, do not include contributions from ice sheet losses (hereafter "cryospheric," IPCC 2007); currently the greatest source of uncertainty in SLR projections (NOAA 2012). Estimates that incorporate cryospheric contributions range from 0.50 m to 1.40 m (Rahmstorf 2007), and from 0.79 m to 2.01 m (Pfeffer *et al.* 2008).

The National Oceanic and Atmospheric Administration (NOAA) presents four recommended SLR projections for the year 2100. The two lower end scenarios are based solely on either observations of historical data, or thermal contributions to SLR (NOAA 2012). Scenarios representing the intermediate-high and highest projections (1.2 m and 2.0 m) consider both thermal expansion and cryospheric sources; the intermediate-high scenario represents an average of multiple semi-empirical based global SLR projections (NOAA 2012). Pfeffer *et al.* (2008) provides the basis for the highest scenario projection.

Rising sea levels can affect surge generation by altering shallow water depths and distances (*e.g.*, Smith *et al.* 2010), as well as land cover (*e.g.*, Irish *et al.* 2013, Bilskie *et al.* 2014), any of which may increase the likelihood of future flooding. Dynamic SLR effects on hurricane surge are generally small at open coast locations, if significant changes in coastal topography do not occur; examples of this are provided in Mousavi *et al.* (2011) for Corpus Christi, TX, and Lin *et al.* (2012) for New York City, NY. Other coastal regions, such as open coast locations near New Orleans, experience considerable differences in surge heights that correspond to coastal wetland losses from encroaching SLR (*e.g.*, Smith *et al.* 2010). These dynamic peak surge effects were caused by the flooded marshlands becoming a large, shallow extension of the Gulf of Mexico (Smith *et al.* 2010); effectively increasing the shallow water distance available for surge generation.

The capacity of SLR to dynamically alter surge generation by affecting coastal land cover changes was reported by Irish *et al.* (2013) for the area near Bay St. Louis, MS. Here, bottom friction changes due to SLR encroachment on protective coastal wetlands has caused significant surge momentum loss reductions. The dynamic SLR effects on surge generation near Bay St. Louis are on the order of 0.5 m to 1.0 m, for surge heights greater than 6.0 m (Irish *et al.* 2013); these effects are comparable to those resulting from the shallow water distance increases observed in Smith *et al.* (2010). Bilskie *et al.* (2014) also examines dynamic SLR effects on surge generation, with respect to changes in land cover and land use (LCLU), for Mississippi Sound and Mobile Bay, AL. When changes in LCLU due to urbanization as well as SLR are considered, dynamic surge effects are confirmed for coastal wetland areas; however, surge effects for many other locations become more static and less dynamic (Bilskie *et al.* 2014).

Significant changes in SLR induced surge response can also be expected within coastal bay interiors (*e.g.*, Mousavi *et al.* 2011, Bilskie *et al.* 2014). Mousavi *et al.* (2011) investigated the surge response characteristics of Corpus Christi Bay, a shallow bay enclosed by low-elevation barrier islands. Locations inside Corpus Christi Bay, sufficiently spaced from the barrier islands, showed significant reductions in surge generation with respect to SLR increases. It is likely that the bathymetric and geographic features of coastal bays, including inlet geometry and the characteristics of any existing barrier islands, will impact SLR based surge response.

3.1.3 Surge Response Functions

SRFs are physics-based algebraic expressions of hurricane surge; once developed, these equations can replace the expensive computational models associated with traditional JPM applications. Irish and Resio (2013) define the JPM, in terms of return period, as a continuous probability density function (PDF) of storm parameters:

$$T_Z = \left\{1 - \int_{c_p}\int_{R_p}\int_{v_f}\int_{\theta}\int_{x_0} f\left(c_p, R_p, v_f, \theta, x_0\right) H\left(Z - \left[\phi\left(x, c_p, R_p, v_f, \theta, x_0, MSL\right) + \varepsilon_z\right]\right) dx_0\, d\theta\, dv_f\, dR_p\, dc_p\right\}^{-1} \tag{1}$$

Z	=	Total maximum flood elevation
T_Z	=	Total maximum flood elevation return period
x	=	Location of interest
ϕ	=	SRF model term
c_p	=	Hurricane central pressure
R_p	=	Hurricane radius of maximum winds
v_f	=	Hurricane forward velocity
θ	=	Hurricane track angle
x_0	=	Hurricane landfall position
MSL	=	Mean sea level

The Heaviside function (H) in Equation 1 represents the nonexceedance limit, where $H(x) = 1$ when $x \geq 0$, and $H(x) = 0$ otherwise.

SRFs are developed using dimensionless surge scaling terms, which are derived from the shallow water momentum equations. Song *et al.* (2012) developed the following SRF model, which incorporates both hurricane central pressure (hereafter intensity), storm size, and L_{30} influences into the dimensionless alongshore surge response, for open coast application:

$$x' = \frac{x-x_0}{R_p} - \lambda(x_0) + cH\left(\frac{x-x_0}{R_p} - \lambda(x_0) - 1\right) H\left(\frac{L_{30}}{L_{30-ref}} - 1\right)\left(\frac{R_p}{L_{30}}\right) - F\left(1 - \frac{R_p}{R_{thres}}\right) H\left(1 - \frac{R_p}{R_{thres}}\right) \tag{2a}$$

$$\zeta' = \frac{\gamma_0 \zeta}{\Delta p} + m_2(x,x')\left(\frac{\Delta p}{\Delta p_{max}}\right)^{\alpha(x,x')} \left(\frac{R_p/L_{30}(x_0)}{\left[R_p/L_{30}\right]_{ref}}\right)^{\beta(x,x')} \tag{2b}$$

$$F\left(1 - \frac{R_p}{R_{thres}}\right) = \begin{cases} a_1\left(1 - \frac{R_p}{R_{thres}}\right) + b_1 & for \quad -\lambda \le x' \le 0 \\ a_2\left(1 - \frac{R_p}{R_{thres}}\right) + b_2 & for \quad 0 < x' \le \lambda \\ 0 & for \quad \lambda < |x'| \end{cases} \tag{2c}$$

$$[m_2(x,x'), \alpha(x,x'), \beta(x,x')] = \begin{cases} [m_{2L}(x), \alpha_L(x), \beta_L(x)] & for\ x' < 0 \\ [m_{2R}(x), \alpha_R(x), \beta_R(x)] & for\ x' \ge 0 \end{cases} \tag{2d}$$

x'	=	Dimensionless alongshore parameter
ζ'	=	Dimensionless surge parameter
ζ	=	Peak surge elevation
$\lambda(x_0)$	=	Ratio between relative maximum peak surge location and R_p
c	=	Dimensionless regional scaling constant
L_{30}	=	Cross shore distance from shoreline to 30 m bathymetric contour, at x_0
L_{30-ref}	=	Threshold value of L_{30}
R_{thres}	=	Threshold value of R_p
a_1, a_2, b_1, b_2	=	Dimensionless scaling coefficients
m_2, α, β	=	Dimensionless scaling coefficients
Δp	=	Ambient pressure and hurricane central pressure difference
Δp_{max}	=	Maximum theoretical hurricane intensity (Tonkin *et al.* 2000)
$\left[R_p/L_{30}\right]_{ref}$	=	Maximum value of R_p/L_{30}
γ_0	=	Reference specific weight of water

This model was developed using hydrodynamic surge simulations for the entire Texas coast. In addition to influencing surge magnitudes, the relative storm size (R_p/L_{30}) also affects the degree of asymmetry in alongshore surge distributions west and east of a storm's landfall position (Song *et al.* 2012). The coefficients α and β are weighting parameters with values ranging between zero and one, and indicate the relative influence of hurricane intensity and size on dimensionless surge. Song *et al.* (2012) reported negligible bias, and a maximum root mean square (RMS) error of 0.22 m, when applying this form of the SRF model to the Texas open coast; significantly lower than the ADCIRC standard deviation of 0.37 m, as reported by Westerink *et al.* 2008.

3.1.4 Epistemic Uncertainty

Epistemic uncertainty is inherent in JPM population inputs created using hydrodynamic models and OS techniques. This uncertainty can be quantified by the standard deviation between actual and estimated flood elevations (*e.g.,* Resio *et al.* 2009, Resio *et al.* 2013, Irish and Resio 2013), and is assumed to be normally distributed:

$$\varepsilon_z^2 = \varepsilon_{tide}^2 + \varepsilon_{waves}^2 + \varepsilon_{winds}^2 + \varepsilon_{model}^2 + \varepsilon_{residual}^2 \qquad (3)$$

ε_z	=	Epistemic uncertainty
ε_{tide}	=	Tide model uncertainty
ε_{model}	=	Hydrodynamic and wind model uncertainty
ε_{waves}	=	Wave model uncertainty
ε_{wind}	=	Wind model uncertainty
$\varepsilon_{residual}$	=	Residual uncertainty

In JPM-OS sampling methods using the SRF approach, the model term in Equation 3 represents the sum of variances for both the hydrodynamic and SRF models. The residual term accounts for additional random modeling errors. Uncertainty estimates within the Gulf of Mexico region, before SRF contributions are considered, range between 0.70 m (Resio *et al.* 2013) and 1.0 m (Irish and Resio 2013).

3.2 Methods

3.2.1 ADCIRC Simulations

Hurricane simulations in the Bay County, FL area were computed using the two-dimensional, depth-integrated shallow water hydrodynamic model ADCIRC (Westerink *et al.* 2008) coupled with the SWAN wave model (Booij *et al.* 1999) to account for wave setup. The model employed the numerical grid used to produce Federal Emergency Management Agency (FEMA) digital flood insurance rate maps for the Florida panhandle and Alabama coastal region (University of Central Florida 2011), with coastline and bay interior resolution between 20 m and 100 m. A nested hurricane vortex, planetary boundary layer (PBL) model (Thompson and Cardone 1996), with enhanced resolution over the northern Gulf of Mexico, was used to develop the wind and barometric pressure field inputs. Values for storm position, size, and central pressure were specified in 1-h intervals, and pressure and wind velocity fields were calculated in 15 minute increments.

Surge simulations for 38 unique hurricane parameter combinations were carried out and analyzed to develop the SRFs, as a subset taken from those used in the recent FEMA study (University of Central Florida 2011). Landfall positions were chosen based on initial x' estimates (Equation 2a, term 1), for values between -6.7 (west) and 3.0 (east); the remaining parameter ranges are summarized in Table 3-1. Parameter combinations for the 38 simulations were chosen so that sufficient variability would be present in the simulated surge data.

A second subset of seven storms was selected to evaluate the relationship between total flood elevation and SLR. Changes in sea level were modeled by statically increasing the water surface elevation throughout the computational domain. To simplify the analysis, localized differences in water surface elevation, sediment transport induced coastline changes, barrier island degradation, LCLU changes, and other topographic adjustments, were not considered. Each storm was simulated at SLR conditions of 0.0 m, 1.2 m, and 2.0 m, relative to MSL c. 2005.

Table 3-1 Parameter values for SRF hurricane simulations.

Parameter	Minimum	Maximum
Δp	41 mb	105 mb
R_p	15 km	99 km
v_f	2.6 m/s	9.7 m/s
θ	-61°	+73°

3.2.2 SRF Development

SRFs were developed for 73 open coast locations, and 259 locations along the bay shoreline, following Song *et al.* (2012). The spacing between locations selected for SRF model development ranged between 0.5 km and 1.5 km in the alongshore direction. A single term exponential or power distribution was applied to the dimensionless surge data (Equation 2), in order to develop the best-fit algebraic model for each location. Values of L_{30}, at corresponding landfall locations, were interpolated from measurements taken at alongshore intervals of 30 km.

3.2.3 Uncertainty Quantification

Epistemic uncertainties introduced by the SRF and SLR models were quantified using RMS errors as estimates of standard deviation. Total epistemic uncertainties were estimated by incorporating these SRF and SLR uncertainty terms into Equation 3, where we assume the smaller total uncertainty estimate of 0.70 m from tide, wave, wind, computational model, and residual sources (Resio *et al.* 2013).

$$\varepsilon_z^2 = \varepsilon_{tide}^2 + \varepsilon_{waves}^2 + \varepsilon_{winds}^2 + \varepsilon_{model}^2 + \varepsilon_{SRF}^2 + \varepsilon_{SLR}^2 + \varepsilon_{residual}^2 \quad (4)$$

ε_{SRF} = SRF model uncertainty
ε_{SLR} = SLR model uncertainty

3.3 Results and Discussion

3.3.1 SRF Development at Open Coast Locations

Because of the region's bathymetry, which features gradual changes in L_{30}, the coefficient c in Equation 2a was determined to be zero. This indicates that the correction term for asymmetry in alongshore surge distributions, caused by changes in L_{30} values (Song *et al.* 2012), is not required for this area. A 30 km R_{thres} value was applied to Equation 2a, and was selected based on an inspection of the data.

Simulated surge data available for this study encompassed an alongshore distance of 98 km, and did not include the alongshore maximum peak surge for most of the simulated hurricanes; therefore, an alternative to the Song *et al.* (2012) method of approximating λ was required. Initial SRF estimates were obtained using the following initial estimates of the dimensionless SRF:

$$x' = \frac{x - x_0}{R_p} \tag{5a}$$

$$\zeta' = \frac{\gamma_0 \zeta}{\Delta p} \tag{5b}$$

Values of λ were calculated as the deviation of the initial SRF's maximum value location from the dimensionless coordinate origin. Using this method, expected values of λ, ranging from 0.7 to 1.3, are obtained.

SRFs are presented in Figure 2, for selected open coast locations. The selected locations include the alongshore reference location for bay interior SRFs, as well as locations near Panama City Beach and Tyndall Air Force Base (AFB). Locations near Panama City Beach and the bay reference point were selected for their geographic importance, and are representative of open coast SRF performance. The location near Tyndall AFB was selected to examine worst-case model performance. A summary of R^2, RMS error, and bias values at the selected open coast locations is provided in Table 3-2.

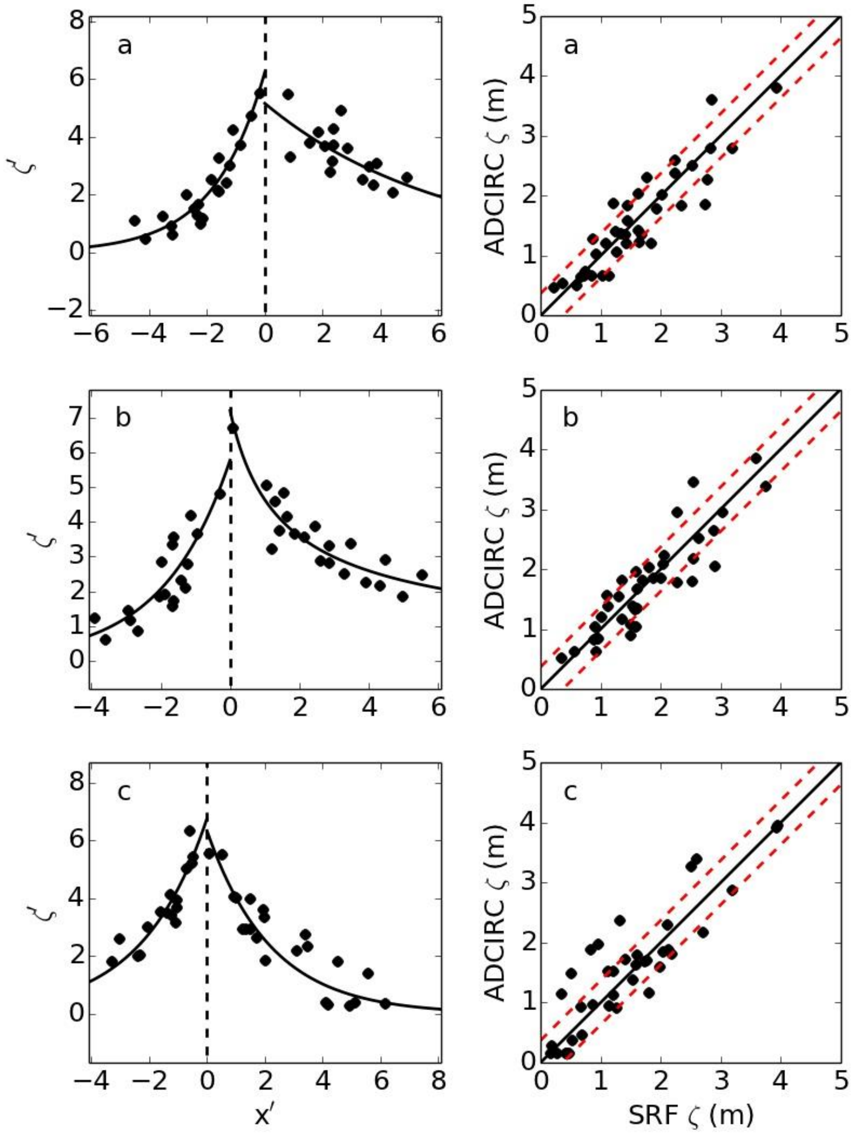

Figure 3-2 Surge response functions (left) and ADCIRC-simulated versus SRF-predicted peak surge (right), with ±0.37 m deviations (from Westerink *et al.* 2008) about an exact match, for selected open coast locations 1 (a, Panama City Beach), 2 (b, bay reference location), and 3 (c, Tyndall Air Force Base). Locations 1 and 2 are representative of model performance at open coast locations. Location 3 represents the worst-case model performance.

RMS errors were below 0.40 m at 93%, and below 0.30 m at 23%, of the 73 open coast locations. Respective mean, minimum, and maximum RMS errors were 0.35 m, 0.25 m, and 0.47 m. The Panama City open coast mean, minimum, and maximum bias values were -0.01 m, -0.10 m, and +0.03 m. RMS errors for the 73 open coast locations are higher than those reported in Song *et al.* (2012). A source of large alongshore RMS errors in this study, relative to those presented in Song *et al.* (2012), is the approximation of λ values at each SRF location.

Table 3-2 Performance statistics of SRF models at selected open coast (top) and bay interior (bottom) locations.

Station	R^2	RMS error (m)	Bias (m)
1	0.83	0.35	+0.02
2	0.80	0.37	+0.03
3	0.80	0.47	-0.10
4	0.76	0.38	+0.03
5	0.74	0.31	+0.01
6	0.67	0.61	+0.02

3.3.2 SRF Development at Bay Interior Locations

Since the initial x' given in Equation 5a represents the offset between peak open coast surge and landfall position, an adjustment for x is required in order to apply Equation 2a at bay interior locations. An alongshore reference value for x was selected by optimizing the performance of Equation 2 for all 259 bay interior locations. The selected reference point corresponded to an alongshore distance of approximately half of the bay width (Figure 3-1). Values of λ in Equation 2a were approximated for each bay interior station using the same methods described for open coast locations. The λ value at the reference location was used for the small storm adjustments in Equation 2c. SRF performance was quantified by evaluating R^2, bias, and RMS error.

SRF models at bay interior locations, selected from the West Bay, East Bay, and St. Andrew Sound, are shown in Figure 3-3. Locations inside the West Bay and East Bay were chosen to evaluate SRF performance at different bay interior regions, are representative of bay interior SRF performance. The St. Andrew Sound location was selected to examine worst-case model performance. A summary of R^2, RMS error, and bias at the selected bay interior locations

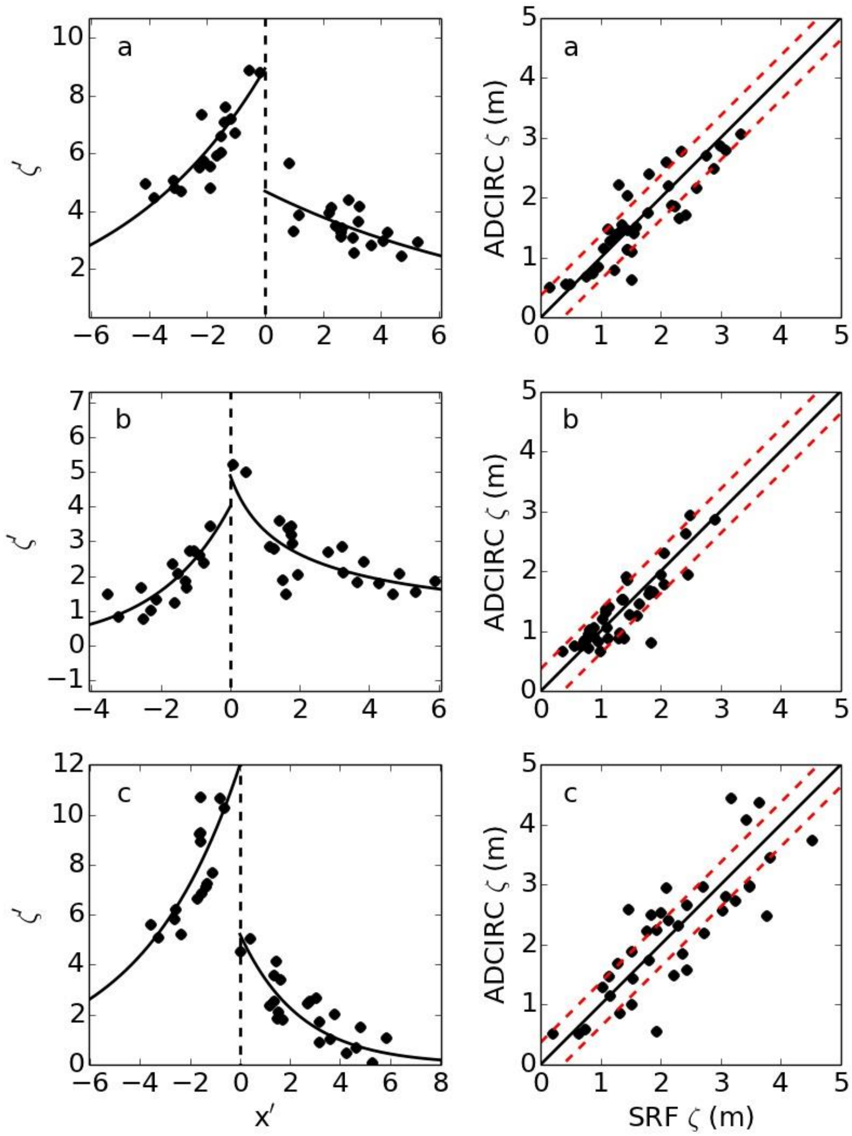

Figure 3-3 Surge response functions (left) and ADCIRC-simulated versus SRF-predicted peak surge (right), with ±0.37 m deviations (from Westerink *et al.* 2008) about an exact match, for selected bay interior locations 4 (a, West Bay), 5 (b, East Bay), and 6 (c, St. Andrew Sound). Locations 4 and 5 are representative of model performance at bay interior locations. Location 6 represents the worst-case model performance.

are summarized in Table 3-2.

RMS errors were below 0.50 m at 96%, below 0.40 m at 76%, and below 0.30 m at 3% of the 259 bay interior locations. Mean, minimum, and maximum RMS errors were 0.39 m, 0.29 m, and 0.61 m, respectively. Bay interior mean, minimum, and maximum biases for all locations were -0.01 m, -0.12 m, and +0.05 m.

3.3.3 Surge Adjustments for SLR

Figure 3-4 shows the total inundated areas for one ADCIRC simulated hurricane at present day, 1.2 m, and 2.0 m of SLR, for the Panama City region. Under present day conditions, the barrier islands remain dry at most locations; this substantially limits floodwater access to bay interior locations. At 1.2 m SLR conditions, barrier island protection is substantially reduced, and floodwater access to bay interior locations within St. Andrew Bay and St. Andrew Sound is largely unhindered. Additional increases in SLR result in further barrier island inundation; however, these increases become less significant under SLR conditions of 2.0 m. The ADCIRC simulations conducted here to evaluate dynamic SLR impacts on surge generation did not account for potential morphological changes such as barrier island break-up or roll-over. Incorporation of these changes can potentially impact surge levels (*e.g.*, Woodruff *et al.* 2013, Bilskie *et al.* 2014).

For all storms simulated, inundation of barrier islands under large SLR has a greater effect on nearby bay interior regions. Under present day conditions, hurricane surge in St. Andrew Bay is considerably less than surge magnitudes along the open coast. The difference in surge levels between bay location 7 and open coast location 3, under present day conditions, ranges from 0.25 m to 0.98 m. With SLR, barrier island overtopping causes flood levels in the easternmost sections of St. Andrew Bay to merge with the Gulf Coast flood levels. Surge

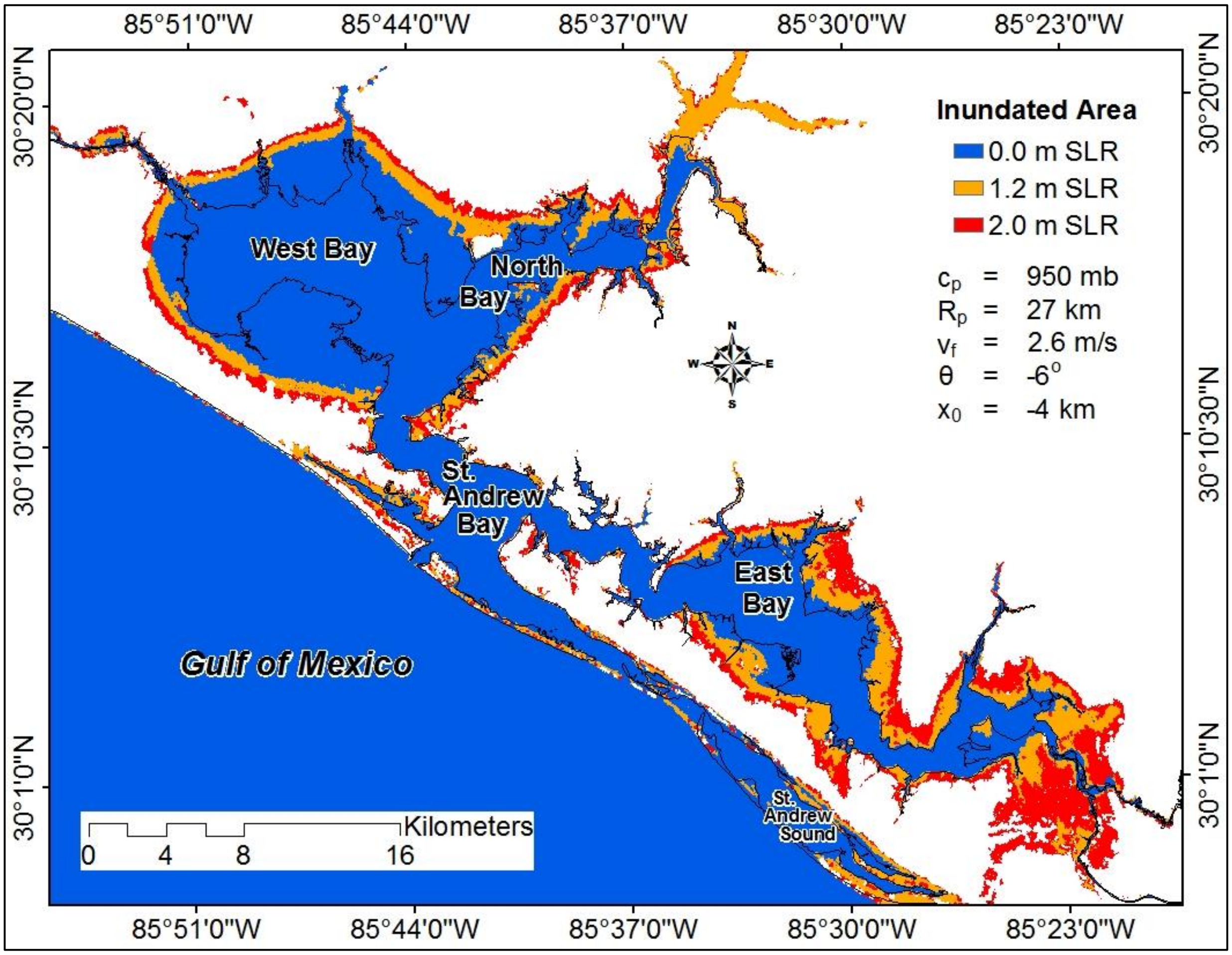

Figure 3-4 Total inundated areas for selected ADCIRC simulated hurricane at present day, 1.2 m, and 2.0 m of SLR.

differences between these locations (relative to open coast location 3) under 1.2 m and 2.0 m of projected SLR, fall to respective ranges of -0.06 m to +0.42 m, and -0.09 m to +0.19 m. Rising sea levels cause surge magnitudes within east St. Andrew Bay to approach open coast values, as encroaching SLR reduces the separation between the bay interior and the Gulf Coast.

Significant reductions in surge generation occur with increasing SLR conditions in the western sections of St. Andrew Sound. In contrast to most other bay interior regions, St. Andrew Sound experiences higher surge generation at present day MSL, relative to open coast locations. With increasing SLR, surge magnitudes within the sound approach those at open coast locations.

Compared to present day conditions, this results in an overall decrease in surge generation. St. Andrew Sound represents a small portion of Panama City's total bay area; furthermore, this effect is confined to the western portion of the sound. Despite this localized decrease in surge, the data shown here provides evidence of a significant increase in the total flooding hazard, inclusive of SLR and surge changes.

Surge trends with SLR were evaluated and quantified at each open coast and bay interior location by examining the simulated surge data. The summation of present day flood elevations (Z_0) and SLR ($Z_0 + SLR$) was compared to the ADCIRC simulated total flood elevations under corresponding SLR conditions. The data exhibited the following trend:

$$Z_{SLR} = k(Z_0 + SLR) + l \tag{6}$$

Z_{SLR}	=	Total flood elevation at projected SLR, relative to present day MSL
Z_0	=	Present day total flood elevation
k, l	=	Location-dependent fit coefficients
SLR	=	SLR, relative to present day conditions

Performance of Equation 6 was quantified by evaluating the R^2, bias, and RMS error. A value of k =1 suggests that the influence of SLR on surge generation is small, and that the total flood elevation can be approximated as the summation of SLR and present day flood elevation.

The summation of present day flood elevation and SLR was compared to total simulated flood elevations under corresponding SLR conditions, at selected open coast (Figure 3-5) and bay interior (Figure 3-6) locations. An additional location in the eastern section of St. Andrew Bay, where SLR effects on surge generation are significant, was also evaluated. The mean, minimum, and maximum RMS errors for all open coast locations were 0.03 m, 0.02 m, and 0.16 m, respectively. Among the bay interior locations, the respective mean, minimum, and maximum RMS errors were 0.10 m, 0.02 m, and 0.36 m. Bias was negligible (< 0.005 m) for all open coast and bay interior locations. The slope (k) for the Panama City region, shown in Figure 3-7, varies from 0.83 to 1.15.

The open coast trends shown in Figure 3-5 display slope (k) terms as low as 0.95 near the barrier islands, indicating that total flood elevations for many Panama City open coast locations cannot be approximated as static SLR increases. West Bay locations (Figure 3-6) also show evidence of dynamic effects with similar magnitudes. Substantially high SLR effects on surge are indicated by k values of 1.15 for the St. Andrew Bay location, and 0.85 for the St. Andrew Sound location. Figures 3-5 and 3-6 also provide evidence of highly correlated trends between SLR and total flood elevations, for both open coast and bay interior locations.

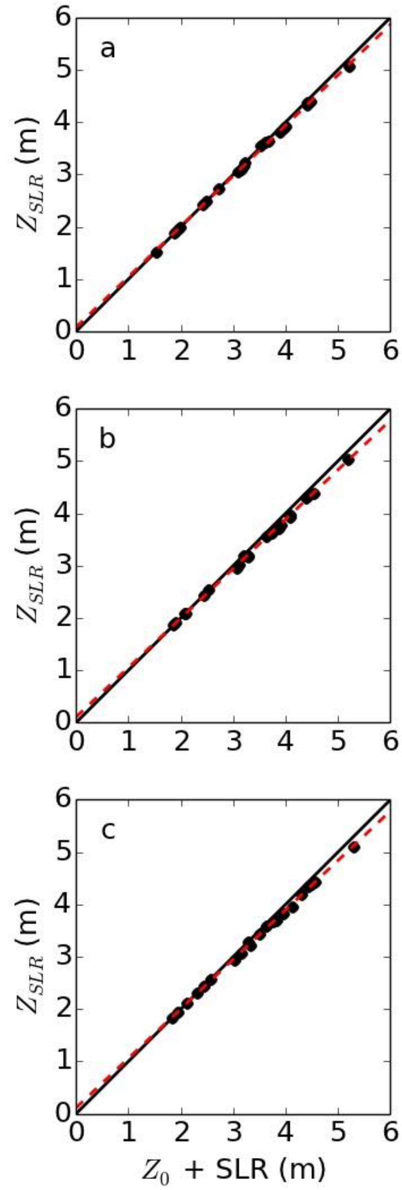

Figure 3-5 Total flood elevation trends at selected open coast locations 1 (a, Panama City Beach), 2 (b, bay reference location), and 3 (c, Tyndall Air Force Base).

The spatial distribution of k, as shown in Figure 3-7, is determined primarily by the geometry of coastline or bay interior features. Along the open coast, values of k decrease at locations close to the shoreline; these changes occur in a predominately alongshore direction. It can be observed, however, that the rate of decrease is not consistent for the entire area. Decreases in k occur more gradually for open coast locations in the west,

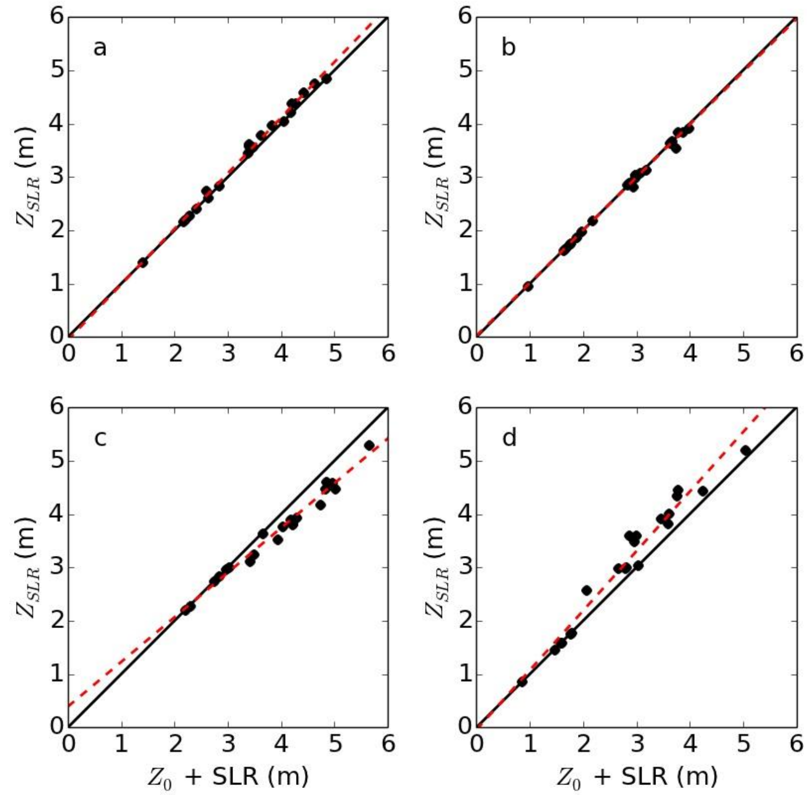

Figure 3-6 Total flood elevation trends at selected bay interior locations 4 (a, West Bay), 5 (b, East Bay), 6 (c, St. Andrew Sound), and 7 (d, St. Andrew Bay).

while eastern locations show slightly accelerated *k* value decreases.

Within the bay interior, spatial distributions of *k* show trends that change with different bay geometries. In the West Bay, which has a comparatively large width relative to its length, *k* gradients are directed predominately to the northwest. St. Andrew Bay, which has outlets to the North Bay and East Bay, displays gradients in *k* that are directed towards these outlets. North Bay, East Bay, and St. Andrew Sound, which have much longer lengths relative to their widths, feature well defined *k* gradients that are directed along their lengths.

SLR effects on surge generation within the bay interior undergo a transition from amplification in western areas, to deamplification towards the east. Values of *k* at bay interior locations are above 1.00 for West Bay, St. Andrew Bay, and most of North Bay; this indicates

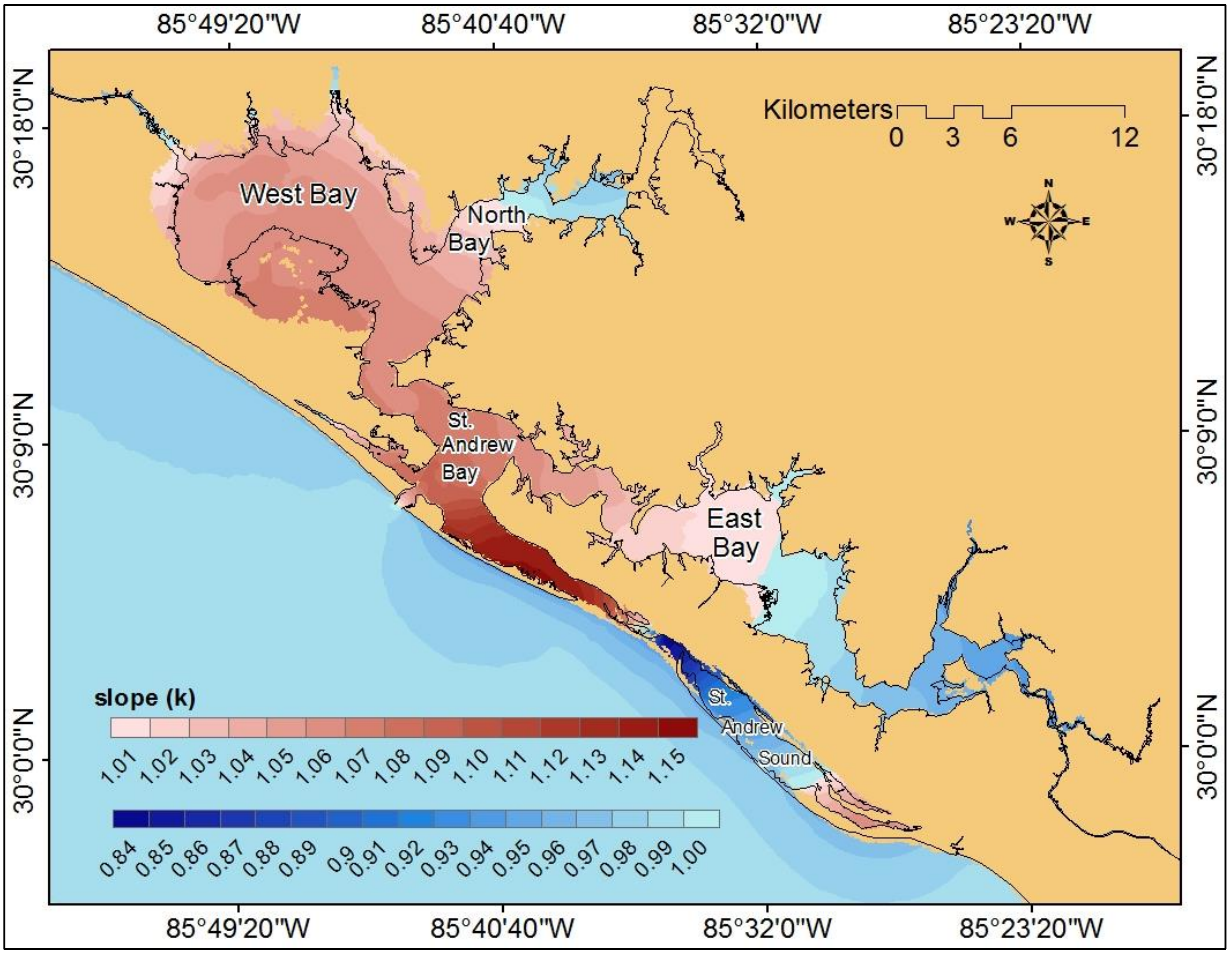

Figure 3-7 Dynamic sea level rise trends for the Panama City region (*k* coefficient from Equation 6).

surge amplification with increasing SLR. Transitions to surge deamplification, with *k* values below 1.00, occur in North Bay and East Bay locations. This effect is most pronounced in East Bay, where *k* is as low as 0.94. The overall transition between amplification and deamplification corresponds with the shift from relatively steep elevation gradients in western Bay County areas, to milder gradients in eastern Bay County (Figure 3-7). The existence of milder elevation gradients will likely result in surge deamplification, at the cost of greater overland inundation extent, as SLR increases.

3.3.4 SRF and SLR Model Contributions to Epistemic Uncertainty

Total epistemic uncertainty values, including SRF and SLR contributions, as well as the initial uncertainty value of 0.70 m, are provided in Table 3 for selected open coast locations and bay interior locations. Mean, minimum, and maximum SRF uncertainty contributions among all open coast locations were 0.08 m, 0.04 m, and 0.14 m, respectively. The mean, minimum, and maximum SRF uncertainty contributions among all bay interior locations were 0.10 m, 0.06 m, and 0.22 m. Mean SLR uncertainty contributions among all open coast and bay interior locations were negligible.

The initial uncertainty value of 0.70 m was selected to examine SRF and SLR error contributions to represent the worst-case. Thus, the relative influence of uncertainty added by the SRF and SLR models will decrease when considering the larger base value of 1.0 m. In summary, we have demonstrated that the SRF and SLR models developed for Panama City, FL marginally increase mean epistemic uncertainties by 0.08 m for open coast locations, and 0.10 m for bay interior locations.

Table 3-3 Total epistemic uncertainty, SRF model uncertainty, and SLR model uncertainty at selected open coast (top) and bay interior (bottom) locations. Values are based on an initial uncertainty estimate of 0.70 m.

Loc.	ε_{new} (m)	ε_{SRF} (m)	ε_{SLR} (m)	% Total Increase
1	0.78	0.08	< 0.01	10
2	0.79	0.09	< 0.01	12
3	0.84	0.14	< 0.01	17
4	0.80	0.10	<0.01	12
5	0.77	0.07	<0.01	9
6	0.93	0.22	0.01	25
7	0.90	0.16	0.03	22

3.4 Conclusions

By extending the SRF approach described in Song *et al.* (2012) to bay interior locations, an expression for estimating extreme surge values has been developed for Panama City, FL. These SRFs incorporate the primary statistical parameters associated with hurricane hazard assessments; central pressure, radius, and landfall location. An adjustment model incorporating dynamic SLR effects into total flood elevation estimates has also been proposed for open coast and bay interior locations. The Panama City SRFs showed RMS error values that were somewhat higher than those reported by Song *et al.* (2012); we hypothesize that the approximation for λ likely contributes to this additional error. Nonetheless, it has been demonstrated that the additional uncertainty from the SRF and SLR models presented in this study is reasonable for application in hazard analysis, and the approximate method used to determine λ makes the SRF approach more universally applicable when applied to datasets of limited spatial extent.

In this study, flood elevation adjustment accuracies were limited due to the absence of SLR induced topographic changes (*e.g.,* barrier island degradation, shoreline morphology, etc.) in the ADCIRC hydrodynamic simulations. Land cover changes have been shown to alter surge generation near coastal wetlands (*e.g.,* Smith *et al.* 2010, Irish *et al.* 2013); however, land cover effects on surge levels can range between +80% and -100% over an entire region (Bilskie *et al.* 2014). Changes in land use due to urbanization can potentially increase surge generation by up to +70% (Bilskie *et al.* 2014). Therefore, future research is recommended that incorporates SLR induced topographic and land cover changes, as well as land use changes from urbanization projections, into the SLR adjustments.

Dynamic SLR effects on surge generation are significant for the Panama City area, and cause total flood elevations to be poorly characterized as static SLR increases. These dynamic effects are greatly influenced by characteristics such as topographic gradients, coastline geometry, and other regional geographic features, and will vary significantly depending on coastal location (*e.g.*, Hagen and Bacopoulos 2012, Bilskie *et al.* 2014). Therefore, it is necessary to study the physical surge dynamics using computational models, for each unique coastal region, to inform SRF and SLR development.

JPM applications coupled with the SRF, and linear SLR adjustments, presented here can be used to provide accurate hazard assessments for decisions requiring return periods in the 50 to 500-year range, or greater, on a regional scale. By extending model development to bays, the geographic restrictions limiting JPM-OS applications coupled with SRFs to open coast locations have been removed. Furthermore, the high resolution coastline and bay shoreline at which SRFs were developed can be used by coastal planners and developers to create flood inundation maps, damage assessments, and other applications useful for surge hazard mitigation.

Acknowledgements

This material is based on the work supported by the National Sea Grant College Program of the U.S. Department of Commerce's National Oceanic and Atmospheric Administration (Grant No. NA10OAR4170099. The views expressed here do not necessarily reflect the views of this organization. The authors wish to thank Dr. James M. Kaihatu, and Patrick W. McLaughlin, for their contributions to this work.

References

Bilskie, M. V., Hagen, S. C., Medeiros, S. C., Passeri, D. L. (2014). Dynamics of sea level rise and coastal flooding on a changing landscape. *Geophys Res Lett*. **41**, 927-934.

Booij, N., Ris, R. C., Holthuijsen, L. H., (1999). A third-generation wave model for coastal regions: 1. Model description and validation. *J Geophys Res*. **104**(C4), 7649-7666.

Condon, A. J., Sheng, Y. P. (2012). Optimal storm generation for evaluation of the storm surge inundation threat. *Ocean Eng*. **43**, 13-22.

Fallah, M. H., Sharma, J. N., Yang, C. Y. (1976). Simulation model for storm surge probabilities. *Coastal Engineering Proceedings*. **1**(15).

Hagen, S. C., Bacopoulos, P. (2012). Coastal flooding in Florida's big bend region with application to sea level rise based on synthetic storm analysis. *Terr Atmos Ocean Sci*. **23**(5), 481-500.

Holland, G. J. (1980). An analytic model of the wind and pressure profiles in hurricanes. *Mon Weather Rev*. **108**(8), 1212-1218.

Irish, J. L., Sleath, A., Cialone, M. A., Knutson, T. R., Jensen, R. E. (2013). Simulations of Hurricane Katrina (2005) under sea level and climate conditions for 1900. *Climatic Change*. 1-15.

Irish, J. L., Resio, D. T. (2013). Method for Estimating Future Hurricane Flood Probabilities and Associated Uncertainty. *J Waterw Port C-ASCE*. **139**(2), 126-134.

Irish, J. L., Resio, D. T. (2010). A hydrodynamics-based surge scale for hurricanes. *Ocean Eng*. **37**(1), 69-81.

Irish, J. L., Resio, D. T., Cialone, M. A. (2009). A surge response function approach to coastal hazard assessment. Part 2: Quantification of spatial attributes of response functions. *Nat Hazards*. **51**(1), 183-205.

Lin, N., Emanuel, K., Oppenheimer, M., Vanmarcke, E. (2012). Physically based assessment of hurricane surge threat under climate change. *Nature Clim Change.* **2**(6), 462-467.

Liu, D., Pang, L., Fu, G., Shi, H., Fan, W. (2006). Joint probability analysis of hurricane Katrina 2005, vol 3. In: Proceeding of international offshore and polar engineering conference, San Francisco, USA, pp 74-80.

Mousavi, M. E., Irish, J. L., Frey, A. E., Olivera, F., Edge, B. L. (2011). Global warming and hurricanes: the potential impact of hurricane intensification and sea level rise on coastal flooding. *Climatic Change*. **104**(3-4), 575-597.

Niedoroda, A. W., Resio, D. T., Toro, G. R., Divoky, D., Das, H. S., Reed, C. W. (2010). Analysis of the coastal Mississippi storm surge hazard. *Ocean Eng.* **37**(1), 82-90.

Parris, A., *et al.* (2012). Global sea level rise scenarios for the United States National Climate Assessment. *NOAA Technical Report OAR CPO-1*. National Oceanic and Atmospheric Administration. Silver Spring, MD.

Pfeffer, W. T., Harper, J. T., O'Neel, S. (2008). Kinematic constraints on glacier contributions to 21st-century sea-level rise. *Science.* **321**(5894), 1340-1343.

Rahmstorf, S. (2007). A semi-empirical approach to projecting future sea-level rise. *Science.* **315**(5810), 368-370.

Resio, D. T., Irish, J. L., Westerink, J. J., Powell, N. J. (2013). The effect of uncertainty on estimates of hurricane surge hazards. *Nat Hazards*. **66**(3), 1443-1459.

Resio, D. T., Irish, J., Cialone, M. (2009). A surge response function approach to coastal hazard assessment–part 1: basic concepts. *Nat Hazards*. **51**(1), 163-182.

Resio, D. T., Boc, S. J., Borgman, L., Cardone, V., Cox, A., Dally, W. R., *et al.* (2007). White paper on estimating hurricane inundation probabilities. *US Army Corps of Engineers Engineer Research and Development Center*. Vicksburg, MS.

Simpson, R. H., Saffir, H. (1974). The hurricane disaster potential scale. *Weatherwise*. **27**(8), 169.

Smith, J. M., Cialone, M. A., Wamsley, T. V., McAlpin, T. O. (2010). Potential impact of sea level rise on coastal surges in southeast Louisiana. *Ocean Eng*. **37**(1), 37-47.

Song, Y. K., Irish, J. L., Udoh, I. E. (2012). Regional attributes of hurricane surge response functions for hazard assessment. *Nat Hazards*. **64**(2), 1475-1490.

Thompson, E. F., Cardone, V. J. (1996). Practical modeling of hurricane surface wind fields. *J Waterw Port C-ASCE*. **122**(4), 195-205.

Tonkin, H., Holland, G. J., Holbrook, N., Henderson-Sellers, A. (2000). An evaluation of the thermodynamic estimates of climatological maximum potential tropical cyclone intensity. *Mon Weather Rev.* **135**, 746-764.

Toro, G. R., Niedoroda, A. W., Reed, C. W., Divoky, D. (2010). Quadrature-based approach for the efficient evaluation of surge hazard. *Ocean Eng*. **37**(1), 114-124.

University of Central Florida (2011). Flood insurance study: Florida Panhandle and Alabama, model validation. *Report.* Federal Emergency Management Agency. Philadelphia, PA.

Westerink, J. J., Luettich, R. A., Feyen, J. C., Atkinson, J. H., Dawson, C., Roberts, H. J., Powell, M. D., Dunion, J. P., Kubatko, E. J., Pourtaheri, H. (2008). A basin-to channel-scale unstructured grid hurricane storm surge model applied to southern Louisiana. *Mon Weather Rev*. **136**(3), 833-864.

Woodruff, J. D., Irish, J. L., Camargo, S. J. (2013). Coastal flooding by tropical cyclones and sea-level rise. *Nature*. **504**(7478), 44-52.

Yang, C. Y., Parisi, A. M., Gaither, W. S. (1970). Statistical prediction of hurricane storm surge. *Coastal Engineering Proceedings*. **1**(12).

Yin, J., Overpeck, J. T., Griffies, S. M., Hu, A., Russell, J. L., Stouffer, R. J. (2011). Different magnitudes of projected subsurface ocean warming around Greenland and Antarctica. *Nature Geosci*. **4**(8), 524-528.

CHAPTER 4

SUMMARY AND CONCLUSIONS

The design of coastal surge protection is based on extreme value hazard assessments, and the accuracy of these assessments is of fundamental importance in the coastal engineering profession. The Joint Probability Method (JPM) has become the preferred hazard assessment method in the United States, due to its high accuracy and robustness in comparison to alternative methods (Divoky and Resio 2007). Because the probability density functions used in JPM hazard assessments are based on hurricane meteorological parameters, rather than surge, accurate modeled estimates of surge heights corresponding to each parameter combination is essential. The long term climate trends inherent in the historical, and simulated, hurricane surge data necessitates the incorporation of these trends into the JPM as a second key phase.

A review of the literature, presented in Chapter 2, demonstrates that surge response functions (SRFs) have been successfully applied at multiple open coast locations, with average root-mean-square (RMS) error contributions ranging from 0.17 m (Song *et al.* 2012) to 0.28 m (Irish *et al.* 2009). The SRFs presented in these studies feature scaling terms that are universally applicable; all region specific terms are limited to coefficients. Therefore, these equations are highly transferrable, although their applications are limited to open coasts. Furthermore, investigations have been limited to select locations. The need for high-resolution alongshore SRF applications at open coast and bay interior locations is one research goal addressed in this study.

Following Song *et al.* (2012), SRFs were developed for 73 open coast, and 259 bay interior locations at Panama City, FL. A total of 38 simulated hurricanes were used to develop these response functions; these simulations were taken from a larger set used in a recent Federal

Emergency Management Agency (FEMA) study (University of Florida 2011). Potential complicating factors include the limited spatial extent of available surge data, as well as the complex coastal and bay interior features of this region. Potential advantages included the relatively narrow regional shelf width. Comparable results were achieved between open coast and bay interior locations, with respective mean RMS errors of 0.34 m and 0.37 m, and negligible bias values.

In developing the sea-level rise (SLR) adjustment models, it has been demonstrated that surge levels at bay interior locations are significantly influenced by the presence of barrier islands. The simulations used in this study were based upon the National Oceanic and Atmospheric Administration (NOAA) intermediate-high (1.2 m) and highest (2.0 m) SLR projections for the year 2100. It was revealed that, in contrast to present-day conditions, significant barrier island inundation occurred during simulated hurricane events under these projected conditions. The inundated area increases were not linear between these scenarios; most land cover losses occurred due to peak hurricane surge under 1.2 m projected SLR conditions. At 2.0 m SLR conditions, the loss in total area was less substantial. Despite the nonlinearity in total land cover reduction, the total flooding hazard with respect to SLR was characterized by a strong linear trend at these, and all other locations considered.

In this study, the accuracy of flood elevation adjustments with respect to SLR was limited due to the absence of topographic changes in the ADIRC hydrodynamic simulations. Land cover changes have been shown to increase surge generation near coastal wetlands (*e.g.*, Smith *et al.* 2010, Irish *et al.* 2013). Surge levels with respect to land cover changes can range between +80% and -100% over an entire region (Bilskie *et al.* 2014). Changes in land use due to urbanization, when considered in tandem with land cover changes, can potentially increase regional surge generation by up to +70% (Bilskie *et al.* 2014).

Bilskie *et al.* (2014) shows that changes in coastline morphology alters the flow paths of hurricane flood waters. The total extent of overland flooding for a single hurricane event will remain largely unchanged because of this; however, dynamic SLR effects on surge generation can be observed, demonstrating an effect on surge heights (Bilskie *et al.* 2014). Hazard assessments using the JPM-OS coupled with SRFs consider all possible hurricane scenarios; therefore, surge heights corresponding to a given return period are determined for each location of interest. Because surge heights are affected by morphologic coastline changes, the total 50, 100, or 500-year inundated area may also be affected.

Recommended future research concerning SLR adjustment models involves incorporating topographic adjustments, such as localized differences in water surface elevation, sediment transport induced changes in the coastline, land cover and land use changes, and changes in coastline morphology, as well as NOAA low (0.2 m) SLR projections for the year 2100, into the simulated hurricane dataset. It has been established that, for bay interior locations in close proximity to barrier islands, the total flood elevation is well characterized by linear adjustments to the SRF model, when SLR is sufficient to cause barrier island inundation. However, surge response at lower SLR conditions, when inundation may not occur, has not been investigated. It is anticipated that, in the absence of land cover loss, SLR trends at these locations will more closely approximate ideal conditions. A possible outcome is the introduction of an SLR "threshold," where *k* values at these bay interior locations experience a sudden decrease. Therefore, bay interior locations in close proximity to barrier islands may best be characterized by not one, but two, *k* values. Incorporating additional topographic effects, such as localized differences in water surface elevation, changes in land cover from sediment transport, or other SLR induced alterations, will add further certainty to these trends.

Hurricane surge and waves of the same return period are not necessarily caused by the same storm. A similar investigation into the development of wave response functions (WRFs) at Panama City, FL, is being conducted in tandem with the development of the SRFs presented here (McLaughlin 2014). Therefore, future research opportunities will include JPM return period analyses for hurricane induced surge and wave heights, which incorporate both SRFs and WRFs. Ultimately, a hazard assessment method by which the JPM is coupled with SRFs and WRFs is sought, in order to incorporate hurricane induced waves into flooding hazard assessments.

REFERENCES

Bacopoulos, P., Dally, W. R., Hagen, S. C., Cox, A. T. (2012). Observations and simulation of winds, surge, and currents on Florida's east coast during hurricane Jeanne (2004). *Coast Eng*. **60**, 84-94.

Bender, M. A., Knutson, T. R., Tuleya, R. E., Sirutis, J. J., Vecchi, G. A., Garner, S. T., Held, I. M. (2010). Modeled impact of anthropogenic warming on the frequency of intense Atlantic hurricanes. *Science*. **327**(5964), 454-458.

Bilskie, M. V., Hagen, S. C., Medeiros, S. C., Passeri, D. L. (2014). Dynamics of sea level rise and coastal flooding on a changing landscape. *Geophys Res Lett*. **41**, 927-934.

Blain, C. A., Westerink, J. J., Luettich, R. A. (1998). Grid convergence studies for the prediction of hurricane storm surge. *Int J Numer Meth Fl*. **26**(4), 369-401.

Condon, A. J., Sheng, Y. P. (2012). Optimal storm generation for evaluation of the storm surge inundation threat. *Ocean Eng*. **43**, 13-22.

Dawson, C., Proft, J. (2004). Coupled discontinuous and continuous Galerkin finite element methods for the depth-integrated shallow water equations. *Comput Method Appl M*. **193**(3), 289-318.

Dietrich, J. C., Dawson, C. N., Proft, J. M., Howard, M. T., Wells, G., Fleming, J. G., Luettich, R. A., Westerink, J. J., Cobell, Z., Vitse, M., Lander, H., Blanton, B. O., Szpilka, C. M., Atkinson, J. H. (2013). Real-Time Forecasting and Visualization of Hurricane Waves and Storm Surge Using SWAN+ADCIRC and FigureGen. In: *Computational Challenges in the Geosciences* (pp. 49-70). Springer. New York.

Divoky, D., Resio, D. T. (2007). Performance of the JPM and EST methods in storm surge studies. In: *10th international workshop on wave hindcasting and forecasting and coastal hazard symposium.* Joint WMO/IOC technical commission for oceanography and marine meteorology. Oahu, Hawaii, USA.

Ferreira, C. M., Olivera, F., Irish, J. L. (2013). Arc StormSurge: Integrating Hurricane Storm Surge Modeling and GIS. *J Am Water Resour As*. **50**, 219-233.

Gringorten, I. I. (1963). A simplified method of estimating extreme values from data samples. *J Appl Meteorol*. **2**(1), 82-89.

Ho, F. P., Myers, V. A. (1975). Joint probability method of tide frequency analysis applied to Apalachicola Bay and St. George Sound, Florida. NOAA Technical Report WS 18.

Holland, G. J., Webster, P. J. (2007). Heightened tropical cyclone activity in the North Atlantic: natural variability or climate trend? *Philos T R Soc A*. **365**(1860), 2695-2716.

Holland, G. J. (1980). An analytic model of the wind and pressure profiles in hurricanes. *Mon Weather Rev*. **108**(8), 1212-1218.

Intergovernmental Panel on Climate Change (2007). Contribution of working group I to the fourth assessment report of the Intergovernmental Panel on Climate Change. *Solomon, S. D. (Ed).*

Irish, J. L., Resio, D. T. (2013). Method for Estimating Future Hurricane Flood Probabilities and Associated Uncertainty. *J Waterw Port C-ASCE*. **139**(2), 126-134.

Irish, J. L., Sleath, A., Cialone, M. A., Knutson, T. R., Jensen, R. E. (2013). Simulations of Hurricane Katrina (2005) under sea level and climate conditions for 1900. *Climatic Change*. 1-15.

Irish, J. L., Song, Y. K., Chang, K. A. (2011). Probabilistic hurricane surge forecasting using parameterized surge response functions. *Geophys Res Lett.* **38**(3).

Irish, J. L., Resio, D. T. (2010). A hydrodynamics-based surge scale for hurricanes. *Ocean Eng.* **37**(1), 69-81.

Irish, J. L., Resio, D. T., Cialone, M. A. (2009). A surge response function approach to coastal hazard assessment. Part 2: Quantification of spatial attributes of response functions. *Nat Hazards*. **51**(1), 183-205.

Irish, J. L., Resio, D. T., Ratcliff, J. J. (2008). The influence of storm size on hurricane surge. *J Phys Oceanogr*. **38**(9), 2003-2013.

Klemeš, V. (1986). Dilettantism in hydrology: transition or destiny? *Water Resour Res*. **22**(9S), 177S-188S.

Knutson, T. R., McBride, J. L., Chan, J., Emanuel, K., Holland, G., Landsea, C., Held, I., Kossin, J. P., Srivastava, A. K., Sugi, M. (2010). Tropical cyclones and climate change. *Nat Geosci*. **3**(3), 157-163.

Knutson, T. R., Tuleya, R. E. (2008). Tropical cyclones and climate change: revisiting recent studies at GFDL. In: *Climate extremes and society* (pp. 120-144). Cambridge University Press. New York.

Knutson, T. R., Tuleya, R. E. (2004). Impact of CO 2-Induced Warming on Simulated Hurricane Intensity and Precipitation: Sensitivity to the Choice of Climate Model and Convective Parameterization. *J Climate*. **17**(18), 3477-3495.

McLaughlin, P. W. (2014). Parameterization and Statistical Analysis of Hurricane Waves (Master's thesis). Texas A&M University. College Station, TX.

Mousavi, M. E., Irish, J. L., Frey, A. E., Olivera, F., Edge, B. L. (2011). Global warming and hurricanes: the potential impact of hurricane intensification and sea level rise on coastal flooding. *Climatic Change*. **104**(3-4), 575-597.

Niedoroda, A. W., Resio, D. T., Toro, G. R., Divoky, D., Das, H. S., Reed, C. W. (2010). Analysis of the coastal Mississippi storm surge hazard. *Ocean Eng*. **37**(1), 82-90.

Resio, D. T., Irish, J. L., Westerink, J. J., Powell, N. J. (2013). The effect of uncertainty on estimates of hurricane surge hazards. *Nat Hazards*. **66**(3), 1443-1459.

Resio, D. T., Irish, J., Cialone, M. (2009). A surge response function approach to coastal hazard assessment–part 1: basic concepts. *Nat Hazards*. **51**(1), 163-182.

Resio, D. T., Westerink, J. J. (2008). Modeling the physics of storm surges. *Phys Today*. **61**, 33-38.

Resio, D. T., Boc, S. J., Borgman, L., Cardone, V., Cox, A., Dally, W. R., *et al.* (2007). White paper on estimating hurricane inundation probabilities. *US Army Corps of Engineers Engineer Research and Development Center*. Vicksburg, MS.

Rossby, C. G. (1940). Planetary flow patterns in the atmosphere. *Quart J Roy Meteor Soc*. **66**, 68-87.

Scheffner, N. W., Borgman, L. E., Mark, D. J. (1996). Empirical simulation technique based storm surge frequency analyses. *J Waterw Port C-ASCE*. **122**(2), 93-101.

Simpson, R. H., Saffir, H. (1974). The hurricane disaster potential scale. *Weatherwise*. **27**(8), 169.

Smith, J. M., Cialone, M. A., Wamsley, T. V., McAlpin, T. O. (2010). Potential impact of sea level rise on coastal surges in southeast Louisiana. *Ocean Eng*. **37**(1), 37-47.

Smith, R. K. (1968). The surface boundary layer of a hurricane. *Tellus*. **20**(3), 473-484.

Song, Y. K., Irish, J. L., Udoh, I. E. (2012). Regional attributes of hurricane surge response functions for hazard assessment. *Nat Hazards*. **64**(2), 1475-1490.

Thompson, E. F., Cardone, V. J. (1996). Practical modeling of hurricane surface wind fields. *J Waterw Port C-ASCE*. **122**(4), 195-205.

Tonkin, H., Holland, G. J., Holbrook, N., Henderson-Sellers, A. (2000). An evaluation of the thermodynamic estimates of climatological maximum potential tropical cyclone intensity. *Mon Weather Rev*. **135**, 746-764.Toro, G. R., Resio, D. T., Divoky, D., Niedoroda, A. W., Reed, C. W. (2010a). Efficient joint-probability methods for hurricane surge frequency analysis. *Ocean Eng.* **37**(1), 125-134.

Toro, G. R., Niedoroda, A. W., Reed, C. W., Divoky, D. (2010b). Quadrature-based approach for the efficient evaluation of surge hazard. *Ocean Eng*. **37**(1), 114-124.

Udoh, I. E. (2012). Robust hurricane surge response functions (Doctoral dissertation). Texas A&M University. College Station, TX.

University of Central Florida (2011). Flood insurance study: Florida Panhandle and Alabama, model validation. *Report.* Federal Emergency Management Agency. Philadelphia, PA.

Westerink, J. J., Luettich, R. A., Feyen, J. C., Atkinson, J. H., Dawson, C., Roberts, H. J., Powell, M. D., Dunion, J. P., Kubatko, E. J., Pourtaheri, H. (2008). A basin-to channel-scale unstructured grid hurricane storm surge model applied to southern Louisiana. *Mon Weather Rev*. **136**(3), 833-864.

Westerink, J. J., Luettich, R. A., Baptists, A. M., Scheffner, N. W., Farrar, P. (1992). Tide and storm surge predictions using finite element model. *J Hydraul Eng-ASCE*. **118**(10), 1373-1390.

Yang, C. Y., Parisi, A. M., Gaither, W. S. (1970). Statistical prediction of hurricane storm surge. *Coastal Engineering Proceedings*. **1**(12).

APPENDIX A

OPEN COAST SURGE RESPONSE FUNCTIONS

Table A-1 Open coast surge response function R^2, root-mean-square error, mean error, and lambda parameter values; geodetic coordinates, and alongshore distances.

Index	Longitude	Latitude	Alongshore Distance (km)	R^2	RMS Error (m)	Bias (m)	λ
0	-86.140250	30.318463	528.7842	0.8410	0.3846	0.0103	0.7102
1	-86.127244	30.314390	530.1141	0.8388	0.3894	0.0126	0.7264
2	-86.115924	30.310820	531.2726	0.8392	0.3889	0.0131	0.7406
3	-86.104069	30.307242	532.4799	0.8415	0.3946	0.0098	0.7559
4	-86.093550	30.303994	533.5539	0.8380	0.3996	0.0131	0.7695
5	-86.082405	30.300195	534.7057	0.8448	0.3746	0.0041	0.7823
6	-86.073106	30.296730	535.6791	0.8460	0.3660	0.0071	0.7952
7	-86.063118	30.292876	536.7307	0.8484	0.3653	0.0059	0.8084
8	-86.051470	30.288419	537.9553	0.8484	0.3636	0.0073	0.8232
9	-86.040309	30.284541	539.1121	0.8621	0.3528	0.0146	0.8367
10	-86.030335	30.280992	540.1492	0.8404	0.3623	0.0018	0.8500
11	-86.020084	30.277326	541.2159	0.8402	0.3705	0.0025	0.8639
12	-86.008894	30.273316	542.3807	0.8403	0.3703	0.0027	0.8786
13	-85.996842	30.268700	543.6483	0.8127	0.3950	0.0038	0.8946
14	-85.986821	30.264600	544.7144	0.8170	0.3888	0.0066	0.9037
15	-85.977651	30.260884	545.6883	0.8086	0.3913	0.0095	0.9200
16	-85.967194	30.256576	546.8021	0.8239	0.3753	0.0129	0.9344
17	-85.958539	30.252933	547.7278	0.8212	0.3803	0.0143	0.9456
18	-85.947536	30.248171	548.9111	0.8196	0.3797	0.0163	0.9620
19	-85.936952	30.243454	550.0561	0.8195	0.3787	0.0162	0.9745
20	-85.926430	30.238515	551.2074	0.8150	0.3800	0.0188	0.9916
21	-85.913343	30.232232	552.6469	0.7997	0.3998	0.0138	1.0113
22	-85.896724	30.224167	554.4796	0.7838	0.4115	0.0195	1.0350
23	-85.885256	30.218434	555.7534	0.7972	0.3920	0.0194	1.0508
24	-85.875716	30.213591	556.8174	0.8073	0.3800	0.0211	1.0651
25	-85.862330	30.206359	558.3352	0.7749	0.4108	0.0181	1.0857
26	-85.852353	30.200787	559.4773	0.7791	0.4023	0.0142	1.0999
27	-85.841698	30.194790	560.6998	0.7816	0.3981	0.0086	1.1146
28	-85.828572	30.187074	562.2261	0.7856	0.3958	0.0069	1.1315
29	-85.819926	30.182066	563.2269	0.7802	0.3960	0.0123	1.1504
30	-85.806487	30.174260	564.7839	0.8265	0.3535	0.0188	1.1701
31	-85.797508	30.168813	565.8386	0.8223	0.3585	0.0181	1.1845
32	-85.780014	30.158129	567.8984	0.8149	0.3577	0.0170	1.2108
33	-85.772152	30.152824	568.8573	0.8250	0.3514	0.0152	1.2263
34	-85.761590	30.144917	570.2004	0.8149	0.3482	0.0141	1.2428
35	-85.753883	30.138837	571.2032	0.8205	0.3389	0.0153	1.2560
36	-85.745410	30.131978	572.3188	0.8119	0.3428	0.0123	1.2709

Index	Longitude	Latitude	Alongshore Distance (km)	R^2	RMS Error (m)	Bias (m)	λ
37	-85.736696	30.124728	573.4812	0.8042	0.3439	0.0113	1.2857
38	-85.724393	30.115025	575.0820	0.8001	0.3544	0.0149	1.3064
39	-85.714882	30.108107	576.2771	0.7694	0.3826	0.0144	1.3224
40	-85.706130	30.102421	577.3302	0.7290	0.4214	-0.0195	1.3392
41	-85.697082	30.097215	578.3759	0.8115	0.3611	0.0292	1.1259
42	-85.684821	30.091082	579.7394	0.8012	0.3698	0.0294	1.1544
43	-85.670679	30.084855	581.2675	0.7918	0.3792	0.0192	1.1854
44	-85.658598	30.079995	582.5508	0.8025	0.3717	0.0150	1.2117
45	-85.649961	30.076543	583.4672	0.8031	0.3717	0.0157	1.2306
46	-85.616067	30.061439	587.1392	0.8293	0.3696	-0.0420	0.8315
47	-85.606200	30.056142	588.2573	0.7953	0.4679	-0.1001	0.8617
48	-85.582803	30.037635	591.3070	0.8816	0.3069	0.0238	0.9202
49	-85.577547	30.032123	592.1008	0.8777	0.3074	0.0219	0.9306
50	-85.571987	30.026035	592.9629	0.8764	0.3073	0.0195	0.9442
51	-85.567194	30.020957	593.6913	0.8747	0.3065	0.0186	0.9559
52	-85.560126	30.013874	594.7312	0.9051	0.2590	0.0191	0.9727
53	-85.553255	30.007386	595.7093	0.8971	0.2655	0.0146	0.9884
54	-85.547073	30.001688	596.5781	0.8387	0.3287	0.0119	1.0022
55	-85.539628	29.994960	597.6136	0.9090	0.2486	0.0149	1.0183
56	-85.536087	29.992025	598.0854	0.9085	0.2477	0.0145	1.0259
57	-85.527592	29.985270	599.1956	0.8909	0.2853	0.0261	1.0446
58	-85.512342	29.974723	601.0753	0.8776	0.2860	0.0174	1.0792
59	-85.504003	29.969627	602.0585	0.8855	0.2861	0.0233	1.0958
60	-85.493756	29.964620	603.1927	0.8980	0.2702	0.0222	1.1149
61	-85.481648	29.960603	604.4434	0.9059	0.2651	0.0248	1.1369
62	-85.469722	29.957539	605.6435	0.9227	0.2538	0.0297	1.1589
63	-85.456609	29.955174	606.9362	0.9170	0.2677	0.0318	1.1815
64	-85.446488	29.953516	607.9303	0.9198	0.2534	0.0259	1.1980
65	-85.434519	29.950532	609.1321	0.9195	0.2531	0.0258	1.2194
66	-85.424162	29.946382	610.2327	0.8712	0.3203	0.0239	0.9129
67	-85.412435	29.940195	611.5564	0.9166	0.2531	0.0293	1.1117
68	-85.402180	29.933505	612.7934	0.9094	0.2579	0.0296	1.1371
69	-85.390668	29.924297	614.3025	0.9045	0.2611	0.0319	1.1678
70	-85.381551	29.915504	615.6159	0.9020	0.2579	0.0221	1.1952
71	-85.374514	29.907445	616.7383	0.8598	0.3028	0.0141	1.0340
72	-85.367691	29.899631	617.8268	0.8539	0.3037	0.0144	1.0538

Table A-2 Dimensionless surge response function regression parameters for open coast locations.

Index	x' < 0					x' >= 0				
	α	β	m	a_1	b_1	α	β	m	a_2	b_2
0	0.10	0.05	-2.1432	1.6188	0.3452	0.05	1.00	4.0129	-1.9687	-1.6494
1	0.10	0.05	-2.0609	1.8462	0.3710	0.05	1.00	3.9624	-2.0623	-1.6100
2	0.10	0.05	-2.0371	1.9287	0.3722	0.05	1.00	3.9114	-2.1293	-1.5467
3	0.10	0.05	-2.1479	2.0534	0.3696	0.05	1.00	4.1657	-1.9696	-1.5405
4	0.00	1.00	-0.3964	-0.3131	0.6898	0.05	1.00	3.8321	-2.2361	-1.4604
5	0.10	0.05	-3.2184	1.4001	0.4637	0.05	1.00	4.1460	-1.4078	-1.3613
6	0.10	0.05	-3.1897	1.4288	0.4570	0.05	1.00	3.6666	-2.6346	-1.2425
7	0.15	0.10	-2.0153	1.4876	0.4530	0.05	1.00	3.6225	-2.5948	-1.2311
8	0.10	0.05	-2.9455	1.7393	0.4449	0.05	1.00	3.5488	-2.7005	-1.1640
9	0.15	0.05	-1.8258	8.5065	0.1816	0.00	1.00	3.1015	-3.2020	-0.7815
10	0.15	0.05	-1.7928	8.2793	0.1886	0.00	1.00	2.8829	3.0416	-1.2698
11	0.15	0.05	-1.7679	8.2375	0.1972	0.00	1.00	2.9647	3.9855	-1.3652
12	0.20	0.05	-1.4846	8.0696	0.1949	0.00	1.00	2.9382	3.8785	-1.3163
13	0.00	1.00	-0.1808	-1.6569	0.8114	0.00	1.00	2.9248	4.4517	-1.3559
14	0.10	0.05	-0.5987	-1.7130	0.8112	0.00	1.00	2.7374	3.2112	-1.1452
15	1.00	0.00	-0.1746	-1.8368	0.8352	0.00	1.00	2.7116	4.0117	-1.2419
16	0.00	1.00	-0.1620	0.0251	0.7239	0.00	1.00	2.6929	3.8669	-1.2047
17	0.00	1.00	-0.1440	0.1732	0.7290	0.00	1.00	2.6376	4.1390	-1.2101
18	0.00	1.00	-0.1504	0.3354	0.7299	0.00	1.00	2.6003	4.5772	-1.2421
19	0.00	1.00	-0.1211	0.4598	0.7423	0.00	1.00	2.5354	3.7060	-1.1058
20	0.00	1.00	-0.1357	0.5715	0.7490	0.00	1.00	2.4978	4.4496	-1.1795
21	0.00	1.00	-0.1836	0.7890	0.6387	0.00	1.00	3.1188	3.6688	-1.6181
22	0.00	1.00	-0.1528	0.9771	0.6587	0.00	1.00	2.9954	2.5192	-1.8044
23	0.00	1.00	-0.1340	0.9420	0.6719	0.00	1.00	2.7437	2.9994	-1.5195
24	0.00	1.00	-0.3705	0.7521	0.8227	0.00	1.00	2.6737	3.3523	-1.5703
25	0.00	1.00	-0.4721	-0.5796	1.1765	0.00	1.00	2.7792	3.9764	-1.6448
26	0.00	1.00	-0.4616	-0.4593	1.1529	0.00	1.00	2.8213	3.4681	-1.6315
27	0.00	1.00	-0.4363	0.1642	0.9723	0.20	1.00	3.1207	8.5537	-2.2752
28	1.00	0.80	1.4785	0.2510	0.9764	0.20	1.00	2.8913	9.8992	-2.3467
29	0.00	1.00	-0.4553	-3.7451	1.3197	0.00	1.00	2.7498	-2.5677	-1.5338
30	0.00	1.00	-0.4664	0.6896	0.7161	0.00	1.00	2.3960	-4.2035	-1.3286
31	0.00	0.95	-0.4503	0.5429	0.6861	0.00	1.00	2.3955	-3.5491	-1.5170
32	0.00	0.95	-0.4247	0.8334	0.7264	0.00	1.00	2.4683	-2.9875	-1.5396
33	0.00	0.95	-0.4141	0.9720	0.7353	0.00	1.00	2.6303	-3.8894	-1.2641
34	0.00	0.45	-0.4947	-2.6308	0.9821	0.00	1.00	2.0188	-0.9830	-1.5048
35	0.00	0.55	-0.4179	1.5333	0.4631	0.00	1.00	1.8752	-1.1308	-1.5052
36	0.00	0.50	-0.4302	1.7311	0.4785	0.00	1.00	1.7227	0.1687	-1.6149

Index	x' < 0					x' >= 0				
	α	β	m	a_1	b_1	α	β	m	a_2	b_2
37	0.00	0.55	-0.3871	1.8810	0.5039	0.00	1.00	1.5233	0.7185	-1.6400
38	0.00	0.60	-0.3471	1.9492	0.5040	0.00	1.00	1.2896	0.9324	-1.7209
39	0.00	1.00	-0.4316	0.6101	0.9357	0.00	1.00	1.1161	1.7374	-1.7599
40	0.05	0.00	5.7669	-0.8944	1.0515	0.05	0.00	-3.0399	3.6278	-1.8212
41	0.00	1.00	-0.6781	-0.6224	1.0523	0.00	1.00	1.4969	-3.5050	-1.0546
42	0.00	1.00	-0.6763	-1.7907	1.1420	0.00	1.00	1.3795	-0.5085	-1.1874
43	0.00	1.00	-0.6861	-1.7488	1.1092	0.00	1.00	1.2898	3.1107	-1.2723
44	0.05	0.00	5.8053	-1.1351	1.0515	0.00	1.00	1.3339	2.8917	-1.2018
45	0.05	0.00	5.7358	-1.1420	1.0507	0.00	1.00	1.3586	3.0592	-1.1961
46	0.00	1.00	-0.2797	0.6628	0.5819	0.00	1.00	1.4365	0.0000	-3.0526
47	0.25	0.05	1.7744	1.0454	0.4425	0.00	1.00	0.2775	0.0000	-0.9877
48	0.00	1.00	-0.6778	0.6204	0.5047	0.00	1.00	0.9492	-2.0281	-1.2327
49	0.00	1.00	-0.7750	0.6916	0.5047	0.00	1.00	0.9190	-0.7106	-1.3210
50	0.00	1.00	-0.8347	0.7493	0.5195	0.00	1.00	0.8951	-0.1807	-1.4404
51	0.00	1.00	-0.8434	0.8070	0.5369	0.00	1.00	0.8701	-0.2735	-1.5109
52	0.15	0.05	-2.0323	1.4074	0.3134	0.00	1.00	0.7876	1.9927	-1.7390
53	0.10	0.05	-2.9929	1.5442	0.2897	0.00	1.00	0.7654	4.6127	-2.0650
54	0.00	1.00	-0.9939	1.1758	0.1697	0.00	1.00	0.7572	4.1277	-2.0263
55	0.10	0.05	-3.2866	-1.5011	0.4712	0.00	1.00	0.7692	-3.1173	-1.3552
56	0.10	0.05	-3.2767	-1.4465	0.4750	0.00	1.00	0.7560	-2.8635	-1.3660
57	0.05	0.05	-0.8701	-1.8328	0.5833	1.00	0.00	-0.8150	-1.0833	-1.3467
58	1.00	0.55	1.8332	-1.7508	0.5712	0.00	1.00	1.2325	0.0844	-1.6405
59	1.00	0.55	1.9293	-1.7093	0.5568	0.00	1.00	1.3670	-3.3622	-1.5023
60	1.00	0.55	2.0083	-1.6592	0.5618	0.00	1.00	1.3750	-4.4486	-1.2584
61	1.00	0.55	1.8459	-1.6144	0.5671	0.00	1.00	1.3429	-4.7981	-1.0684
62	1.00	0.70	2.0759	-1.5165	0.5547	0.00	1.00	1.4040	-5.5503	-0.5679
63	1.00	0.60	2.1614	-1.4013	0.5609	0.00	1.00	1.2306	-7.6054	-0.3177
64	1.00	0.60	2.1858	-1.3433	0.5815	0.00	1.00	1.2227	-6.4135	-0.6600
65	1.00	0.60	2.1987	-1.2187	0.5978	0.00	1.00	1.1954	-7.0570	-0.5964
66	0.00	0.05	-2.5310	-1.1102	0.6180	1.00	0.00	-0.8267	0.6270	-1.0296
67	0.00	0.05	-2.3259	-1.0075	0.6534	0.00	0.70	0.7176	-4.7239	-0.8055
68	0.00	0.05	-2.1116	-0.9265	0.7020	0.00	0.60	0.7591	-4.6994	-0.8657
69	0.00	0.05	-1.8143	-0.7933	0.7499	0.00	0.30	1.1041	-5.3560	-0.8407
70	1.00	0.00	0.3116	-0.6768	0.8040	0.00	0.75	0.6233	-7.3262	-0.7350
71	1.00	0.00	0.3338	-0.5186	0.8377	1.00	0.00	-0.6283	0.0445	-0.9746
72	1.00	0.00	0.3269	-0.3257	0.8731	1.00	0.00	-0.6214	-0.1239	-0.9623

Table A-3 Surge response function least-squares based model distribution and coefficients for open coast locations.

	x' < 0		$\zeta' = c_1 e^{c_2(x'+c_3)}$			x' >= 0		$\zeta' = \begin{cases} c_1 e^{(x')c_2} \\ c_1(x'+1)^{c_2} \end{cases}$	
Index	SRF model	ζ'*	c_1	c_2	c_3	SRF model	ζ'*	c_1	c_2
0	exp	1.5025	2.1866	0.7747	1.1769	exp	0	5.7433	-0.1797
1	exp	1.4220	2.1654	0.7790	1.2103	exp	0	5.7561	-0.1783
2	exp	1.3981	0.1777	0.7844	4.4006	exp	0	5.7459	-0.1785
3	exp	1.5051	0.2136	0.8061	4.1061	exp	0	5.9321	-0.1822
4	exp	0	1.9314	0.6426	1.6523	exp	0	5.8102	-0.1743
5	exp	2.4012	1.3627	0.7859	1.8791	exp	0	5.9816	-0.1906
6	exp	2.3716	0.2024	0.7763	4.3199	exp	0	5.6476	-0.1784
7	exp	1.1457	1.7254	0.7941	1.5351	exp	0	5.6663	-0.1769
8	exp	2.1514	0.9692	0.7865	2.2963	exp	0	5.6308	-0.1767
9	exp	1.1923	0.2217	0.7454	4.3604	exp	0	5.6974	-0.1869
10	exp	1.1547	0.2046	0.7475	4.4517	exp	0	5.2365	-0.1688
11	exp	1.1396	0.2136	0.7530	4.4046	exp	0	5.4117	-0.1726
12	exp	0.8787	1.8104	0.7485	1.5778	exp	0	5.4148	-0.1738
13	exp	0	2.3314	0.6025	1.5136	exp	0	5.4222	-0.1745
14	exp	0.1605	0.3004	0.7421	4.0193	exp	0	5.3358	-0.1732
15	exp	0	0.7193	0.6205	3.3638	exp	0	5.2852	-0.1735
16	exp	0	1.2282	0.5933	2.6352	exp	0	5.2790	-0.1746
17	exp	0	4.5347	0.5905	0.4532	exp	0	5.2891	-0.1740
18	exp	0	5.3400	0.5856	0.1706	exp	0	5.2792	-0.1742
19	exp	0	1.4737	0.5846	2.3779	exp	0	5.2381	-0.1759
20	exp	0	1.2430	0.5744	2.7010	exp	0	5.2218	-0.1752
21	exp	0	0.9105	0.5919	3.2046	exp	0	5.4193	-0.1735
22	exp	0	1.5454	0.5737	2.3677	exp	0	5.4002	-0.1674
23	exp	0	0.8859	0.5720	3.3227	exp	0	5.2057	-0.1687
24	exp	0	1.5210	0.5688	2.4297	exp	0	5.2193	-0.1696
25	exp	0	0.6210	0.5588	4.0914	exp	0	5.3396	-0.1708
26	exp	0	1.7954	0.5590	2.1695	exp	0	5.3811	-0.1805
27	exp	0	1.7429	0.5763	2.1837	exp	0	5.2572	-0.1727
28	exp	0	1.4906	0.5791	2.6662	exp	0	5.1817	-0.1653
29	exp	0	1.4588	0.5756	2.5192	exp	0	5.2782	-0.1708
30	exp	0	1.0880	0.5690	3.0703	exp	0	5.1625	-0.1616
31	exp	0	2.2603	0.5708	1.7714	exp	0	5.1859	-0.1613
32	exp	0	1.5591	0.5615	2.4454	exp	0	5.1814	-0.1643
33	exp	0	1.7435	0.5678	2.2519	exp	0	5.2947	-0.1721
34	exp	0	1.7836	0.5783	2.1059	exp	0	4.9241	-0.1636
35	exp	0	4.6835	0.5726	0.4505	exp	0	4.9451	-0.1672
36	exp	0	1.6018	0.5718	2.3102	exp	0	4.8124	-0.1658

	x' < 0		$\zeta' = c_1 e^{c_2(x'+c_3)}$			x' >= 0		$\zeta' = \begin{cases} c_1 e^{(x')c_2} \\ c_1(x'+1)^{c_2} \end{cases}$	
Index	SRF model	ζ'*	c_1	c_2	c_3	SRF model	ζ'*	c_1	c_2
37	exp	0	1.4178	0.5538	2.5933	exp	0	4.5844	-0.1564
38	exp	0	4.8280	0.5470	0.4404	exp	0	4.6761	-0.1584
39	exp	0	3.0695	0.5117	1.3845	exp	0	4.6190	-0.1557
40	exp	0	5.7923	0.1597	4.0675	exp	1.4405	3.7168	-0.4207
41	exp	0	2.5432	0.5222	1.5298	pwr	0	7.2546	-0.6420
42	exp	0	2.3260	0.5152	1.7693	pwr	0	7.2080	-0.6358
43	exp	0	2.1798	0.5246	1.9034	pwr	0	6.7120	-0.6026
44	exp	0	8.0641	0.1649	1.9178	pwr	0	6.7758	-0.6084
45	exp	0	7.5695	0.1673	2.2627	pwr	0	6.8130	-0.6095
46	exp	0	1.0104	0.6721	2.4292	pwr	0	5.9110	-0.7034
47	exp	0	1.9305	0.4447	2.8190	exp	0	6.3343	-0.4534
48	exp	0	1.6614	0.7073	1.9314	pwr	0	6.8341	-0.6030
49	exp	0	0.8392	0.7176	2.8361	pwr	0	6.7527	-0.6027
50	exp	0	0.7409	0.7293	2.9628	pwr	0	6.7753	-0.6099
51	exp	0	2.0385	0.7316	1.5645	pwr	0	6.7456	-0.6127
52	exp	0.9125	0.8888	1.0410	2.0243	pwr	0	6.7012	-0.6193
53	exp	1.7548	1.3453	1.0602	1.5820	pwr	0	6.6371	-0.6235
54	exp	0	1.1005	0.6332	2.5946	pwr	0	6.6190	-0.6253
55	exp	1.9812	0.8347	1.0598	2.0182	pwr	0	6.5606	-0.6343
56	exp	1.9513	0.8525	1.0624	1.9881	pwr	0	6.5178	-0.6339
57	exp	0	0.5129	0.9953	2.6321	pwr	0	5.9018	-0.7306
58	exp	0	3.5439	0.5475	1.1271	pwr	0	7.0847	-0.6358
59	exp	0	1.9185	0.5565	2.2520	pwr	0	7.5949	-0.6634
60	exp	0	2.4745	0.5595	1.7901	pwr	0	7.5596	-0.6739
61	exp	0	0.6904	0.5605	4.0886	pwr	0	7.6111	-0.6744
62	exp	0	1.2950	0.5731	2.9624	pwr	0	7.5781	-0.6630
63	exp	0	1.6785	0.5543	2.6179	pwr	0	7.3677	-0.6503
64	exp	0	2.5250	0.5428	1.9077	pwr	0	7.5417	-0.6744
65	exp	0	4.1655	0.5338	1.0003	pwr	0	7.4381	-0.6685
66	exp	1.0332	0.9465	0.9990	1.6682	exp	0	4.3684	-0.1872
67	exp	0.7783	0.4434	0.9823	2.6105	pwr	0	7.1178	-0.6398
68	exp	0.5231	0.9721	0.9608	1.8087	pwr	0	7.0066	-0.6243
69	exp	0.1728	2.0581	0.9369	1.0069	pwr	0	7.1418	-0.5510
70	exp	0	3.6189	0.5031	1.1084	pwr	0	6.5434	-0.6162
71	exp	0	2.2338	0.4890	1.9349	pwr	0	5.7269	-0.6861
72	exp	0	1.0386	0.4756	3.5800	pwr	0	5.6284	-0.6819

APPENDIX B

BAY INTERIOR SURGE RESPONSE FUNCTIONS

Table B-1 Bay interior surge response function R^2, root-mean-square error, mean error, and lambda parameter values; geodetic coordinates, and alongshore distances.

Index	Longitude	Latitude	Alongshore Distance (km)	R^2	RMS Error (m)	Bias (m)	λ
0	-85.724633	30.127531	579.7394	0.7772	0.3438	0.0108	1.3636
1	-85.728747	30.132150	579.7394	0.7361	0.3751	0.0024	1.3594
2	-85.734721	30.137026	579.7394	0.7342	0.3880	0.0049	1.3590
3	-85.741467	30.140495	579.7394	0.7382	0.3966	0.0126	1.3596
4	-85.745999	30.144869	579.7394	0.7646	0.3921	0.0216	1.3600
5	-85.745022	30.147778	579.7394	0.7720	0.3930	0.0243	1.3599
6	-85.737238	30.147480	579.7394	0.7813	0.3805	0.0227	1.3595
7	-85.733973	30.146896	579.7394	0.7822	0.3742	0.0193	1.3585
8	-85.727756	30.145688	579.7394	0.7748	0.3734	0.0128	1.3565
9	-85.732258	30.142687	579.7394	0.7595	0.3801	0.0118	1.3579
10	-85.728101	30.138711	579.7394	0.7556	0.3725	0.0039	1.3582
11	-85.721124	30.137234	579.7394	0.7502	0.3694	0.0043	1.3575
12	-85.716909	30.138885	579.7394	0.7638	0.3470	-0.0023	1.1831
13	-85.712189	30.143360	579.7394	0.7602	0.3451	-0.0030	1.1833
14	-85.713515	30.149098	579.7394	0.7669	0.3236	0.0124	1.3613
15	-85.719367	30.154986	579.7394	0.7705	0.3177	0.0146	1.3617
16	-85.732719	30.162799	579.7394	0.7724	0.3147	0.0185	1.3622
17	-85.741524	30.163240	579.7394	0.7686	0.3138	0.0194	1.3636
18	-85.747129	30.169077	579.7394	0.7717	0.3150	0.0200	1.3638
19	-85.751327	30.174008	579.7394	0.7694	0.3220	0.0199	1.3642
20	-85.752184	30.183329	579.7394	0.7682	0.3320	0.0215	1.3648
21	-85.747146	30.188046	579.7394	0.7808	0.3277	0.0209	1.3634
22	-85.751507	30.194708	579.7394	0.7760	0.3355	0.0209	1.3647
23	-85.744980	30.202055	579.7394	0.7870	0.3367	0.0208	1.3637
24	-85.742311	30.213669	579.7394	0.7928	0.3472	0.0241	1.3643
25	-85.751150	30.217033	579.7394	0.7594	0.3727	0.0178	1.3659
26	-85.758854	30.214599	579.7394	0.7668	0.3595	0.0234	1.3672
27	-85.763404	30.223197	579.7394	0.7789	0.3608	0.0235	1.3687
28	-85.768732	30.230626	579.7394	0.7913	0.3573	0.0235	1.3707
29	-85.762293	30.231706	579.7394	0.7798	0.3702	0.0189	1.3691
30	-85.758999	30.236046	579.7394	0.7967	0.3659	0.0279	1.3687
31	-85.763550	30.240969	579.7394	0.7831	0.3794	0.0172	1.3704
32	-85.770291	30.244149	579.7394	0.8011	0.3702	0.0249	1.3722
33	-85.777789	30.245853	579.7394	0.7967	0.3763	0.0252	1.3736
34	-85.786202	30.246064	579.7394	0.7870	0.3805	0.0203	1.3752
35	-85.791120	30.250994	579.7394	0.7912	0.3841	0.0249	1.3759
36	-85.797652	30.252206	579.7394	0.7976	0.3770	0.0195	1.3774

Index	Longitude	Latitude	Alongshore Distance (km)	R^2	RMS Error (m)	Bias (m)	λ
37	-85.805115	30.249626	579.7394	0.7823	0.3860	0.0210	1.3800
38	-85.813396	30.243473	579.7394	0.7626	0.3922	0.0282	1.3836
39	-85.824198	30.235200	579.7394	0.7367	0.3932	0.0245	1.3875
40	-85.825184	30.226175	579.7394	0.7513	0.3799	0.0282	1.3881
41	-85.831653	30.226837	579.7394	0.7401	0.3767	0.0196	1.3903
42	-85.841739	30.228839	579.7394	0.7519	0.3740	0.0273	1.3920
43	-85.847889	30.232381	579.7394	0.7578	0.3794	0.0322	1.3927
44	-85.850947	30.238528	579.7394	0.7020	0.4268	0.0300	1.3929
45	-85.851191	30.248222	579.7394	0.7065	0.4465	0.0294	1.3912
46	-85.853263	30.257732	579.7394	0.6976	0.4764	0.0271	1.3908
47	-85.851868	30.268577	579.7394	0.6963	0.5047	0.0279	1.3900
48	-85.845705	30.274128	579.7394	0.7004	0.5093	0.0284	1.3883
49	-85.840967	30.285629	579.7394	0.7668	0.4713	0.0368	1.3871
50	-85.829462	30.285905	579.7394	0.7789	0.4476	0.0280	1.3849
51	-85.818092	30.285580	579.7394	0.8096	0.4125	0.0309	1.3815
52	-85.807892	30.291286	579.7394	0.8317	0.3985	0.0320	1.3815
53	-85.803181	30.295487	579.7394	0.8431	0.3948	0.0307	1.3807
54	-85.795730	30.286016	579.7394	0.8168	0.4008	0.0264	1.3790
55	-85.792570	30.290272	579.7394	0.8314	0.3963	0.0202	1.3809
56	-85.783644	30.289028	579.7394	0.8302	0.3941	0.0205	1.3780
57	-85.777368	30.287728	579.7394	0.8338	0.3903	0.0263	1.3755
58	-85.768907	30.293537	579.7394	0.8414	0.3935	0.0297	1.3727
59	-85.764599	30.298182	579.7394	0.8551	0.3852	0.0160	1.1526
60	-85.760707	30.308361	579.7394	0.8585	0.3988	0.0146	1.1566
61	-85.757785	30.297110	579.7394	0.8496	0.3901	0.0149	1.1527
62	-85.752897	30.290563	579.7394	0.8330	0.4038	0.0197	1.1514
63	-85.749305	30.283951	579.7394	0.8317	0.3894	0.0253	1.3674
64	-85.746189	30.278472	579.7394	0.8330	0.3824	0.0273	1.3675
65	-85.739112	30.279327	579.7394	0.8310	0.3866	0.0236	1.3659
66	-85.738799	30.272918	579.7394	0.8233	0.3822	0.0211	1.3653
67	-85.734603	30.260802	579.7394	0.8218	0.3758	0.0250	1.3645
68	-85.727911	30.258063	579.7394	0.8244	0.3692	0.0216	1.3632
69	-85.724288	30.248672	579.7394	0.8174	0.3633	0.0225	1.3616
70	-85.724718	30.239623	579.7394	0.8095	0.3619	0.0220	1.3612
71	-85.711979	30.237452	579.7394	0.8074	0.3635	0.0231	1.3580
72	-85.703533	30.247959	579.7394	0.8051	0.3752	0.0073	1.1491
73	-85.699880	30.254693	579.7394	0.8180	0.3707	0.0095	1.1508
74	-85.693766	30.260486	579.7394	0.8179	0.3794	0.0096	1.1528
75	-85.686228	30.263127	579.7394	0.8140	0.3881	0.0104	1.1550
76	-85.675488	30.264004	579.7394	0.8144	0.3889	0.0142	1.1576
77	-85.670935	30.267976	579.7394	0.8162	0.3939	0.0234	1.1592

Index	Longitude	Latitude	Alongshore Distance (km)	R^2	RMS Error (m)	Bias (m)	λ
78	-85.661558	30.266910	579.7394	0.8142	0.3923	0.0203	1.1601
79	-85.651250	30.271244	579.7394	0.8135	0.4011	0.0270	1.1617
80	-85.642179	30.263281	579.7394	0.8133	0.3914	0.0231	1.1635
81	-85.630440	30.268775	579.7394	0.8093	0.3977	0.0211	1.1659
82	-85.623524	30.272569	579.7394	0.8065	0.4066	0.0242	1.1667
83	-85.614354	30.269939	579.7394	0.8040	0.4081	0.0249	1.1671
84	-85.605889	30.262835	579.7394	0.8023	0.4052	0.0254	1.1672
85	-85.616314	30.256017	579.7394	0.8036	0.3976	0.0239	1.1665
86	-85.631169	30.256224	579.7394	0.8084	0.3910	0.0225	1.1648
87	-85.641237	30.254872	579.7394	0.8103	0.3884	0.0219	1.1632
88	-85.647166	30.254534	579.7394	0.8111	0.3870	0.0169	1.1621
89	-85.653842	30.256195	579.7394	0.8082	0.3913	0.0210	1.1608
90	-85.661336	30.253509	579.7394	0.8035	0.3925	0.0159	1.1580
91	-85.666355	30.249687	579.7394	0.8018	0.3905	0.0140	1.1569
92	-85.677192	30.249714	579.7394	0.8092	0.3808	0.0122	1.1545
93	-85.680028	30.243583	579.7394	0.8122	0.3706	0.0115	1.1519
94	-85.676474	30.234739	579.7394	0.8123	0.3624	0.0120	1.1511
95	-85.686044	30.232991	579.7394	0.7919	0.3762	0.0080	1.1490
96	-85.687076	30.225033	579.7394	0.7861	0.3733	0.0077	1.1474
97	-85.689547	30.219879	579.7394	0.7839	0.3706	0.0086	1.1466
98	-85.698309	30.215559	579.7394	0.7874	0.3626	0.0229	1.3564
99	-85.705211	30.208159	579.7394	0.7904	0.3524	0.0229	1.3572
100	-85.711351	30.199321	579.7394	0.7857	0.3466	0.0219	1.3580
101	-85.723807	30.190613	579.7394	0.7808	0.3393	0.0218	1.3600
102	-85.736235	30.188446	579.7394	0.7798	0.3324	0.0197	1.3621
103	-85.732862	30.182559	579.7394	0.7752	0.3313	0.0185	1.3614
104	-85.729164	30.176112	579.7394	0.7752	0.3275	0.0169	1.3615
105	-85.718778	30.179119	579.7394	0.7813	0.3337	0.0139	1.3605
106	-85.707999	30.174808	579.7394	0.7804	0.3336	0.0120	1.3596
107	-85.701978	30.165686	579.7394	0.7801	0.3355	0.0128	1.3599
108	-85.692683	30.163872	579.7394	0.7784	0.3393	0.0089	1.3585
109	-85.675204	30.160380	579.7394	0.7632	0.3486	-0.0066	1.1827
110	-85.665807	30.152943	579.7394	0.7628	0.3384	0.0085	1.3556
111	-85.659346	30.147573	579.7394	0.7631	0.3270	0.0116	1.3559
112	-85.650161	30.142323	579.7394	0.7601	0.3189	0.0151	1.3563
113	-85.642599	30.133681	579.7394	0.7549	0.3054	0.0214	1.3571
114	-85.632242	30.135178	579.7394	0.7526	0.3023	0.0161	1.3569
115	-85.626182	30.137296	579.7394	0.7487	0.3035	0.0172	1.3567
116	-85.618220	30.135649	579.7394	0.7449	0.3056	0.0185	1.3562
117	-85.611382	30.126527	579.7394	0.7195	0.3109	0.0182	1.3559
118	-85.601533	30.122864	579.7394	0.7107	0.3176	0.0192	1.3548

Index	Longitude	Latitude	Alongshore Distance (km)	R^2	RMS Error (m)	Bias (m)	λ
119	-85.604306	30.105767	579.7394	0.6935	0.3083	0.0201	1.3571
120	-85.596407	30.114908	579.7394	0.6997	0.3109	0.0228	1.3568
121	-85.586543	30.116933	579.7394	0.6674	0.3335	0.0152	0.7934
122	-85.569458	30.117952	579.7394	0.6894	0.3281	0.0169	0.7914
123	-85.557387	30.122166	579.7394	0.6999	0.3293	0.0173	0.7906
124	-85.552285	30.124634	579.7394	0.7039	0.3318	0.0175	0.7896
125	-85.542982	30.124783	579.7394	0.6975	0.3395	0.0159	0.7885
126	-85.534699	30.122040	579.7394	0.6782	0.3509	0.0113	0.7869
127	-85.526094	30.115087	579.7394	0.6758	0.3489	0.0089	0.7854
128	-85.523924	30.105639	579.7394	0.6777	0.3415	0.0089	0.7848
129	-85.520316	30.093533	579.7394	0.7275	0.3118	0.0197	0.7840
130	-85.504990	30.092451	579.7394	0.7358	0.3125	0.0166	0.7826
131	-85.496230	30.090515	579.7394	0.7387	0.3132	0.0136	0.7812
132	-85.490687	30.081671	579.7394	0.7335	0.3104	0.0078	0.7792
133	-85.494084	30.069325	579.7394	0.7181	0.3121	0.0129	0.7784
134	-85.492349	30.062179	579.7394	0.7175	0.3089	0.0158	0.7774
135	-85.490203	30.053829	579.7394	0.7230	0.3025	0.0157	0.7760
136	-85.486410	30.046886	579.7394	0.7276	0.2957	0.0146	0.7741
137	-85.483923	30.037624	579.7394	0.7246	0.2938	0.0143	0.7738
138	-85.476060	30.030094	579.7394	0.7061	0.3009	0.0150	0.7725
139	-85.467698	30.031561	579.7394	0.7050	0.3042	0.0145	0.7720
140	-85.456164	30.029258	579.7394	0.7040	0.3079	0.0137	0.7712
141	-85.451575	30.037984	579.7394	0.7078	0.3107	0.0145	0.7709
142	-85.446472	30.043178	579.7394	0.7139	0.3105	0.0151	0.7706
143	-85.440446	30.052736	579.7394	0.7249	0.3098	0.0164	0.7703
144	-85.435893	30.057293	579.7394	0.7263	0.3119	0.0168	0.7701
145	-85.425738	30.053606	579.7394	0.7276	0.3120	0.0154	0.7689
146	-85.416617	30.049037	579.7394	0.7208	0.3172	0.0150	0.7680
147	-85.408213	30.050587	579.7394	0.7181	0.3219	0.0152	0.7671
148	-85.402707	30.052966	579.7394	0.7004	0.3344	0.0132	0.7664
149	-85.396572	30.051376	579.7394	0.6993	0.3364	0.0120	0.7656
150	-85.401853	30.043550	579.7394	0.6990	0.3316	0.0110	0.7664
151	-85.394414	30.031081	579.7394	0.6930	0.3337	0.0104	0.7656
152	-85.409728	30.034772	579.7394	0.6922	0.3307	0.0103	0.7672
153	-85.418669	30.035964	579.7394	0.6926	0.3281	0.0117	0.7681
154	-85.425625	30.044879	579.7394	0.7208	0.3125	0.0144	0.7688
155	-85.434032	30.041303	579.7394	0.7216	0.3087	0.0143	0.7696
156	-85.442020	30.031942	579.7394	0.7079	0.3110	0.0136	0.7701
157	-85.439557	30.022733	579.7394	0.7043	0.3108	0.0124	0.7697
158	-85.437055	30.017304	579.7394	0.7016	0.3122	0.0117	0.7695
159	-85.451396	30.020068	579.7394	0.7011	0.3083	0.0132	0.7707

Index	Longitude	Latitude	Alongshore Distance (km)	R^2	RMS Error (m)	Bias (m)	λ
160	-85.462108	30.018610	579.7394	0.7016	0.3042	0.0132	0.7713
161	-85.468851	30.017341	579.7394	0.7002	0.3022	0.0137	0.7723
162	-85.475195	30.023396	579.7394	0.7028	0.3012	0.0144	0.7723
163	-85.487803	30.027133	579.7394	0.7085	0.2964	0.0156	0.7736
164	-85.497443	30.031089	579.7394	0.7171	0.2925	0.0175	0.7752
165	-85.506323	30.040952	579.7394	0.7156	0.2950	0.0188	0.7768
166	-85.509536	30.046336	579.7394	0.7195	0.2937	0.0175	0.7772
167	-85.515106	30.052634	579.7394	0.7073	0.3036	0.0190	0.7786
168	-85.524733	30.056024	579.7394	0.7095	0.3004	0.0178	0.7798
169	-85.536908	30.060669	579.7394	0.7043	0.3012	0.0190	0.7818
170	-85.529238	30.065104	579.7394	0.7095	0.3040	0.0187	0.7813
171	-85.531886	30.078698	579.7394	0.7267	0.3030	0.0197	0.7837
172	-85.545135	30.080751	579.7394	0.6761	0.3240	0.0148	0.7851
173	-85.554460	30.082360	579.7394	0.6592	0.3255	0.0118	0.7861
174	-85.564517	30.092091	579.7394	0.6537	0.3302	0.0113	0.7886
175	-85.571502	30.093721	579.7394	0.6571	0.3278	0.0129	0.7896
176	-85.579537	30.094901	579.7394	0.6611	0.3245	0.0143	0.7905
177	-85.587525	30.100076	579.7394	0.6621	0.3256	0.0154	0.7922
178	-85.592336	30.095502	579.7394	0.6585	0.3233	0.0145	0.7922
179	-85.603612	30.091274	579.7394	0.6534	0.3200	0.0150	0.7926
180	-85.609706	30.096063	579.7394	0.6900	0.3027	0.0216	1.3578
181	-85.614028	30.102116	579.7394	0.6952	0.3039	0.0206	1.3579
182	-85.621481	30.111941	579.7394	0.7009	0.3057	0.0210	1.3581
183	-85.618930	30.121235	579.7394	0.7149	0.3067	0.0200	1.3574
184	-85.631764	30.120250	579.7394	0.7443	0.2977	0.0172	1.3566
185	-85.642273	30.121774	579.7394	0.7474	0.2961	0.0190	1.3577
186	-85.650946	30.124980	579.7394	0.7505	0.3036	0.0190	1.3573
187	-85.659765	30.125752	579.7394	0.7466	0.3065	0.0180	1.3583
188	-85.673688	30.139093	579.7394	0.7657	0.3283	0.0109	1.3561
189	-85.679639	30.130324	579.7394	0.7590	0.3301	0.0091	1.3565
190	-85.686504	30.124073	579.7394	0.7496	0.3435	-0.0061	1.1852
191	-85.683158	30.115073	579.7394	0.7300	0.3879	-0.0186	1.1903
192	-85.674626	30.107906	579.7394	0.7168	0.4151	-0.0250	1.1925
193	-85.665162	30.102390	579.7394	0.7018	0.4398	-0.0309	1.1937
194	-85.654066	30.098243	579.7394	0.6612	0.4734	-0.0471	0.7033
195	-85.648678	30.091667	579.7394	0.6623	0.4725	-0.0512	0.6969
196	-85.643081	30.087196	579.7394	0.6601	0.4828	-0.0549	0.6920
197	-85.634156	30.082600	579.7394	0.6604	0.4990	-0.0592	0.6869
198	-85.624561	30.078589	579.7394	0.6628	0.5087	-0.0650	0.6845
199	-85.616397	30.073885	579.7394	0.6563	0.5234	-0.0714	0.6853
200	-85.610897	30.066642	579.7394	0.7641	0.4363	-0.0425	0.6957

Index	Longitude	Latitude	Alongshore Distance (km)	R^2	RMS Error (m)	Bias (m)	λ
201	-85.602767	30.066310	579.7394	0.8461	0.3483	-0.0077	0.7038
202	-85.598817	30.062006	579.7394	0.8414	0.3557	-0.0174	0.7016
203	-85.607222	30.066004	579.7394	0.8269	0.3671	-0.0170	0.6998
204	-85.604663	30.061049	579.7394	0.7926	0.4613	0.0437	0.7086
205	-85.596924	30.058829	579.7394	0.7971	0.4751	0.0506	0.7098
206	-85.597283	30.058476	579.7394	0.7913	0.4803	0.0505	0.7096
207	-85.604048	30.058713	579.7394	0.7574	0.5152	-0.1151	0.7048
208	-85.613027	30.063363	579.7394	0.7503	0.4458	-0.0459	0.6944
209	-85.616219	30.065839	579.7394	0.6670	0.5135	-0.0608	0.6924
210	-85.621433	30.071570	579.7394	0.6522	0.5135	-0.0666	0.6811
211	-85.636619	30.074766	579.7394	0.6647	0.4800	-0.0572	0.6811
212	-85.648454	30.082620	579.7394	0.6581	0.4764	-0.0547	0.6894
213	-85.656948	30.084221	579.7394	0.6482	0.4767	-0.0563	0.6896
214	-85.667120	30.089628	579.7394	0.6639	0.4432	-0.0418	0.7003
215	-85.683802	30.093371	579.7394	0.6833	0.4144	-0.0307	0.7075
216	-85.695554	30.103008	579.7394	0.6759	0.4026	-0.0231	0.7173
217	-85.704494	30.105538	579.7394	0.6750	0.4015	-0.0191	0.7202
218	-85.710098	30.118788	579.7394	0.7391	0.3474	-0.0069	1.1837
219	-85.719023	30.123786	579.7394	0.7498	0.3542	0.0055	1.3617
220	-85.583923	30.053393	579.7394	0.6739	0.6062	0.0168	0.8377
221	-85.575973	30.048000	579.7394	0.7383	0.5360	0.0209	0.7123
222	-85.568619	30.041159	579.7394	0.7602	0.4970	0.0440	0.7070
223	-85.560894	30.036353	579.7394	0.7770	0.4649	0.0368	0.7013
224	-85.552137	30.030563	579.7394	0.7977	0.4318	0.0331	0.6961
225	-85.542382	30.024618	579.7394	0.8046	0.4135	0.0297	0.6903
226	-85.535760	30.015294	579.7394	0.8101	0.3923	0.0197	0.6853
227	-85.527782	30.007022	579.7394	0.8038	0.3886	0.0151	0.6782
228	-85.517795	30.002594	579.7394	0.8246	0.3696	0.0148	0.6689
229	-85.508912	29.993602	579.7394	0.8182	0.3672	0.0047	0.6565
230	-85.501182	29.985909	579.7394	0.7856	0.3977	0.0019	0.6440
231	-85.497327	29.987442	579.7394	0.7957	0.3947	0.0011	0.6419
232	-85.487937	29.979546	579.7394	0.7740	0.4181	-0.0022	0.3145
233	-85.479236	29.974541	579.7394	0.7672	0.4320	-0.0070	0.3096
234	-85.469457	29.971388	579.7394	0.7620	0.4539	-0.0164	0.3059
235	-85.476862	29.972825	579.7394	0.7659	0.4354	-0.0094	0.3081
236	-85.489050	29.975959	579.7394	0.7638	0.4225	-0.0046	0.3140
237	-85.497129	29.982672	579.7394	0.7813	0.4050	0.0019	0.6380
238	-85.498569	29.978528	579.7394	0.7720	0.4040	0.0007	0.6380
239	-85.490666	29.972845	579.7394	0.7899	0.3894	-0.0014	0.6289
240	-85.481303	29.969761	579.7394	0.7816	0.4049	-0.0043	0.3135
241	-85.470408	29.965923	579.7394	0.7925	0.4078	-0.0084	0.3137

Index	Longitude	Latitude	Alongshore Distance (km)	R^2	RMS Error (m)	Bias (m)	λ
242	-85.458390	29.964191	579.7394	0.7677	0.4522	-0.0200	0.3107
243	-85.465789	29.963961	579.7394	0.7670	0.4417	-0.0170	0.3135
244	-85.477536	29.963907	579.7394	0.7830	0.4009	-0.0029	0.3111
245	-85.488691	29.968277	579.7394	0.7884	0.3889	-0.0031	0.3152
246	-85.499064	29.972782	579.7394	0.7642	0.4033	-0.0026	0.6349
247	-85.505646	29.983011	579.7394	0.7742	0.4008	0.0016	0.6461
248	-85.516766	29.982864	579.7394	0.7885	0.3764	0.0125	0.6589
249	-85.530119	29.991352	579.7394	0.7923	0.3695	0.0133	0.6772
250	-85.541256	29.998863	579.7394	0.7989	0.3684	0.0131	0.6828
251	-85.549357	30.005878	579.7394	0.7978	0.3697	0.0161	0.6875
252	-85.550947	30.014068	579.7394	0.7973	0.4005	0.0203	0.6915
253	-85.556493	30.017448	579.7394	0.7998	0.3970	0.0255	0.6944
254	-85.565613	30.022089	579.7394	0.8021	0.3768	0.0164	0.6963
255	-85.569674	30.029950	579.7394	0.7724	0.4550	0.0344	0.7041
256	-85.573002	30.038523	579.7394	0.7492	0.4974	0.0404	0.7081
257	-85.579067	30.041054	579.7394	0.7442	0.5133	0.0432	0.7112
258	-85.579787	30.047703	579.7394	0.6794	0.5842	0.0132	0.8392

Table B-2 Dimensionless surge response function regression parameters for bay interior locations.

Index	x' < 0					x' >= 0				
	α	β	m	a_1	b_1	α	β	m	a_2	b_2
0	0.10	0.05	-2.1432	1.6188	0.3452	0.05	1.00	4.0129	-1.9687	-1.6494
1	0.10	0.05	-2.0609	1.8462	0.3710	0.05	1.00	3.9624	-2.0623	-1.6100
2	0.10	0.05	-2.0371	1.9287	0.3722	0.05	1.00	3.9114	-2.1293	-1.5467
3	0.10	0.05	-2.1479	2.0534	0.3696	0.05	1.00	4.1657	-1.9696	-1.5405
4	0.00	1.00	-0.3964	-0.3131	0.6898	0.05	1.00	3.8321	-2.2361	-1.4604
5	0.10	0.05	-3.2184	1.4001	0.4637	0.05	1.00	4.1460	-1.4078	-1.3613
6	0.10	0.05	-3.1897	1.4288	0.4570	0.05	1.00	3.6666	-2.6346	-1.2425
7	0.15	0.10	-2.0153	1.4876	0.4530	0.05	1.00	3.6225	-2.5948	-1.2311
8	0.10	0.05	-2.9455	1.7393	0.4449	0.05	1.00	3.5488	-2.7005	-1.1640
9	0.15	0.05	-1.8258	8.5065	0.1816	0.00	1.00	3.1015	-3.2020	-0.7815
10	0.15	0.05	-1.7928	8.2793	0.1886	0.00	1.00	2.8829	3.0416	-1.2698
11	0.15	0.05	-1.7679	8.2375	0.1972	0.00	1.00	2.9647	3.9855	-1.3652
12	0.20	0.05	-1.4846	8.0696	0.1949	0.00	1.00	2.9382	3.8785	-1.3163
13	0.00	1.00	-0.1808	-1.6569	0.8114	0.00	1.00	2.9248	4.4517	-1.3559
14	0.10	0.05	-0.5987	-1.7130	0.8112	0.00	1.00	2.7374	3.2112	-1.1452
15	1.00	0.00	-0.1746	-1.8368	0.8352	0.00	1.00	2.7116	4.0117	-1.2419
16	0.00	1.00	-0.1620	0.0251	0.7239	0.00	1.00	2.6929	3.8669	-1.2047
17	0.00	1.00	-0.1440	0.1732	0.7290	0.00	1.00	2.6376	4.1390	-1.2101
18	0.00	1.00	-0.1504	0.3354	0.7299	0.00	1.00	2.6003	4.5772	-1.2421
19	0.00	1.00	-0.1211	0.4598	0.7423	0.00	1.00	2.5354	3.7060	-1.1058
20	0.00	1.00	-0.1357	0.5715	0.7490	0.00	1.00	2.4978	4.4496	-1.1795
21	0.00	1.00	-0.1836	0.7890	0.6387	0.00	1.00	3.1188	3.6688	-1.6181
22	0.00	1.00	-0.1528	0.9771	0.6587	0.00	1.00	2.9954	2.5192	-1.8044
23	0.00	1.00	-0.1340	0.9420	0.6719	0.00	1.00	2.7437	2.9994	-1.5195
24	0.00	1.00	-0.3705	0.7521	0.8227	0.00	1.00	2.6737	3.3523	-1.5703
25	0.00	1.00	-0.4721	-0.5796	1.1765	0.00	1.00	2.7792	3.9764	-1.6448
26	0.00	1.00	-0.4616	-0.4593	1.1529	0.00	1.00	2.8213	3.4681	-1.6315
27	0.00	1.00	-0.4363	0.1642	0.9723	0.20	1.00	3.1207	8.5537	-2.2752
28	1.00	0.80	1.4785	0.2510	0.9764	0.20	1.00	2.8913	9.8992	-2.3467
29	0.00	1.00	-0.4553	-3.7451	1.3197	0.00	1.00	2.7498	-2.5677	-1.5338
30	0.00	1.00	-0.4664	0.6896	0.7161	0.00	1.00	2.3960	-4.2035	-1.3286
31	0.00	0.95	-0.4503	0.5429	0.6861	0.00	1.00	2.3955	-3.5491	-1.5170
32	0.00	0.95	-0.4247	0.8334	0.7264	0.00	1.00	2.4683	-2.9875	-1.5396
33	0.00	0.95	-0.4141	0.9720	0.7353	0.00	1.00	2.6303	-3.8894	-1.2641
34	0.00	0.45	-0.4947	-2.6308	0.9821	0.00	1.00	2.0188	-0.9830	-1.5048
35	0.00	0.55	-0.4179	1.5333	0.4631	0.00	1.00	1.8752	-1.1308	-1.5052
36	0.00	0.50	-0.4302	1.7311	0.4785	0.00	1.00	1.7227	0.1687	-1.6149

Index	x' < 0					x' >= 0				
	α	β	m	a_1	b_1	α	β	m	a_2	b_2
37	0.00	0.05	-2.3916	-6.3640	1.2481	0.00	1.00	2.7252	-1.7111	-1.8535
38	0.00	0.05	-2.5524	-2.6030	0.9745	0.00	1.00	2.5291	-0.3176	-2.0937
39	0.00	0.05	-2.2559	-1.6933	0.8867	0.00	1.00	1.9804	5.2401	-2.6979
40	0.05	0.00	3.5769	-1.0250	0.7835	0.00	1.00	2.5027	-1.8505	-2.0817
41	0.05	0.00	5.0172	-3.5603	0.9248	0.00	1.00	2.1043	4.1357	-2.4207
42	0.05	0.00	4.8380	-3.0711	0.8599	0.00	1.00	2.5716	1.9381	-2.4526
43	0.05	0.00	3.9673	-2.5069	0.7823	0.00	1.00	2.8909	0.2061	-2.2449
44	0.05	0.00	5.6394	1.2470	1.1376	0.00	1.00	2.7868	2.1388	-2.5180
45	0.05	0.00	6.0632	-2.9446	1.3836	0.00	1.00	2.7628	-0.0820	-1.7699
46	0.05	0.00	6.3669	-5.0071	1.5336	0.00	1.00	2.8333	1.5460	-1.7331
47	0.05	0.00	6.9946	-6.1342	1.6440	0.00	1.00	2.8172	1.3116	-1.4367
48	0.05	0.00	7.3237	-5.9248	1.6186	0.00	1.00	3.0112	1.8682	-1.7071
49	0.00	0.25	-0.9689	-5.7379	1.6091	0.00	1.00	3.0683	1.8904	-1.5879
50	0.00	0.05	-3.3836	-3.5673	1.4243	0.00	1.00	2.8466	3.7803	-2.0460
51	0.05	0.05	-3.2082	-1.9480	1.0234	0.00	1.00	3.1542	0.9979	-1.7376
52	0.05	0.05	-3.2555	-0.8163	0.9149	0.00	1.00	3.0484	0.5502	-1.4606
53	0.05	0.05	-2.9341	-2.1787	1.0240	0.00	1.00	2.9912	0.5308	-1.2835
54	0.05	0.05	-2.7699	-1.3456	1.0759	0.00	1.00	2.7022	0.8783	-1.8119
55	0.00	0.05	-2.0876	-8.1485	1.6316	0.00	1.00	2.7735	0.2738	-1.4551
56	0.00	0.05	-2.1064	-5.9972	1.4368	0.00	1.00	2.7722	-0.7768	-1.3921
57	0.05	0.05	-2.6476	-0.0301	0.8675	0.00	1.00	2.8103	-1.1240	-1.4000
58	0.10	0.05	-2.6431	1.2059	0.6874	0.00	1.00	2.9005	-1.0555	-1.1860
59	0.05	0.05	-5.3775	0.5634	0.6943	0.00	0.80	1.9752	-0.1009	-1.3852
60	0.05	0.05	-5.5589	0.0235	0.6908	0.10	1.00	2.0924	1.2056	-1.5704
61	0.05	0.05	-5.4056	0.3646	0.6829	0.00	0.75	1.9578	0.0288	-1.4755
62	0.10	0.05	-4.6892	0.5344	0.6299	0.00	0.65	1.9802	-0.6091	-1.5738
63	0.10	0.05	-2.7563	0.2526	0.6205	0.00	1.00	2.7005	0.1770	-1.4631
64	0.10	0.05	-2.7963	0.1439	0.6159	0.00	1.00	3.0076	-1.9944	-1.1881
65	0.10	0.05	-2.7878	-0.5107	0.5873	0.00	1.00	2.6950	0.1826	-1.4387
66	0.10	0.05	-2.7910	0.0928	0.5795	0.00	1.00	2.5528	0.7293	-1.5234
67	0.10	0.05	-2.4798	0.7404	0.5708	0.00	1.00	2.9865	-3.2080	-1.2014
68	0.10	0.05	-2.4645	0.5755	0.5528	0.00	1.00	2.6001	-1.0342	-1.1961
69	0.05	0.05	-2.4029	0.4974	0.5873	0.00	0.90	2.8171	-3.1951	-1.2240
70	0.05	0.05	-2.3945	0.5486	0.6419	0.00	1.00	2.9296	-3.3695	-1.2254
71	0.05	0.05	-1.9924	-0.2271	0.6564	0.00	0.80	2.6579	-2.9101	-1.1879
72	0.05	0.05	-3.5443	-0.7478	0.6166	0.15	1.00	2.1216	0.9089	-1.7547
73	0.05	0.05	-3.3426	-1.0322	0.6061	0.10	1.00	2.1127	0.1235	-1.5087
74	0.05	0.05	-3.4045	-1.1668	0.5891	0.15	1.00	2.2605	-0.1943	-1.4989
75	0.05	0.05	-3.5026	-1.2589	0.5816	0.20	1.00	2.3843	-0.4717	-1.4858
76	0.05	0.05	-3.6336	-1.4588	0.5962	0.25	1.00	2.6289	-1.1454	-1.3016
77	0.05	0.05	-3.7352	-1.5583	0.6002	0.00	0.40	2.4059	-1.3892	-1.1683

Index	x' < 0					x' >= 0				
	α	β	m	a_1	b_1	α	β	m	a_2	b_2
78	0.05	0.05	-3.6357	-1.7002	0.6216	0.20	1.00	2.6109	-1.3844	-1.0868
79	0.10	0.15	-1.5504	-1.8064	0.6259	0.00	0.50	2.2673	-1.3260	-0.9784
80	0.30	1.00	-0.8175	-2.3938	0.6993	0.00	0.60	2.2198	-0.8509	-0.9321
81	0.25	1.00	-0.6931	-2.9696	0.7452	0.10	1.00	2.3874	-0.1290	-0.9956
82	0.25	1.00	-0.6523	-3.0525	0.7404	0.00	0.60	2.1850	-0.1331	-0.9941
83	0.30	1.00	-0.6436	-3.1588	0.7516	0.00	0.50	2.3342	-0.2352	-0.9794
84	0.30	1.00	-0.6073	-3.2369	0.7707	0.00	0.40	2.5916	-0.3398	-0.9595
85	0.20	1.00	-0.5863	-3.1198	0.7774	0.00	0.50	2.3452	-0.3111	-0.9624
86	0.20	1.00	-0.6767	-2.7764	0.7482	0.00	0.65	2.1571	-0.3343	-0.9667
87	0.20	1.00	-0.7263	-2.4208	0.7157	0.00	0.60	2.1890	-0.6741	-0.9902
88	0.25	0.70	-0.7569	-2.1227	0.6849	0.15	1.00	2.4907	-0.8113	-1.0598
89	0.05	0.05	-3.4561	-1.8256	0.6494	0.20	1.00	2.5996	-0.9911	-1.1293
90	0.05	0.05	-3.3790	-1.4365	0.6113	0.25	1.00	2.6933	-1.1204	-1.3297
91	0.05	0.05	-3.3107	-1.3775	0.6113	0.25	1.00	2.6255	-0.7238	-1.4453
92	0.05	0.05	-3.3438	-1.2051	0.6010	0.20	1.00	2.4308	-0.4236	-1.4614
93	0.05	0.05	-3.1414	-0.7741	0.5814	0.15	1.00	2.2350	-0.3211	-1.4128
94	0.05	0.05	-3.1372	-0.5358	0.5859	0.10	1.00	2.1368	-0.3187	-1.3905
95	0.05	0.05	-3.1758	-0.2065	0.5977	0.20	1.00	2.1847	1.0011	-1.8152
96	0.05	0.05	-3.2576	0.0661	0.6397	0.25	1.00	2.3710	0.2811	-1.8141
97	0.05	0.05	-3.3409	0.0433	0.6804	0.30	1.00	2.7715	-2.0243	-1.6838
98	0.05	0.05	-1.5861	0.1893	0.7075	0.00	0.75	2.5433	-2.9744	-1.2547
99	0.05	0.05	-1.8929	0.9905	0.5867	0.00	0.90	2.6574	-3.4828	-1.2392
100	0.05	0.05	-2.1003	1.1098	0.6239	0.00	1.00	2.7022	-3.5735	-1.1562
101	0.05	0.05	-2.3032	1.2273	0.6861	0.00	1.00	2.6706	-3.9756	-1.0692
102	0.05	0.05	-2.4187	1.6919	0.7125	0.00	1.00	2.3158	-2.0565	-1.1909
103	0.05	0.05	-2.1123	1.4792	0.7545	0.00	1.00	2.2746	-2.2411	-1.1620
104	0.05	0.05	-1.9804	2.7847	0.6373	0.00	1.00	2.2469	-2.3357	-1.1311
105	0.05	0.05	-1.6831	2.7372	0.5816	0.00	1.00	2.2418	-2.2424	-1.1684
106	0.00	0.05	-1.3960	2.6952	0.5741	0.00	1.00	2.2852	-2.1799	-1.2192
107	0.05	0.05	-1.3862	4.3141	0.3913	0.00	1.00	2.3213	-2.3523	-1.2468
108	0.00	0.05	-0.9692	4.4716	0.3657	0.05	1.00	2.4356	-2.2030	-1.2707
109	0.00	0.30	-0.6463	2.4238	0.5982	0.30	1.00	2.1453	-1.5845	-1.6426
110	0.00	0.05	-0.8134	2.5700	0.5936	0.05	1.00	2.3587	-1.9664	-1.3212
111	0.05	0.05	-1.0125	3.1135	0.5611	0.00	1.00	2.2358	-1.8057	-1.2980
112	0.10	0.05	-1.5387	3.4901	0.5448	0.00	1.00	2.2146	-1.9008	-1.2664
113	0.15	0.05	-1.7469	3.8735	0.5576	0.00	1.00	2.1782	-2.2243	-1.1751
114	0.15	0.05	-0.8900	-2.5626	0.9823	0.00	1.00	2.1568	-2.0897	-1.1950
115	0.15	0.05	-0.9701	-2.1386	0.9990	0.00	1.00	2.1455	-2.0564	-1.2070
116	0.20	0.05	-0.9435	-1.6956	0.9810	0.00	1.00	2.1423	-1.9786	-1.2281
117	0.10	0.05	-1.1751	-0.0517	1.0710	0.00	1.00	2.0265	-1.0948	-1.3455
118	0.15	0.05	-1.1264	-0.0117	1.0631	0.00	1.00	2.0299	-1.0987	-1.3788

Index	x' < 0					x' >= 0				
	α	β	m	a_1	b_1	α	β	m	a_2	b_2
119	0.10	0.05	-1.0730	-0.8823	1.2566	0.00	1.00	1.8873	-0.4873	-1.4534
120	0.10	0.05	-1.0854	-1.2929	1.2602	0.00	1.00	1.9888	-1.4037	-1.3856
121	0.00	0.05	1.1282	2.7561	0.7444	0.05	1.00	0.9604	12.3314	-3.0081
122	1.00	0.00	-0.1482	3.0233	0.6883	0.00	1.00	0.9153	10.2746	-2.5898
123	1.00	0.00	-0.1786	3.1839	0.6379	0.00	1.00	0.9188	8.7554	-2.3607
124	1.00	0.00	-0.1949	3.3777	0.5967	0.00	1.00	0.9246	8.5563	-2.2656
125	1.00	0.00	-0.2166	3.3965	0.5746	0.00	1.00	0.9215	11.5098	-2.5589
126	1.00	0.00	-0.2393	3.3185	0.5631	0.25	1.00	1.2200	17.3606	-3.2071
127	1.00	0.00	-0.2697	2.8161	0.6034	0.30	1.00	1.3124	19.7367	-3.2886
128	1.00	0.00	-0.2771	2.3756	0.6646	0.25	1.00	1.2137	18.1997	-3.2137
129	1.00	0.00	-0.4041	2.0602	0.5594	0.00	0.95	0.9766	-4.5858	-1.0076
130	1.00	0.00	-0.3914	1.6910	0.6022	0.00	0.90	1.0348	-2.9672	-0.8571
131	1.00	0.15	-0.5911	1.1066	0.6541	0.00	0.90	1.0411	-1.4344	-0.8993
132	0.15	0.05	-2.1365	0.1586	0.7032	0.00	0.90	0.9458	5.2760	-1.6593
133	1.00	0.35	-1.1016	0.6913	0.6036	0.00	0.85	0.9132	4.5305	-1.7950
134	1.00	0.00	-0.2553	2.8407	0.4021	0.00	0.85	0.9043	3.4143	-1.7242
135	1.00	0.00	-0.1818	2.7917	0.3434	0.00	0.80	0.9211	0.2283	-1.4531
136	0.00	1.00	0.2720	2.5963	0.3517	0.00	0.80	0.9361	-0.9924	-1.2896
137	0.00	1.00	0.2613	2.3886	0.3576	0.00	0.80	0.9542	-0.1781	-1.2526
138	1.00	0.00	-0.2187	1.7677	0.4935	0.00	0.80	0.9136	4.3757	-1.7710
139	1.00	0.05	-0.2667	1.5733	0.5236	0.00	0.80	0.9016	4.3749	-1.8255
140	1.00	0.15	-0.2674	1.7855	0.5595	0.00	0.80	0.8880	3.3880	-1.7952
141	1.00	0.15	-0.3184	1.5497	0.5407	0.00	0.80	0.8875	2.3539	-1.7396
142	1.00	0.10	-0.2739	1.6796	0.5190	0.00	0.80	0.9102	2.7301	-1.6547
143	1.00	0.00	-0.2253	1.7126	0.4641	0.00	0.80	0.9633	2.6893	-1.4347
144	1.00	0.00	-0.2188	1.8274	0.4275	0.00	0.80	0.9491	1.8072	-1.4339
145	0.00	1.00	0.2841	2.6119	0.4011	0.00	0.75	0.9654	-0.0577	-1.2858
146	0.00	1.00	0.2755	3.3130	0.4068	0.00	0.75	0.9378	2.2252	-1.5170
147	0.00	1.00	0.2580	3.5138	0.4155	0.00	0.75	0.9073	2.5040	-1.6552
148	0.00	1.00	0.2727	3.5025	0.4139	0.00	0.80	0.8299	8.3431	-2.4263
149	0.00	1.00	0.2337	3.3405	0.4536	0.00	0.75	0.8447	8.5514	-2.4254
150	0.00	1.00	0.1832	3.2613	0.4758	0.00	0.75	0.8694	9.7697	-2.3981
151	1.00	0.35	-0.3423	2.8312	0.6480	0.00	0.75	0.8643	9.9434	-2.4121
152	0.00	1.00	0.1457	3.1926	0.4997	0.00	0.75	0.8644	9.6145	-2.4121
153	0.00	1.00	0.1631	3.3252	0.4790	0.00	0.75	0.8648	9.3904	-2.4125
154	0.00	1.00	0.2115	2.6793	0.4714	0.00	0.75	0.9449	1.9143	-1.4736
155	0.00	1.00	0.2024	2.5736	0.4735	0.00	0.75	0.9651	0.5616	-1.3137
156	0.00	1.00	0.2125	2.9836	0.4715	0.00	0.75	0.9082	1.4343	-1.6151
157	0.00	1.00	0.1331	3.1743	0.5219	0.00	0.75	0.9062	0.9418	-1.5554
158	1.00	0.55	-0.9223	1.0998	0.7428	0.00	0.75	0.9160	0.2867	-1.4427
159	0.00	1.00	0.1658	3.2938	0.4964	0.00	0.75	0.9117	2.9460	-1.6847

Index	x' < 0					x' >= 0				
	α	β	m	a_1	b_1	α	β	m	a_2	b_2
160	1.00	0.15	-0.2308	1.9487	0.5769	0.00	0.80	0.9045	4.0553	-1.7392
161	1.00	0.25	-0.4434	1.3024	0.6349	0.00	0.80	0.9153	4.7671	-1.7731
162	1.00	0.10	-0.2926	1.5684	0.5639	0.00	0.80	0.9141	4.6600	-1.7762
163	1.00	0.00	-0.1950	1.9983	0.4838	0.00	0.80	0.9391	3.9657	-1.6283
164	1.00	0.00	-0.1645	2.3909	0.4482	0.00	0.75	1.0044	0.7318	-1.1893
165	1.00	0.00	-0.1884	2.8344	0.3706	0.00	0.80	0.9777	2.2387	-1.3580
166	0.00	1.00	0.3072	3.0713	0.3097	0.00	0.80	0.9739	2.0797	-1.3819
167	1.00	0.00	-0.2609	3.1137	0.3639	0.00	0.80	0.9308	5.7112	-1.8777
168	1.00	0.15	-0.6637	0.7422	0.5645	0.00	0.85	0.9438	6.1165	-1.8343
169	1.00	0.20	-0.8993	0.2228	0.6154	0.00	0.85	0.9660	7.1347	-1.8731
170	1.00	0.20	-0.9865	0.1299	0.6405	0.00	0.85	0.9623	4.7626	-1.6971
171	1.00	0.10	-0.6102	1.0349	0.6116	0.00	0.90	1.0668	-2.3655	-0.8137
172	1.00	0.00	-0.4017	1.6131	0.5644	0.25	1.00	1.1417	14.2049	-3.2358
173	1.00	0.00	-0.1582	1.4307	0.8562	0.25	1.00	1.1512	14.7402	-3.3371
174	1.00	0.00	-0.1410	1.9977	0.8100	0.35	1.00	1.3142	16.8828	-3.6061
175	0.00	0.05	0.8432	2.0842	0.8113	0.25	1.00	1.1530	13.2391	-3.3155
176	0.00	0.05	0.9397	2.0133	0.8340	0.10	1.00	0.9817	11.5966	-3.1201
177	0.00	0.05	1.0680	2.2162	0.8249	0.05	1.00	0.9371	10.8159	-3.0170
178	0.00	0.05	1.1904	1.8729	0.8700	0.05	1.00	0.9403	10.9728	-3.0573
179	0.00	0.05	1.3968	1.4652	0.9390	0.00	1.00	0.8939	10.4037	-3.0325
180	0.10	0.05	-1.0237	-1.2146	1.3423	0.00	1.00	1.8884	-0.9237	-1.4160
181	0.10	0.05	-1.0096	-0.9171	1.2841	0.00	1.00	1.8971	-0.7414	-1.4222
182	0.10	0.05	-0.8559	-0.8815	1.2463	0.00	1.00	1.9370	-0.8212	-1.3943
183	0.10	0.05	-0.8901	-0.5859	1.1662	0.00	1.00	2.0614	-1.7849	-1.2986
184	0.15	0.05	-0.9872	-2.5893	1.0382	0.00	1.00	2.0934	-1.8156	-1.2200
185	0.15	0.05	-1.1298	-0.9988	0.9502	0.00	1.00	2.1220	-2.1259	-1.1810
186	0.10	0.05	-1.6720	3.2196	0.6627	0.00	1.00	2.1263	-1.9033	-1.2193
187	0.10	0.05	-1.4002	2.6244	0.7491	0.00	1.00	2.1583	-2.1404	-1.2140
188	0.00	0.05	-0.7945	3.9200	0.4649	0.00	1.00	2.2336	-2.0722	-1.3038
189	0.00	0.05	-0.9120	4.2893	0.4619	0.05	1.00	2.3307	-2.0299	-1.3026
190	0.00	0.75	-0.5147	4.8994	0.4076	0.35	1.00	2.2943	-2.2067	-1.5861
191	0.00	1.00	-0.5896	4.0710	0.5019	0.60	1.00	3.1667	-3.6787	-1.4392
192	0.00	1.00	-0.6138	3.6179	0.5498	0.70	1.00	3.3838	-4.8754	-1.3430
193	0.00	1.00	-0.6231	3.2663	0.5846	0.80	1.00	3.6846	-4.6592	-1.3769
194	0.00	1.00	-0.3088	0.4250	0.5354	1.00	1.00	2.9399	7.1116	-2.4032
195	1.00	0.50	0.5084	0.3814	0.5384	1.00	1.00	2.9624	6.4211	-2.3398
196	1.00	0.60	0.6390	0.3816	0.5377	1.00	1.00	3.0921	6.3357	-2.2932
197	1.00	0.65	0.6487	0.4502	0.5251	1.00	1.00	3.3130	7.4216	-2.2923
198	1.00	0.80	0.7612	0.1027	0.5440	1.00	1.00	3.5147	9.1276	-2.2373
199	1.00	0.85	0.8352	-0.0212	0.5474	0.95	1.00	3.6911	11.6452	-2.3160
200	0.00	0.05	1.0934	0.2565	0.4113	0.15	1.00	1.4730	4.3029	-1.4189

Index	x' < 0					x' >= 0				
	α	β	m	a_1	b_1	α	β	m	a_2	b_2
201	0.75	0.85	0.5808	0.3880	0.3214	0.00	1.00	1.0625	-3.9213	-0.3331
202	0.65	0.60	0.7205	0.2163	0.3266	0.00	1.00	1.0805	-3.9033	-0.3521
203	1.00	0.00	-0.1331	0.6668	0.2972	0.00	1.00	1.1663	-4.9929	-0.2337
204	1.00	0.05	-0.7511	0.0412	0.3689	0.60	1.00	1.1960	8.7081	-1.8253
205	1.00	0.00	-1.0208	0.1822	0.4053	0.40	1.00	0.7219	0.4604	-1.6208
206	1.00	0.00	-1.0127	0.2666	0.3988	0.55	1.00	0.8040	-2.6996	-1.6003
207	0.15	0.05	3.0634	0.7820	0.2966	1.00	0.35	-0.7523	-2.7629	-0.4870
208	0.00	0.05	1.1905	0.5668	0.4391	0.15	1.00	1.4477	1.6458	-1.4766
209	0.00	0.05	1.3967	0.5169	0.4855	0.60	1.00	2.5545	14.5906	-2.7175
210	1.00	0.85	0.6496	0.4262	0.5176	0.95	1.00	3.5362	10.2608	-2.3359
211	1.00	0.75	0.8359	0.3371	0.5377	1.00	1.00	3.0602	6.1426	-2.2933
212	1.00	0.60	0.6838	0.2780	0.5491	1.00	1.00	3.0369	5.0319	-2.2396
213	1.00	0.55	0.5039	0.0474	0.5982	1.00	1.00	3.0263	3.1870	-2.2218
214	0.00	1.00	-0.3475	0.1370	0.5761	0.90	1.00	2.4680	3.1295	-2.2366
215	0.00	1.00	-0.5240	0.8333	0.5469	0.70	1.00	1.9372	-2.6500	-1.7119
216	0.00	1.00	-0.7986	2.0283	0.4623	0.60	1.00	1.6867	-1.0515	-2.0028
217	0.00	1.00	-1.1086	4.4871	0.3061	0.45	1.00	1.5256	-3.4932	-1.6120
218	0.00	0.50	-0.6848	6.7049	0.4030	0.30	1.00	2.1770	-2.3914	-1.4936
219	0.00	0.05	-2.0109	6.8584	0.4773	0.00	1.00	2.3166	-2.3813	-1.3829
220	0.05	0.05	5.3148	-1.4841	1.3624	0.05	0.00	-3.3287	10.4326	-2.3126
221	0.00	0.05	5.1970	-1.0511	1.0181	0.05	0.00	-3.5980	9.8651	-2.2826
222	0.00	0.05	37.9654	-1.0637	0.9804	0.00	1.00	0.3462	9.1928	-2.2722
223	0.00	0.05	4.2343	-0.8927	0.8703	0.00	1.00	0.3899	8.6057	-2.2381
224	0.00	0.05	3.5114	-0.8028	0.7928	0.00	1.00	0.4461	6.9734	-2.0312
225	0.00	0.05	3.6871	-0.8455	0.7724	0.00	1.00	0.4825	5.4879	-1.9053
226	1.00	0.00	-0.2735	-1.4515	0.8849	0.00	1.00	0.5641	4.1479	-1.7918
227	0.00	0.05	2.3703	-1.1782	0.9120	0.00	1.00	0.6321	1.7722	-1.5439
228	1.00	0.00	-0.4763	-1.0487	0.8878	0.00	1.00	0.7047	-0.3164	-1.2551
229	1.00	0.70	2.3596	0.8433	0.4051	0.00	1.00	0.7975	-3.2619	-0.9400
230	1.00	0.70	2.5386	2.0205	0.3175	0.00	1.00	0.8097	3.3406	-1.6562
231	1.00	0.75	2.8015	1.7854	0.3343	0.00	1.00	0.8716	5.4899	-1.5606
232	1.00	0.50	3.2444	2.9623	-0.5037	0.00	1.00	0.8776	3.9681	-1.4676
233	1.00	0.55	2.9156	2.8470	-0.4703	0.00	1.00	0.8203	3.6534	-1.4531
234	1.00	0.55	2.7455	2.8363	-0.4515	0.30	1.00	1.0558	2.6542	-1.4217
235	1.00	0.55	2.7429	2.8032	-0.4523	0.05	1.00	0.8517	3.3942	-1.4370
236	1.00	0.50	2.7601	2.7826	-0.4523	0.00	1.00	0.8816	4.0581	-1.5809
237	1.00	0.75	2.3717	2.4630	0.3060	0.00	1.00	0.8658	2.9806	-1.5861
238	1.00	0.70	2.0578	2.5834	0.3116	0.00	1.00	0.8551	2.0901	-1.6250
239	1.00	0.80	2.1215	2.2979	0.4027	0.00	1.00	1.1006	-1.5831	-0.6927
240	1.00	0.60	1.6827	2.2283	-0.2481	0.00	1.00	0.8932	3.5185	-1.3513
241	1.00	0.70	1.4052	1.9457	-0.1542	0.10	1.00	1.0774	2.5387	-1.0026

Index	x' < 0					x' >= 0				
	α	β	m	a_1	b_1	α	β	m	a_2	b_2
242	1.00	0.80	1.4008	1.8183	-0.1050	0.40	1.00	1.2473	3.3371	-1.5544
243	1.00	0.85	1.2953	1.7401	-0.0757	0.30	1.00	1.1772	3.4413	-1.5805
244	0.00	0.05	2.0234	1.7398	-0.0506	0.00	1.00	0.9308	2.6550	-1.0673
245	1.00	0.75	1.5320	1.9665	-0.1356	0.00	1.00	1.0059	2.9284	-1.0950
246	1.00	0.75	1.9600	2.3579	0.3803	0.00	1.00	0.8865	1.2985	-1.6114
247	1.00	0.70	2.2049	2.3226	0.3314	0.00	1.00	0.8100	3.2115	-1.8163
248	0.00	0.05	3.0329	0.9142	0.8055	0.00	1.00	0.8681	0.6679	-1.3833
249	0.00	0.05	2.3055	-1.3801	1.0319	0.00	1.00	0.7380	1.5573	-1.3349
250	0.00	0.05	3.2592	-1.0008	0.9801	0.00	1.00	0.7658	1.1614	-1.2468
251	0.00	0.05	3.3696	-0.8927	0.9236	0.00	1.00	0.7389	2.4174	-1.3634
252	0.00	0.05	1.3730	-1.6424	0.9517	0.00	1.00	0.6703	3.7802	-1.5589
253	0.00	0.05	1.7544	-1.4345	0.9153	0.00	1.00	0.6391	4.9685	-1.6316
254	1.00	0.00	-0.2047	-1.5326	0.8807	0.00	1.00	0.6663	4.3299	-1.6205
255	0.00	0.05	4.8443	-1.3459	0.9721	0.00	1.00	0.5088	7.7209	-1.9709
256	0.00	0.05	5.4325	-1.2280	1.0109	0.00	1.00	0.3735	9.0765	-2.2796
257	0.00	0.05	5.2736	-1.1939	0.9918	0.00	1.00	0.3572	9.0057	-2.2965
258	0.05	0.05	5.9242	-1.5881	1.3788	0.05	0.00	-3.5851	9.8269	-2.2985

Table B-3 Surge response function least-squares based model distribution and coefficients for bay interior locations.

	x' < 0		$\zeta' = c_1 e^{c_2(x'+c_3)}$			x' >= 0		$\zeta' = \begin{cases} c_1 e^{(x')c_2} \\ c_1(x'+1)^{c_2} \end{cases}$	
Index	SRF model	ζ'*	c_1	c_2	c_3	SRF model	ζ'*	c_1	c_2
0	exp	0.0000	2.3877	0.6414	1.1473	exp	0.0000	4.0535	-0.1501
1	exp	1.6553	2.4240	0.6912	0.9477	pwr	0.0000	4.9487	-0.4922
2	exp	1.6686	1.3382	0.7035	1.8342	pwr	0.0000	5.1107	-0.4983
3	exp	0.0000	1.7806	0.6856	1.5526	exp	0.0000	4.2921	-0.1384
4	exp	0.0000	4.9122	0.6481	0.1387	exp	0.0000	4.2929	-0.1399
5	exp	0.7364	1.8200	0.7159	1.5246	exp	0.0000	4.4463	-0.1469
6	exp	0.6748	3.0074	0.7235	0.8048	exp	0.0000	4.4670	-0.1466
7	exp	1.6028	3.9802	0.7272	0.3944	exp	0.0000	4.4291	-0.1446
8	exp	1.2825	2.5574	0.7178	0.9914	exp	0.0000	4.3811	-0.1420
9	exp	1.5382	4.5485	0.7149	0.1574	exp	0.0000	4.3093	-0.1438
10	exp	1.5100	4.7575	0.7060	0.0415	exp	0.0000	3.9688	-0.1382
11	exp	1.3555	4.5538	0.6770	0.0710	pwr	0.0000	5.0100	-0.4918
12	exp	1.1022	3.7358	0.7423	0.2414	pwr	0.0000	5.1710	-0.5408
13	exp	1.0792	2.1844	0.7430	0.9530	pwr	0.0000	5.0203	-0.5289
14	exp	1.1266	1.0673	0.6621	2.1597	exp	0.0000	3.7967	-0.1308
15	exp	1.1840	2.2338	0.6647	1.0517	exp	0.0000	3.8153	-0.1297
16	exp	1.2549	1.8719	0.6777	1.3472	exp	0.0000	3.8378	-0.1246
17	exp	1.4322	2.8764	0.6685	0.7061	exp	0.0000	3.7463	-0.1204
18	exp	1.4066	2.8217	0.6763	0.7521	exp	0.0000	3.7948	-0.1202
19	exp	1.5049	2.6506	0.6844	0.8513	pwr	0.0000	4.7515	-0.4305
20	exp	1.6435	4.9529	0.6821	-0.0099	pwr	0.0000	4.8448	-0.4306
21	exp	1.6139	3.4188	0.7013	0.5491	exp	0.0000	4.0861	-0.1258
22	exp	1.8330	4.5349	0.6938	0.1560	exp	0.0000	4.0527	-0.1223
23	exp	1.8429	3.0543	0.7158	0.7422	exp	0.0000	4.2516	-0.1274
24	exp	1.9872	2.1497	0.7284	1.2628	exp	0.0000	4.5637	-0.1296
25	exp	1.7609	3.2304	0.7127	0.7043	exp	0.0000	4.6595	-0.1295
26	exp	1.3592	2.4100	0.6952	1.1484	exp	0.0000	4.5443	-0.1281
27	exp	1.5926	3.2313	0.7200	0.7306	exp	0.0000	4.6857	-0.1264
28	exp	1.7085	2.8776	0.7393	0.8916	exp	0.0000	4.7079	-0.1253
29	exp	1.7980	4.4199	0.7432	0.3070	exp	0.0000	4.7683	-0.1257
30	exp	2.3095	2.9147	0.7389	0.8980	exp	0.0000	4.8530	-0.1263
31	exp	1.6929	2.6471	0.7581	1.0228	exp	0.0000	4.9411	-0.1280
32	exp	1.9988	3.4270	0.7685	0.7084	exp	0.0000	4.9876	-0.1268
33	exp	1.9295	3.2834	0.7695	0.7713	exp	0.0000	5.0095	-0.1241
34	exp	1.8255	2.2072	0.7681	1.2655	exp	0.0000	4.8992	-0.1245
35	exp	1.9422	2.5026	0.7677	1.1390	exp	0.0000	4.9802	-0.1233
36	exp	1.6503	3.6271	0.8081	0.6208	exp	0.0000	4.9699	-0.1204

	x' < 0		$\zeta' = c_1 e^{c_2(x'+c_3)}$			x' >= 0		$\zeta' = \begin{cases} c_1 e^{(x')c_2} \\ c_1(x'+1)^{c_2} \end{cases}$	
Index	SRF model	ζ'*	c_1	c_2	c_3	SRF model	ζ'*	c_1	c_2
37	exp	1.6601	2.6200	0.7916	1.0261	exp	0.0000	4.9150	-0.1178
38	exp	1.8030	4.3593	0.7401	0.3715	exp	0.0000	4.7093	-0.1123
39	exp	1.5474	2.9829	0.6856	0.9143	exp	0.0000	3.9803	-0.0750
40	exp	0.0000	140.3429	0.2059	-	exp	0.0000	4.5020	-0.1114
41	exp	0.0000	8.1083	0.1597	1.1124	exp	0.0000	3.9748	-0.0802
42	exp	0.0000	7.9421	0.1642	1.1726	pwr	0.0000	5.2873	-0.3552
43	exp	0.0000	11.6043	0.1904	-1.3641	exp	0.0000	4.6943	-0.1065
44	exp	0.0000	148.5885	0.1494	-	exp	0.0000	4.7108	-0.1035
45	exp	0.0000	119.0340	0.1502	-	exp	0.0000	4.9469	-0.1152
46	exp	0.0000	37.9148	0.1479	-8.0941	exp	0.0000	5.1599	-0.1207
47	exp	0.0000	23.5541	0.1411	-4.7398	exp	0.0000	5.3462	-0.1244
48	exp	0.0000	6.9136	0.1373	4.1990	exp	0.0000	5.4918	-0.1252
49	exp	0.0000	6.4899	0.7620	-0.0187	exp	0.0000	5.8233	-0.1307
50	exp	2.5560	3.1402	0.7573	0.9428	exp	0.0000	5.5263	-0.1204
51	exp	2.3362	2.5842	0.7901	1.1840	exp	0.0000	5.6396	-0.1276
52	exp	2.3737	3.9781	0.8067	0.6467	exp	0.0000	5.7000	-0.1289
53	exp	2.0937	8.7335	0.8238	-0.2855	exp	0.0000	5.7888	-0.1305
54	exp	1.9479	2.9345	0.7962	1.0120	exp	0.0000	5.4579	-0.1265
55	exp	1.4082	2.6590	0.8301	1.1215	exp	0.0000	5.6107	-0.1278
56	exp	1.4097	5.7852	0.8258	0.1800	exp	0.0000	5.5853	-0.1296
57	exp	1.8331	2.6239	0.8169	1.1496	exp	0.0000	5.5748	-0.1309
58	exp	1.7740	1.8137	0.8153	1.6511	exp	0.0000	5.7147	-0.1344
59	exp	4.1637	3.0425	0.9515	0.8087	pwr	0.0000	7.8276	-0.5178
60	exp	4.3184	2.4005	0.9746	1.0828	pwr	0.0000	8.0442	-0.5371
61	exp	4.1808	1.4634	0.9491	1.5820	pwr	0.0000	7.8698	-0.5169
62	exp	3.4765	3.4235	0.8986	0.7201	pwr	0.0000	7.8389	-0.5031
63	exp	1.8412	3.7198	0.8005	0.7469	exp	0.0000	5.5382	-0.1381
64	exp	1.8718	2.5506	0.7985	1.1979	exp	0.0000	5.5359	-0.1371
65	exp	1.8429	4.9461	0.8044	0.3738	exp	0.0000	5.4942	-0.1394
66	exp	1.8417	3.6336	0.7908	0.7340	exp	0.0000	5.2535	-0.1359
67	exp	1.6196	2.2221	0.7772	1.3505	exp	0.0000	5.3051	-0.1382
68	exp	1.5729	1.7367	0.7783	1.6565	exp	0.0000	5.1106	-0.1383
69	exp	1.5470	2.3095	0.7722	1.2381	exp	0.0000	5.2098	-0.1361
70	exp	1.5451	3.3746	0.7655	0.7233	exp	0.0000	5.0149	-0.1372
71	exp	1.2149	2.8047	0.7577	0.9845	exp	0.0000	5.1475	-0.1348
72	exp	2.5295	1.6478	0.8694	1.4533	pwr	0.0000	6.7834	-0.5608

	$x' < 0$		$\zeta' = c_1 e^{c_2(x'+c_3)}$			$x' >= 0$		$\zeta' = \begin{cases} c_1 e^{(x')c_2} \\ c_1(x'+1)^{c_2} \end{cases}$	
Index	SRF model	ζ'*	c_1	c_2	c_3	SRF model	ζ'*	c_1	c_2
73	exp	2.3512	2.5187	0.8775	0.9839	pwr	0.0000	6.9870	-0.5728
74	exp	2.3987	3.7991	0.8775	0.5383	pwr	0.0000	7.1780	-0.5782
75	exp	2.4759	1.9493	0.8671	1.3227	pwr	0.0000	7.2689	-0.5807
76	exp	2.5786	2.1925	0.8455	1.2205	pwr	0.0000	7.3233	-0.5827
77	exp	2.6618	1.7175	0.8363	1.5375	pwr	0.0000	8.0949	-0.4895
78	exp	2.5638	1.5608	0.8175	1.6922	pwr	0.0000	7.3734	-0.5873
79	exp	0.4316	4.3153	0.8086	0.4646	pwr	0.0000	7.9116	-0.5216
80	exp	0.0000	1.9992	0.6043	1.8822	pwr	0.0000	7.6779	-0.5408
81	exp	0.0000	3.4347	0.5983	1.0456	pwr	0.0000	7.4349	-0.5956
82	exp	0.0000	5.0744	0.5981	0.4218	pwr	0.0000	7.8435	-0.5494
83	exp	0.0000	5.5697	0.5906	0.2743	pwr	0.0000	8.0163	-0.5272
84	exp	0.0000	7.5117	0.5795	-0.2475	pwr	0.0000	8.2233	-0.4946
85	exp	0.0000	4.3776	0.5794	0.6507	pwr	0.0000	7.8611	-0.5241
86	exp	0.0000	5.3593	0.5890	0.2627	pwr	0.0000	7.5613	-0.5534
87	exp	0.0000	2.9950	0.5970	1.2075	pwr	0.0000	7.6067	-0.5421
88	exp	0.0000	3.7058	0.6257	0.8051	pwr	0.0000	7.2765	-0.5907
89	exp	2.3952	5.2205	0.8003	0.2044	pwr	0.0000	7.2971	-0.5893
90	exp	2.3329	2.9100	0.8167	0.8984	pwr	0.0000	7.2595	-0.5850
91	exp	2.2841	1.5947	0.8259	1.6078	pwr	0.0000	7.1911	-0.5820
92	exp	2.3279	4.6915	0.8448	0.2870	pwr	0.0000	7.0992	-0.5805
93	exp	2.1412	2.7521	0.8433	0.8961	pwr	0.0000	6.8996	-0.5780
94	exp	2.1134	1.4265	0.8317	1.6714	pwr	0.0000	6.7843	-0.5791
95	exp	2.1698	3.7004	0.8339	0.5134	pwr	0.0000	6.5921	-0.5608
96	exp	2.2382	2.4692	0.8241	0.9837	pwr	0.0000	6.5296	-0.5589
97	exp	2.3164	3.3294	0.8217	0.6061	pwr	0.0000	6.5672	-0.5524
98	exp	0.8221	7.1460	0.7253	-0.3350	exp	0.0000	4.9522	-0.1316
99	exp	1.0933	3.0485	0.7318	0.7956	exp	0.0000	4.7147	-0.1338
100	exp	1.2843	5.7991	0.7222	-0.1236	exp	0.0000	4.4939	-0.1347
101	exp	1.4876	3.5822	0.7113	0.5100	exp	0.0000	4.3446	-0.1319
102	exp	1.6064	3.3569	0.7068	0.5824	exp	0.0000	4.1297	-0.1279
103	exp	1.3511	2.3312	0.6953	1.0960	exp	0.0000	4.0501	-0.1276
104	exp	1.2455	3.8979	0.6819	0.3207	exp	0.0000	3.9491	-0.1271
105	exp	0.9885	4.1519	0.6867	0.2477	exp	0.0000	4.0210	-0.1300
106	exp	0.7593	1.6125	0.6884	1.6019	exp	0.0000	4.0357	-0.1333
107	exp	0.7233	2.1384	0.6729	1.2030	exp	0.0000	4.0316	-0.1361
108	exp	0.3695	1.4072	0.6726	1.8082	exp	0.0000	4.0125	-0.1379

	x' < 0		$\zeta' = c_1 e^{c_2(x'+c_3)}$			x' >= 0		$\zeta' = \begin{cases} c_1 e^{(x')c_2} \\ c_1(x'+1)^{c_2} \end{cases}$	
Index	SRF model	ζ'*	c_1	c_2	c_3	SRF model	ζ'*	c_1	c_2
109	exp	0.0000	2.5196	0.6668	0.9515	pwr	0.0000	5.2383	-0.5368
110	exp	0.1933	4.7760	0.6515	-0.0535	exp	0.0000	3.8921	-0.1384
111	exp	0.3307	6.3809	0.6475	-0.5265	exp	0.0000	3.8048	-0.1363
112	exp	0.7381	7.7672	0.6433	-0.8606	exp	0.0000	3.7439	-0.1346
113	exp	0.8608	1.6442	0.6300	1.5496	exp	0.0000	3.6244	-0.1310
114	exp	0.1363	1.5501	0.6595	1.5857	exp	0.0000	3.6233	-0.1307
115	exp	0.1922	2.9518	0.6556	0.6100	exp	0.0000	3.6225	-0.1308
116	exp	0.1431	3.3679	0.6514	0.4180	exp	0.0000	3.6280	-0.1313
117	exp	0.3520	1.1854	0.6348	1.9959	exp	0.0000	3.5106	-0.1285
118	exp	0.2688	1.3170	0.6312	1.8486	exp	0.0000	3.5280	-0.1302
119	exp	0.2315	1.9508	0.6224	1.1585	exp	0.0000	3.3473	-0.1240
120	exp	0.2249	9.4940	0.6225	-1.3505	exp	0.0000	3.4848	-0.1276
121	exp	0.0000	17.4150	0.2500	-5.5540	pwr	0.0000	4.6608	-0.5228
122	exp	0.0000	3.5978	0.4187	0.0006	pwr	0.0000	4.7532	-0.5335
123	exp	0.0000	1.8430	0.4200	1.6359	pwr	0.0000	4.8289	-0.5360
124	exp	0.0000	2.6461	0.4206	0.8000	pwr	0.0000	4.8735	-0.5377
125	exp	0.0000	2.2462	0.4234	1.2179	pwr	0.0000	4.9097	-0.5398
126	exp	0.0000	5.4708	0.4265	-0.8458	pwr	0.0000	4.8992	-0.5333
127	exp	0.0000	6.5093	0.4334	-1.2053	pwr	0.0000	4.8385	-0.5336
128	exp	0.0000	4.9083	0.4370	-0.5460	pwr	0.0000	4.7990	-0.5415
129	exp	0.0000	7.7937	0.4602	-1.5546	pwr	0.0000	4.7983	-0.5564
130	exp	0.0000	2.0850	0.4600	1.3874	pwr	0.0000	4.8712	-0.5600
131	exp	0.0000	7.8229	0.4683	-1.4292	pwr	0.0000	4.8924	-0.5662
132	exp	0.8719	1.1898	0.7550	1.5794	pwr	0.0000	4.8594	-0.5758
133	exp	0.0000	2.0900	0.4530	1.2716	pwr	0.0000	4.7836	-0.5705
134	exp	0.0000	2.9794	0.3979	0.5656	pwr	0.0000	4.7397	-0.5685
135	exp	0.0000	1.9842	0.3838	1.6201	pwr	0.0000	4.7060	-0.5649
136	exp	0.0000	1.9760	0.3703	1.8033	pwr	0.0000	4.6653	-0.5633
137	exp	0.0000	5.9932	0.3637	-1.2501	pwr	0.0000	4.6277	-0.5653
138	exp	0.0000	3.5131	0.3765	0.1120	pwr	0.0000	4.6298	-0.5668
139	exp	0.0000	2.8417	0.3764	0.7020	pwr	0.0000	4.6712	-0.5681
140	exp	0.0000	2.0406	0.3610	1.6857	pwr	0.0000	4.7233	-0.5722
141	exp	0.0000	7.4447	0.3633	-1.8651	pwr	0.0000	4.7918	-0.5707
142	exp	0.0000	8.3003	0.3590	-2.1623	pwr	0.0000	4.8403	-0.5717
143	exp	0.0000	2.1608	0.3570	1.6298	pwr	0.0000	4.9041	-0.5697
144	exp	0.0000	3.0218	0.3514	0.7064	pwr	0.0000	4.9506	-0.5707
145	exp	0.0000	3.8587	0.3280	0.1531	pwr	0.0000	4.9832	-0.5692

	x’ < 0		$\zeta' = c_1 e^{c_2 (x' + c_3)}$			x’ >= 0		$\zeta' = \begin{cases} c_1 e^{(x')^{c_2}} \\ c_1 (x' + 1)^{c_2} \end{cases}$	
Index	SRF model	ζ'*	c_1	c_2	c_3	SRF model	ζ'*	c_1	c_2
146	exp	0.0000	3.9132	0.3138	0.1049	pwr	0.0000	4.9951	-0.5744
147	exp	0.0000	2.6627	0.3063	1.3863	pwr	0.0000	5.0359	-0.5741
148	exp	0.0000	3.7321	0.3040	0.3181	pwr	0.0000	5.0124	-0.5715
149	exp	0.0000	8.4164	0.3010	-2.3689	pwr	0.0000	5.0513	-0.5716
150	exp	0.0000	9.6272	0.3043	-2.8354	pwr	0.0000	4.9980	-0.5752
151	exp	0.0000	1.9755	0.3044	2.2518	pwr	0.0000	4.9532	-0.5803
152	exp	0.0000	3.7224	0.3071	0.2342	pwr	0.0000	4.9391	-0.5771
153	exp	0.0000	2.6688	0.3097	1.2846	pwr	0.0000	4.9166	-0.5725
154	exp	0.0000	3.3566	0.3252	0.5593	pwr	0.0000	4.9513	-0.5724
155	exp	0.0000	8.9918	0.3308	-2.4617	pwr	0.0000	4.8953	-0.5704
156	exp	0.0000	7.2266	0.3283	-1.8771	pwr	0.0000	4.8177	-0.5713
157	exp	0.0000	6.3077	0.3222	-1.5321	pwr	0.0000	4.7774	-0.5741
158	exp	0.0000	6.5249	0.3483	-1.6363	pwr	0.0000	4.7643	-0.5767
159	exp	0.0000	7.2962	0.3256	-2.0002	pwr	0.0000	4.7271	-0.5716
160	exp	0.0000	4.0924	0.3589	-0.2723	pwr	0.0000	4.6496	-0.5742
161	exp	0.0000	1.7652	0.3721	1.9555	pwr	0.0000	4.6217	-0.5711
162	exp	0.0000	3.9075	0.3791	-0.1647	pwr	0.0000	4.6139	-0.5684
163	exp	0.0000	4.8822	0.3782	-0.7848	pwr	0.0000	4.5743	-0.5640
164	exp	0.0000	5.5924	0.3778	-1.1569	pwr	0.0000	4.5649	-0.5519
165	exp	0.0000	2.1412	0.3797	1.3367	pwr	0.0000	4.5592	-0.5545
166	exp	0.0000	1.4464	0.3669	2.5738	pwr	0.0000	4.5861	-0.5543
167	exp	0.0000	6.8428	0.3941	-1.6604	pwr	0.0000	4.6226	-0.5555
168	exp	0.0000	1.8177	0.4676	1.4674	pwr	0.0000	4.5803	-0.5550
169	exp	0.0000	1.4734	0.4937	1.7695	pwr	0.0000	4.5474	-0.5449
170	exp	0.0000	2.6018	0.5033	0.6398	pwr	0.0000	4.6243	-0.5521
171	exp	0.0000	1.7331	0.4938	1.5610	pwr	0.0000	4.6339	-0.5472
172	exp	0.0000	3.5966	0.4812	0.0646	pwr	0.0000	4.5867	-0.5334
173	exp	0.0000	4.0995	0.4378	-0.2172	pwr	0.0000	4.5617	-0.5273
174	exp	0.0000	3.3276	0.4308	0.2077	pwr	0.0000	4.5590	-0.5148
175	exp	0.0000	23.7278	0.2838	-6.1004	pwr	0.0000	4.5513	-0.5160
176	exp	0.0000	3.3337	0.2738	0.8750	pwr	0.0000	4.5250	-0.5185
177	exp	0.0000	9.2884	0.2588	-2.9919	pwr	0.0000	4.5338	-0.5184
178	exp	0.0000	17.7159	0.2514	-5.5680	pwr	0.0000	4.4794	-0.5171
179	exp	0.0000	18.0923	0.2370	-5.8795	pwr	0.0000	4.4039	-0.5141
180	exp	0.1927	1.4928	0.6188	1.5685	exp	0.0000	3.3142	-0.1240
181	exp	0.1951	2.3601	0.6220	0.8446	exp	0.0000	3.3296	-0.1236
182	exp	0.0000	2.4318	0.6612	0.7647	exp	0.0000	3.3804	-0.1237

	x' < 0		$\zeta' = c_1 e^{c_2(x'+c_3)}$			x' >= 0		$\zeta' = \begin{cases} c_1 e^{(x')c_2} \\ c_1(x'+1)^{c_2} \end{cases}$	
Index	SRF model	ζ'^*	c_1	c_2	c_3	SRF model	ζ'^*	c_1	c_2
183	exp	0.1180	2.7162	0.6330	0.6762	exp	0.0000	3.5077	-0.1283
184	exp	0.2099	1.5030	0.6526	1.6108	exp	0.0000	3.5140	-0.1290
185	exp	0.3469	2.6964	0.6443	0.7269	exp	0.0000	3.5216	-0.1282
186	exp	0.8407	5.1244	0.6321	-0.2858	exp	0.0000	3.5567	-0.1293
187	exp	0.6270	4.7736	0.6314	-0.1671	exp	0.0000	3.5778	-0.1296
188	exp	0.1763	7.3592	0.6523	-0.7494	exp	0.0000	3.7959	-0.1366
189	exp	0.2924	2.0726	0.6429	1.1771	exp	0.0000	3.7311	-0.1358
190	exp	0.0000	2.1307	0.5414	1.3428	pwr	0.0000	4.9406	-0.5341
191	exp	0.0000	4.4613	0.5322	0.0426	pwr	0.0000	5.0234	-0.5339
192	exp	0.0000	7.1709	0.5312	-0.8088	pwr	0.0000	4.9532	-0.5290
193	exp	0.0000	3.2705	0.5280	0.7071	pwr	0.0000	4.9429	-0.5301
194	exp	0.0000	2.1789	0.6362	1.1520	pwr	0.0000	5.0777	-0.5596
195	exp	0.0000	6.8476	0.6230	-0.5788	pwr	0.0000	5.0374	-0.5645
196	exp	0.0000	2.2848	0.6280	1.2024	pwr	0.0000	5.0988	-0.5730
197	exp	0.0000	2.4765	0.6302	1.1145	pwr	0.0000	5.2614	-0.5847
198	exp	0.0000	1.8272	0.6388	1.6280	pwr	0.0000	5.3651	-0.6017
199	exp	0.0000	2.3481	0.6311	1.2863	pwr	0.0000	5.4929	-0.6181
200	exp	0.0000	4.3501	0.3967	0.7256	pwr	0.0000	6.1885	-0.7181
201	exp	0.0000	5.2776	0.5573	0.1447	pwr	0.0000	6.8081	-0.7197
202	exp	0.0000	5.6121	0.5194	0.0260	pwr	0.0000	6.9463	-0.7626
203	exp	0.0000	3.9288	0.5923	0.5171	pwr	0.0000	6.3404	-0.7085
204	exp	0.3323	3.6966	1.0239	0.7626	pwr	0.0000	5.9573	-0.4498
205	exp	0.5876	1.7691	0.9796	1.6061	pwr	0.0000	6.3898	-0.4937
206	exp	0.5808	2.8189	0.9724	1.1275	pwr	0.0000	6.3352	-0.4853
207	exp	0.0000	7.5476	0.3099	0.0556	exp	0.0000	7.0032	-0.5976
208	exp	0.0000	6.4638	0.3744	-0.3269	pwr	0.0000	6.2448	-0.7478
209	exp	0.0000	3.9359	0.3559	1.0874	pwr	0.0000	5.8273	-0.6735
210	exp	0.0000	2.9991	0.6243	0.8445	pwr	0.0000	5.3734	-0.6134
211	exp	0.0000	2.6930	0.6307	0.9436	pwr	0.0000	5.0990	-0.5878
212	exp	0.0000	5.4379	0.6310	-0.1969	pwr	0.0000	5.0082	-0.5708
213	exp	0.0000	3.3619	0.6512	0.5122	pwr	0.0000	4.8875	-0.5627
214	exp	0.0000	1.4527	0.6426	1.6914	pwr	0.0000	4.8003	-0.5489
215	exp	0.0000	1.8185	0.6218	1.2745	pwr	0.0000	4.6960	-0.5440
216	exp	0.0000	1.9814	0.5665	1.0623	pwr	0.0000	4.6028	-0.5289
217	exp	0.0000	1.7013	0.5117	1.2416	pwr	0.0000	4.5884	-0.5292
218	exp	0.0000	1.9019	0.5891	1.3373	pwr	0.0000	4.7640	-0.5279
219	exp	1.3177	1.4838	0.6556	1.7224	exp	0.0000	3.8396	-0.1384

	x’ < 0		$\zeta' = c_1 e^{c_2(x'+c_3)}$			x’ >= 0		$\zeta' = \begin{cases} c_1 e^{(x')c_2} \\ c_1(x'+1)^{c_2} \end{cases}$	
Index	SRF model	ζ'*	c_1	c_2	c_3	SRF model	ζ'*	c_1	c_2
220	exp	0.0000	8.5404	0.2531	1.3445	exp	1.3232	5.2176	-0.4152
221	exp	0.0000	11.0105	0.2643	0.2583	exp	1.6603	5.3611	-0.4137
222	exp	0.0000	23.5941	-0.0452	-8.2665	pwr	0.0000	7.6608	-0.5858
223	exp	0.0000	8.5615	0.2907	0.7701	pwr	0.0000	7.5342	-0.5925
224	exp	0.0000	14.1225	0.3146	-1.1013	pwr	0.0000	7.4064	-0.6031
225	exp	0.0000	47.1797	0.2949	-5.2672	pwr	0.0000	7.3015	-0.6147
226	exp	0.0000	3.0298	0.6770	1.3354	pwr	0.0000	7.2217	-0.6318
227	exp	0.0000	151.9656	0.3317	-8.6863	pwr	0.0000	7.1089	-0.6482
228	exp	0.0000	2.5386	0.6361	1.6200	pwr	0.0000	7.1152	-0.6656
229	exp	0.0000	6.5979	0.4705	0.0417	pwr	0.0000	6.8851	-0.6767
230	exp	0.0000	2.2684	0.4222	2.4932	pwr	0.0000	6.6781	-0.6803
231	exp	0.0000	3.2169	0.4250	1.7077	pwr	0.0000	6.7130	-0.6837
232	exp	0.0000	2.2180	0.3585	2.6709	pwr	0.0000	7.3894	-0.7642
233	exp	0.0000	15.9241	0.3519	-2.9034	pwr	0.0000	7.2494	-0.7816
234	exp	0.0000	6.3555	0.3434	-0.2519	pwr	0.0000	7.2629	-0.8027
235	exp	0.0000	10.1072	0.3501	-1.6260	pwr	0.0000	7.1888	-0.7860
236	exp	0.0000	3.2568	0.3615	1.5166	pwr	0.0000	7.2848	-0.7673
237	exp	0.0000	11.6707	0.4049	-1.4922	pwr	0.0000	6.6118	-0.6880
238	exp	0.0000	4.1005	0.3956	1.0321	pwr	0.0000	6.4426	-0.6829
239	exp	0.0000	3.5495	0.3841	1.4315	pwr	0.0000	6.0204	-0.6677
240	exp	0.0000	4.0901	0.3680	0.8058	pwr	0.0000	7.0491	-0.7657
241	exp	0.0000	2.2585	0.3559	2.5355	pwr	0.0000	6.8402	-0.7635
242	exp	0.0000	29.8747	0.3476	-4.7448	pwr	0.0000	7.3612	-0.8217
243	exp	0.0000	4.4212	0.3532	0.6741	pwr	0.0000	7.2929	-0.8118
244	exp	0.0000	5.0739	0.2350	1.3453	pwr	0.0000	6.6116	-0.7508
245	exp	0.0000	11.3206	0.3877	-1.9089	pwr	0.0000	6.6887	-0.7318
246	exp	0.0000	1.8099	0.3930	3.0641	pwr	0.0000	6.2450	-0.6806
247	exp	0.0000	4.1371	0.4220	1.0058	pwr	0.0000	6.5562	-0.6717
248	exp	0.0000	8.3306	0.2494	0.0653	pwr	0.0000	6.5264	-0.6665
249	exp	0.0000	1.8109	0.3101	4.7519	pwr	0.0000	6.6151	-0.6404
250	exp	0.0000	4.3699	0.2723	2.5251	pwr	0.0000	6.6856	-0.6519
251	exp	0.0000	20.8462	0.2667	-3.2447	pwr	0.0000	6.6999	-0.6409
252	exp	0.0000	6.1342	0.4407	0.5595	pwr	0.0000	7.0946	-0.6168
253	exp	0.0000	8.6150	0.4123	-0.1318	pwr	0.0000	6.9784	-0.6000
254	exp	0.0000	11.0140	0.6317	-0.7976	pwr	0.0000	6.9772	-0.6317
255	exp	0.0000	3.0225	0.2633	4.8801	pwr	0.0000	7.3631	-0.5897
256	exp	0.0000	5.5349	0.2497	2.9883	pwr	0.0000	7.6033	-0.5833
257	exp	0.0000	10.9740	0.2588	0.2214	pwr	0.0000	7.7253	-0.5803
258	exp	0.0000	13.1077	0.2336	-0.2577	exp	1.6358	5.0801	-0.4127

APPENDIX C

SEA-LEVEL RISE

Table C-1 Sea level rise slope, intercept, R^2, and root-mean-square error values for open coast locations at Panama City, FL.

Index	*k*	*l*	R^2 (SLR)	RMS error (m, SLR)
0	0.9630	0.0786	0.9994	0.0253
1	0.9637	0.0768	0.9994	0.0244
2	0.9642	0.0752	0.9995	0.0237
3	0.9648	0.0736	0.9995	0.0230
4	0.9670	0.0672	0.9996	0.0206
5	0.9656	0.0699	0.9996	0.0204
6	0.9689	0.0655	0.9995	0.0223
7	0.9671	0.0684	0.9995	0.0225
8	0.9661	0.0705	0.9995	0.0224
9	0.9653	0.0725	0.9995	0.0223
10	0.9620	0.0802	0.9995	0.0222
11	0.9628	0.0774	0.9995	0.0229
12	0.9591	0.0852	0.9995	0.0232
13	0.9604	0.0820	0.9995	0.0235
14	0.9610	0.0825	0.9995	0.0224
15	0.9618	0.0807	0.9995	0.0229
16	0.9628	0.0786	0.9994	0.0236
17	0.9603	0.0872	0.9996	0.0212
18	0.9613	0.0814	0.9994	0.0240
19	0.9628	0.0782	0.9994	0.0241
20	0.9644	0.0752	0.9994	0.0243
21	0.9586	0.0878	0.9992	0.0274
22	0.9565	0.0918	0.9993	0.0253
23	0.9544	0.0977	0.9993	0.0268
24	0.9564	0.0921	0.9993	0.0263
25	0.9593	0.0840	0.9993	0.0266
26	0.9584	0.0865	0.9992	0.0273
27	0.9619	0.0789	0.9991	0.0288
28	0.9663	0.0695	0.9990	0.0313
29	0.9589	0.0862	0.9992	0.0274
30	0.9640	0.0808	0.9993	0.0257
31	0.9622	0.0786	0.9992	0.0269
32	0.9630	0.0758	0.9993	0.0254
33	0.9586	0.0854	0.9993	0.0250
34	0.9625	0.0764	0.9993	0.0262
35	0.9663	0.0685	0.9993	0.0263
36	0.9707	0.0594	0.9992	0.0267

Index	k	l	R^2 (SLR)	RMS error (m, SLR)
37	0.9716	0.0594	0.9992	0.0277
38	0.9641	0.0702	0.9992	0.0266
39	0.9538	0.0914	0.9991	0.0277
40	0.9442	0.1093	0.9988	0.0316
41	0.9431	0.1143	0.9990	0.0291
42	0.9450	0.1063	0.9986	0.0348
43	0.9463	0.1053	0.9989	0.0310
44	0.9437	0.1116	0.9989	0.0311
45	0.9426	0.1153	0.9989	0.0304
46	0.9463	0.1118	0.9989	0.0309
47	0.9453	0.1133	0.9989	0.0306
48	0.9548	0.0917	0.9992	0.0273
49	0.9578	0.0859	0.9992	0.0261
50	0.9537	0.0949	0.9993	0.0248
51	0.9537	0.0934	0.9993	0.0254
52	0.9601	0.0794	0.9994	0.0232
53	0.9639	0.0712	0.9994	0.0230
54	0.9651	0.0690	0.9994	0.0229
55	0.9697	0.0608	0.9994	0.0233
56	0.9712	0.0574	0.9994	0.0239
57	0.9692	0.0591	0.9993	0.0250
58	0.9775	0.0575	0.9960	0.0610
59	1.0037	-0.0133	0.9909	0.0936
60	1.0244	-0.0637	0.9731	0.1632
61	0.9956	-0.0046	0.9948	0.0705
62	0.9671	0.0730	0.9993	0.0263
63	0.9667	0.0638	0.9994	0.0247
64	0.9713	0.0541	0.9994	0.0238
65	0.9748	0.0458	0.9994	0.0239
66	0.9793	0.0360	0.9995	0.0227
67	0.9829	0.0279	0.9995	0.0220
68	0.9865	0.0198	0.9995	0.0216
69	0.9902	0.0126	0.9996	0.0206
70	0.9952	0.0025	0.9996	0.0207
71	1.0015	-0.0099	0.9995	0.0217
72	1.0068	-0.0203	0.9994	0.0249

Table C-2 Sea level rise slope, intercept, R^2, and root-mean-square error values for bay interior locations at Panama City, FL.

Index	*k*	*l*	R^2 (SLR)	RMS error (m, SLR)
0	1.0451	-0.0205	0.9871	0.1186
1	1.0785	-0.0925	0.9925	0.0915
2	1.0733	-0.0901	0.993	0.0879
3	1.0655	-0.0866	0.9939	0.0816
4	1.0555	-0.0806	0.9952	0.0714
5	1.048	-0.0602	0.9939	0.0802
6	1.0509	-0.0559	0.993	0.0867
7	1.0504	-0.0549	0.9933	0.0852
8	1.0509	-0.0569	0.9933	0.0847
9	1.0636	-0.0795	0.994	0.0808
10	1.0705	-0.0853	0.9934	0.0853
11	1.0656	-0.0675	0.9908	0.1006
12	1.0796	-0.0984	0.9917	0.0957
13	1.0763	-0.078	0.9893	0.1098
14	1.0715	-0.0902	0.9943	0.0778
15	1.0717	-0.0996	0.9959	0.0648
16	1.0587	-0.0807	0.997	0.0546
17	1.0622	-0.0901	0.9974	0.0507
18	1.0608	-0.0879	0.9972	0.0524
19	1.0625	-0.0924	0.9971	0.0536
20	1.061	-0.0912	0.997	0.0545
21	1.0583	-0.09	0.9978	0.0459
22	1.0616	-0.0977	0.9975	0.0491
23	1.0575	-0.0912	0.9978	0.0466
24	1.0539	-0.0856	0.9973	0.0518
25	1.0553	-0.0904	0.9974	0.0506
26	1.0608	-0.1003	0.9974	0.0507
27	1.0571	-0.0964	0.9974	0.0506
28	1.055	-0.0963	0.9978	0.0459
29	1.0541	-0.0919	0.9974	0.0509
30	1.0529	-0.0898	0.9974	0.0506
31	1.0528	-0.0908	0.9974	0.0502
32	1.053	-0.0927	0.9975	0.0494
33	1.054	-0.0955	0.9975	0.0496
34	1.0562	-0.1002	0.9974	0.0505
35	1.0539	-0.0969	0.9974	0.0505
36	1.0532	-0.0955	0.9972	0.0522
37	1.054	-0.096	0.997	0.0545
38	1.0541	-0.0935	0.9964	0.0594
39	1.0522	-0.0851	0.9956	0.0663

Index	k	l	R^2 (SLR)	RMS error (m, SLR)
40	1.0545	-0.0851	0.9949	0.0718
41	1.0511	-0.0782	0.9951	0.0707
42	1.0464	-0.0679	0.9951	0.0708
43	1.0422	-0.0572	0.9947	0.0736
44	1.041	-0.0642	0.9954	0.0682
45	1.0412	-0.0778	0.9954	0.0679
46	1.0409	-0.0941	0.9937	0.0788
47	1.0315	-0.0882	0.9916	0.0888
48	1.0378	-0.107	0.9936	0.0774
49	1.0239	-0.083	0.9924	0.0825
50	1.0379	-0.1082	0.9963	0.0585
51	1.0466	-0.1091	0.9983	0.0403
52	1.0457	-0.1131	0.998	0.0438
53	1.0395	-0.1022	0.9977	0.0473
54	1.0497	-0.1118	0.9986	0.0373
55	1.0446	-0.1099	0.9978	0.0464
56	1.044	-0.1	0.9981	0.0434
57	1.043	-0.0904	0.9981	0.0436
58	1.0333	-0.0648	0.9978	0.047
59	1.027	-0.0498	0.9975	0.05
60	1.0111	-0.013	0.9965	0.059
61	1.0258	-0.0419	0.9972	0.0526
62	1.0279	-0.043	0.9971	0.0543
63	1.0317	-0.0484	0.9969	0.0562
64	1.0347	-0.0552	0.997	0.0548
65	1.0288	-0.0395	0.9966	0.0582
66	1.0371	-0.0595	0.9968	0.0571
67	1.0391	-0.0639	0.997	0.0544
68	1.0344	-0.0489	0.9965	0.0589
69	1.0407	-0.0605	0.9968	0.0568
70	1.0435	-0.0665	0.9969	0.0556
71	1.0359	-0.0505	0.9968	0.0559
72	1.0247	-0.0262	0.9963	0.0605
73	1.0176	-0.0087	0.9956	0.0655
74	1.0105	0.0076	0.9954	0.0671
75	1.0063	0.0183	0.995	0.0702
76	0.998	0.0377	0.9942	0.0754
77	0.9923	0.0524	0.9935	0.0798
78	0.9899	0.0568	0.9933	0.0812
79	0.9845	0.0706	0.9927	0.0848
80	0.981	0.0716	0.9925	0.0851
81	0.9746	0.0838	0.9916	0.0895
82	0.9728	0.0881	0.9915	0.0907

Index	k	l	R^2 (SLR)	RMS error (m, SLR)
83	0.9754	0.0803	0.9917	0.0896
84	0.872	0.6072	NaN	NaN
85	0.9022	0.4706	0.9049	0.3564
86	0.9634	0.1943	0.9704	0.1802
87	0.9854	0.0615	0.9926	0.0847
88	0.9885	0.0555	0.9932	0.0813
89	0.9933	0.0471	0.9934	0.0804
90	1.0012	0.0304	0.9941	0.0758
91	1.0033	0.0249	0.9944	0.0738
92	1.0094	0.0098	0.9952	0.0681
93	1.0208	-0.0185	0.9964	0.0592
94	1.0246	-0.0255	0.9965	0.0581
95	1.0313	-0.0393	0.9968	0.0559
96	1.0366	-0.0505	0.9971	0.053
97	1.039	-0.0556	0.9973	0.0518
98	1.0446	-0.0667	0.9974	0.0505
99	1.0492	-0.0753	0.9975	0.0491
100	1.0528	-0.0811	0.9976	0.0481
101	1.0553	-0.0822	0.9975	0.0499
102	1.0589	-0.0862	0.9971	0.0538
103	1.0563	-0.0825	0.9975	0.0499
104	1.0534	-0.0779	0.9967	0.057
105	1.0609	-0.0906	0.996	0.0637
106	1.0585	-0.0788	0.9953	0.0693
107	1.0602	-0.0769	0.9942	0.0781
108	1.0612	-0.0746	0.9931	0.0859
109	1.0576	-0.064	0.9923	0.0907
110	1.0553	-0.0636	0.9935	0.0828
111	1.0526	-0.0633	0.9951	0.0712
112	1.0484	-0.0607	0.9965	0.0592
113	1.0443	-0.0597	0.9978	0.0458
114	1.0407	-0.0573	0.9983	0.0406
115	1.0395	-0.0561	0.9984	0.0394
116	1.0372	-0.0537	0.9985	0.0382
117	1.034	-0.0492	0.9988	0.0337
118	1.0283	-0.0405	0.999	0.0294
119	1.0154	-0.0212	0.9989	0.0304
120	1.0113	-0.0134	0.9989	0.0312
121	1.0104	-0.0116	0.9988	0.0318
122	1.0088	-0.0096	0.9988	0.0317
123	1.0071	-0.0073	0.999	0.0291
124	1.0062	-0.0058	0.9991	0.0282
125	1.0051	-0.0042	0.999	0.0296

Index	k	l	R^2 (SLR)	RMS error (m, SLR)
126	1.0034	-0.0025	0.9985	0.0364
127	1.0009	0.0006	0.9977	0.0448
128	0.9997	0.002	0.997	0.0503
129	0.9972	0.0065	0.9967	0.0528
130	0.9919	0.0184	0.996	0.0581
131	0.9895	0.0238	0.9955	0.061
132	0.9865	0.0311	0.9946	0.0672
133	0.9859	0.0326	0.9943	0.0687
134	0.9837	0.0363	0.9944	0.0677
135	0.9808	0.0423	0.9939	0.0706
136	0.9778	0.0484	0.9938	0.071
137	0.9723	0.0588	0.9937	0.0715
138	0.9678	0.0694	0.9934	0.0735
139	0.965	0.0749	0.9934	0.0731
140	0.961	0.0828	0.9934	0.0733
141	0.9586	0.0871	0.9934	0.0729
142	0.9565	0.0909	0.9936	0.0718
143	0.9533	0.0961	0.9939	0.0701
144	0.9519	0.0987	0.9939	0.07
145	0.9495	0.1044	0.9936	0.0718
146	0.9464	0.1112	0.9932	0.074
147	0.9423	0.1191	0.9932	0.0739
148	0.9398	0.124	0.9932	0.0737
149	0.9376	0.1295	0.9928	0.0763
150	0.9419	0.1213	0.9928	0.0765
151	0.9378	0.1314	0.9917	0.0822
152	0.9454	0.1153	0.9925	0.0783
153	0.9474	0.11	0.9928	0.0763
154	0.9493	0.106	0.9932	0.0738
155	0.9536	0.0974	0.9934	0.0732
156	0.958	0.0897	0.9934	0.0735
157	0.9587	0.0894	0.9932	0.0749
158	0.9585	0.0906	0.9929	0.0763
159	0.9613	0.0836	0.9932	0.0744
160	0.9633	0.0787	0.9932	0.0746
161	0.9645	0.0762	0.9932	0.0742
162	0.9677	0.07	0.9934	0.0734
163	0.9734	0.0585	0.9935	0.0729
164	0.9783	0.0477	0.9939	0.0705
165	0.9832	0.0379	0.9942	0.0687
166	0.9847	0.0346	0.9944	0.0679
167	0.9898	0.0246	0.9948	0.0652
168	0.9926	0.0188	0.995	0.0642

Index	*k*	*l*	R^2 (SLR)	RMS error (m, SLR)
169	0.9968	0.01	0.9958	0.0591
170	0.9953	0.0127	0.9957	0.0598
171	0.9993	0.0058	0.9964	0.0551
172	1.0028	-0.0011	0.997	0.05
173	1.0064	-0.0063	0.9979	0.0424
174	1.0103	-0.0112	0.9986	0.0344
175	1.0101	-0.0109	0.9987	0.0337
176	1.0086	-0.0089	0.9987	0.0329
177	1.0117	-0.0132	0.9987	0.0332
178	1.0067	-0.0058	0.9989	0.0307
179	1.0076	-0.0055	0.9988	0.0316
180	1.0082	-0.0052	0.9988	0.0326
181	1.0191	-0.0241	0.9991	0.0285
182	1.0263	-0.0362	0.9993	0.0247
183	1.0323	-0.0463	0.9989	0.0313
184	1.0468	-0.0708	0.998	0.0435
185	1.0455	-0.0637	0.9982	0.0417
186	1.0486	-0.0643	0.9974	0.05
187	1.0395	-0.0448	0.9969	0.0548
188	1.0858	-0.1134	0.9932	0.0859
189	1.0682	-0.0792	0.9921	0.0917
190	1.083	-0.0984	0.9897	0.1077
191	1.1189	-0.1496	0.9861	0.1315
192	1.1252	-0.1356	0.98	0.1627
193	1.1333	-0.1376	0.9773	0.1768
194	1.1375	-0.1372	0.976	0.1837
195	1.1358	-0.1253	0.974	0.1923
196	1.1364	-0.1133	0.971	0.2053
197	1.1268	-0.078	0.966	0.2242
198	1.1159	-0.0442	0.9634	0.2338
199	1.0978	-0.0002	0.9602	0.2431
200	1.0683	0.011	0.9746	0.1859
201	1.0325	0.0084	0.99	0.1092
202	1.025	0.0304	0.9892	0.1132
203	1.057	-0.0478	0.9854	0.1328
204	1.0053	-0.0167	0.9957	0.0659
205	0.9739	0.0468	0.9962	0.0601
206	0.9751	0.0444	0.9963	0.0596
207	1.0235	-0.0195	0.9966	0.0607
208	1.0719	-0.0104	0.9788	0.1679
209	1.0776	0.0272	0.9655	0.2216
210	1.1089	-0.021	0.961	0.2412
211	1.1355	-0.09	0.9667	0.222

Index	k	l	R^2 (SLR)	RMS error (m, SLR)
212	1.1399	-0.1183	0.9713	0.2037
213	1.1467	-0.1273	0.9718	0.2022
214	1.1412	-0.147	0.9776	0.1755
215	1.138	-0.1562	0.9809	0.159
216	1.1276	-0.146	0.9834	0.1448
217	1.1279	-0.1436	0.9831	0.1458
218	1.0925	-0.0964	0.9867	0.1238
219	1.077	-0.0849	0.9887	0.1125
220	0.8375	0.3901	0.981	0.1148
221	0.8522	0.3455	0.986	0.0999
222	0.873	0.2862	0.9911	0.0815
223	0.8957	0.2276	0.9945	0.0657
224	0.9092	0.1942	0.9962	0.0551
225	0.9241	0.159	0.9975	0.0459
226	0.9375	0.1322	0.9985	0.0359
227	0.9528	0.1025	0.9988	0.0326
228	0.9633	0.0872	0.9983	0.0402
229	0.9854	0.0494	0.9962	0.0609
230	1.0074	0.0182	0.9919	0.0921
231	1.0085	0.0194	0.9907	0.099
232	1.0326	-0.0054	0.9834	0.1371
233	1.0424	-0.0037	0.9782	0.1612
234	1.046	0.0172	0.9701	0.1947
235	1.042	0.0038	0.9767	0.1676
236	1.0387	-0.0104	0.9818	0.1446
237	1.0195	0.0064	0.9881	0.1136
238	1.025	-0.006	0.9878	0.1151
239	1.042	-0.0245	0.9833	0.1379
240	1.0479	-0.0212	0.9792	0.1568
241	1.0511	-0.0043	0.9714	0.1879
242	1.0441	0.0375	0.9613	0.2241
243	1.0519	0.013	0.9651	0.2114
244	1.0506	-0.0171	0.9771	0.1657
245	1.0519	-0.0336	0.9804	0.1515
246	1.0354	-0.0173	0.9858	0.1257
247	1.0099	0.0135	0.992	0.0913
248	0.9987	0.0252	0.9958	0.0646
249	0.9679	0.0639	0.9991	0.0284
250	0.965	0.0708	0.9994	0.0238
251	0.9613	0.0769	0.9993	0.0243
252	0.933	0.1376	0.9983	0.0377
253	0.9297	0.1401	0.9976	0.0449
254	0.9453	0.1114	0.999	0.0293

Index	*k*	*l*	R^2 (SLR)	RMS error (m, SLR)
255	0.8975	0.219	0.9945	0.0654
256	0.8715	0.289	0.9908	0.0826
257	0.8607	0.3213	0.9886	0.0907
258	0.8483	0.3558	0.9846	0.1045